Grid Impact Study For Old Crow Solar Project

Version 1.2 – September 21, 2018

YUKON RESEARCH CENTRE
Yukon College

This publication may be obtained online at yukoncollege.yk.ca/research

THIS PUBLICATION MAY BE OBTAINED FROM:

Northern Energy Innovation

Yukon Research Centre, Yukon College

520 College Drive, PO Box 2799

Whitehorse, Yukon Y1A 5K4

867.668.8895 or 1.800.661.0504

Recommended Citation:

Ross, M., Zrum, J., Bos-Jabbar, T., Bulut, S., Dohring, T., Favreau, G., Hynes, A., Rahman, T., Ross, J., Sumanik, S., Thompson, S., Tutton, R., "Grid Impact Study for Old Crow Solar Project – Version 1.1", Northern Energy Innovation, Yukon Research Centre, Yukon College. Feb. 9, 2018.

Front cover photograph: Old Crow, Yukon. Site visit with Northern Energy Innovation Team. July 24, 2017.

Photo Credit: Sara Thompson

PROJECT TEAM

Lead Authors

Dr. Michael Ross	Northern Energy Innovation, Yukon Research Centre, Yukon College
Jason Zrum	Northern Energy Innovation, Yukon Research Centre, Yukon College
Spencer Ryan Deehr Sumanik	Northern Energy Innovation, Yukon Research Centre, Yukon College

Contributing Authors

Tarek Bos-Jabbar	Northern Energy Innovation, Yukon Research Centre, Yukon College
Dr. Sinan Bulut	Northern Energy Innovation, Yukon Research Centre, Yukon College
Tim Dohring	Northern Energy Innovation, Yukon Research Centre, Yukon College
Geneviève Favreau	Northern Energy Innovation, Yukon Research Centre, Yukon College
Adrienne Hynes	Northern Energy Innovation, Yukon Research Centre, Yukon College
Dr. Tanvir Rahman	Northern Energy Innovation, Yukon Research Centre, Yukon College
John Ross	Northern Energy Innovation, Yukon Research Centre, Yukon College
Sara Thompson	Northern Energy Innovation, Yukon Research Centre, Yukon College
Rosamond Tutton	Northern Energy Innovation, Yukon Research Centre, Yukon College

FOREWORD

This report details the grid impact study for the Old Crow Solar Project. The objective of this project was to analyze solar generation at various levels and determine the potential impact on the electrical generation and distribution system in the community of Old Crow, Yukon. The analyses performed focused on the power and energy balance issues pertinent to the Old Crow electric power system: frequency and voltage stability, voltage regulation and distribution system voltage profile, conductor loading limit analysis, system faults, operation of the protection system, and reverse power flow.

DISCLAIMER

Results from this study are based on predicted responses and may not inherently capture all phenomena. The modelling was performed with every effort to use real equipment data; where real equipment data were not available, industry standard models were implemented. It should be noted that equipment models should be validated from real system data from recorded disturbances, which were not performed due to the lack of data for system events in Old Crow. Several reasonable assumptions have been made and described throughout the analyses due to unavailable data and parameters, and any equipment that has not yet been installed in Old Crow has been modelled through generic models. Results are shown with and without an Energy Storage System as this has been identified a priority by both Vuntut Gwitchin Government and ATCO Electric Ltd. as a resource that will be implemented for the Project. The scope of this study focused on technical aspects of this research, while system planning, parameters, control, and other aspects of the Old Crow Solar Project are not meant to be addressed nor designed by the Northern Energy Innovation team. This was intended to ensure unbiased and transparent results that are pertinent and valuable to all parties involved in the Old Crow Solar Project design.

ACKNOWLEDGMENTS

The project team would like to thank all participants for their commitment and hard work throughout this project. We would especially like to thank Vuntut Gwitchin Government and the Vuntut Gwichin First Nation for supporting this project and welcoming us on their lands and within their Traditional Territory. We appreciate the support and involvement that led to an engaging collaboration which has enriched the lens of this research. A special thank you to William Josie and Rosa Brown for your insight and contribution throughout this project.

Funding for this project was made possible by Vuntut Gwitchin Government through the Indigenous and Northern Affairs Canada Northern REACHE program. In addition, financial support was provided from Natural Sciences and Engineering Research Council through the Industrial Research Chair for Colleges program. The Northern Energy Consortium, comprised of ATCO Electric Ltd., Northwest Territories Power Corporation, Qulliq Energy Corporation, and Yukon Energy Corporation provided continued financial support, access to data, and their invaluable expertise.

Thank you to the many contributors involved in this project, including Solvest Inc. for providing solar data, and MathWorks for answering questions regarding the automation and technical aspects of the project relating to Simulink models. Sean MacKinnon from the Energy Solutions Centre, Yukon Government, and Gordon Howell from Howell-Mayhew Engineering both provided valuable information and data from existing photovoltaic arrays in Old Crow, Yukon.

We would like to especially note the open communication and ongoing availability of Phil Borgel, Norm Curzon, Tom East, and Jay Massie at ATCO Electric Yukon as resources throughout the project, as well as Alexandre Vigneault and Nick Hawley from 3EYOND Consulting Group providing insight and direction on behalf of VGG. The Northern Energy Innovation Team is grateful for everyone's support and input, ensuring a consistent direction for the vision of the Old Crow Solar Project.

EXECUTIVE SUMMARY

This report details the methodology, analyses, and results of the energy balance and power system studies performed for the Old Crow Solar Project. The focus of the studies is on frequency and voltage stability, voltage regulation and distribution system voltage profile, conductor loading limits, system faults, and protection coordination.

The existing system was found to be capable of maintaining frequency and voltage stability under normal operating conditions with a proposed solar plant capacity of 260kW and an existing solar capacity of 20.1kW without the implementation of an energy storage system. Normal operating conditions assume a maximum rate of connection and a maximum rate of loss of output of the solar plant. The diesel generator G3O is also assumed to not be in operation. However, the solar plant capacity is limited by the economic implications associated with curtailing a large fraction of the energy produced by the plant. The proposed solar plant had relatively little impact on the protection coordination. It contributed a slight increase in the maximum observed current, a slight decrease in the clearing time of the fuses, and comparable operation of the feeder relays. The solar plant should incorporate protection that is capable of detecting series faults between the solar plant and the diesel plants, which may be caused by blown fuses, in addition to any other protection required by ATCO.

The existing system, with the addition of a battery energy storage system, was found to be capable of maintaining system frequency and voltage stability under normal and abnormal operating conditions in diesel-off with a solar plant capacity of 450kW; however, a significant, but acceptable, phase imbalance was observed. The phase imbalance must be taken into consideration when designing and specifying the battery energy storage system. The battery energy storage system should be capable of operating on an unbalanced system and maintaining the phase imbalance at an acceptable level. Furthermore, the battery energy storage system should be specified to have a sufficient response time to maintain system frequency and voltage under normal operating conditions and a sufficient fault current contribution to ensure proper protection coordination.

In the proposed system, over-voltages and under-voltages were observed through the energy balance study. The over-voltage is caused by voltage rise between the diesel/storage plant bus and the solar plant. The under-voltage is caused by voltage drop on feeder 2. The over- and under-voltage issues should be addressed. The over-voltage caused by the proposed solar plant may be managed through an appropriate power factor setting. Current through the distribution lines does not exceed the thermal loading limit of the lines at any point in the system. For the given battery dispatch logic: a battery capacity of 400kWh or greater is required to provide a lifespan greater than 20 years, a battery capacity of 600kWh or greater is required to prevent operation in diesel-off mode for less than 1 hour, and a battery capacity of 800kWh or greater is required to achieve diesel-off for greater than 24 hours. Increasing the battery size, however, did not greatly affect the total number of hours of diesel-off, which was found to be between 95 to 105 days, distributed throughout the year, for battery capacities of 400kWh or greater.

It is noted that future system disturbances should be recorded to allow for validation of equipment models. This will improve the accuracy of future studies.

TABLE OF CONTENTS

1 INTRODUCTION

This report details the methodology and results of the grid impact study performed for the Old Crow Solar Project. The following sections provide an overview of the project and the Old Crow system.

1.1 PROJECT OVERVIEW

Yukon College's Industrial Research Chair in Northern Energy Innovation was established to address the specific needs of the Northern Energy Consortium, which comprises the four electric power utilities in the Canadian territories: ATCO Electric, Northwest Territories Power Corporation, Qulliq Energy Corporation, and Yukon Energy Corporation. This project addresses two areas of research identified as priorities of research by the Northern Energy Consortium.

The first research area is the integration of renewables into existing power systems. To address this, the Northern Energy Innovation (NEI) team is developing a grid impact study tool which automates the process of modeling and evaluating how much renewable generation a power system can integrate without affecting stability or reliability. The tool can be applied to identify integration limits of renewables through an analysis that not only identifies the technical bottlenecks preventing a higher penetration level, but also identifies the sensitivities so that potential solutions can be conceptualized. The intent is to standardize and expand on this tool to use in other remote communities so that utilities can confidently move away from generic blanket statements for renewable integration limits in isolated systems.

The second research area is energy storage technologies and controls. An analysis of available storage technologies that may be viable in the North has been completed, and continuing work focuses on the control validation and potential effects on northern and remote systems.

Old Crow, Yukon was chosen as the first community to be modeled as an alpha/development test for the grid impact study tool due to the concurrent timeline of the Old Crow Solar Project. The intent was to model a system where the results could be used to further a current project. The first and second research areas were combined for this study in order to account for the proposed energy storage system from the Old Crow Solar Project.

The Vuntut Gwitchin Government (VGG) received funding through Indigenous and Northern Affairs Canada's (INAC) Northern REACHE program to accelerate the work conducted by NEI. The scope of the deliverables for the research program has been pre-approved by the Northern Energy Consortium (through "Project 01.01: Barriers to Integrating a High Penetration of Renewables" and "Project 02.01: Energy Storage Technologies and Control"); however, the original project timelines, would not have provided pertinent deliverables in sufficient time to meet the needs of VGG. The additional resources covered the salaries and administration to hire and extend contracts for the technical personnel required to expedite the deliverables and to perform specific case studies for VGG. The intent is to provide VGG the technical support and necessary studies to make an informed decision regarding the

planning of the Old Crow Solar Project. The overall objective is to ensure that the proposed solar and storage installation will not affect system stability or cause detrimental effects in Old Crow, and to support the success of the Old Crow Solar Project for both VGG and ATCO Electric.

1.2 OLD CROW SYSTEM

Old Crow is the northernmost community in the Yukon Territory. The community is situated on the Porcupine River, north of the Arctic Circle. It has a population of approximately 250 [1], with a majority belonging to the Vuntut Gwitchin First Nation. The community is isolated, and almost exclusively accessible by air. Yukon is a large territory, with the weather varying widely between communities. The average temperature in Old Crow is among the coldest in the Yukon, with average temperatures ranging from -15°C to -35°C in the winter months and rising to 20°C in the summer [2]. Spring temperatures are more consistent with the rest of the territory, with the cool days having plenty of sunshine, causing the sunlight to reflect off the snow and ice. Long stretches of cloudless days without precipitation are common in Old Crow with the total annual precipitation reaching 278mm [2]. In Old Crow, cool temperatures generally mean that snow cover doesn't finish melting until early summer and the little rainfall that Old Crow gets usually falls from June to early September.

The Old Crow system is a radially configured overhead distribution system with a primary voltage of 2.4kV line-to-line. Power is generated from five diesel-electric generators (G1, G2, G3O, G3N, and G4), located in two plants (the new plant and the old plant), however G3O is now used infrequently due to load growth. The diesel-electric generators are delta connected and generate directly at the primary voltage. Service to customers is provided mainly as single-phase 120/240V through secondary distribution from pole-mounted transformers. There are several three-phase loads on the system; however, the majority of loads are single-phase, and are connected line-to-line on the primary side. Three existing distributed solar photovoltaic (PV) arrays (R1E, R2E, and R3E) are connected to the system through the secondary distribution. Figure 1 provides a single-line diagram of the system, with relevant equipment tags, ratings, and bus numbers shown. The proposed solar PV array (R1N) and battery energy storage system (B1N) are shown at their proposed connection points.

The Old Crow system has an annual average load of approximately 255kW, and a peak load of approximately 555kW.

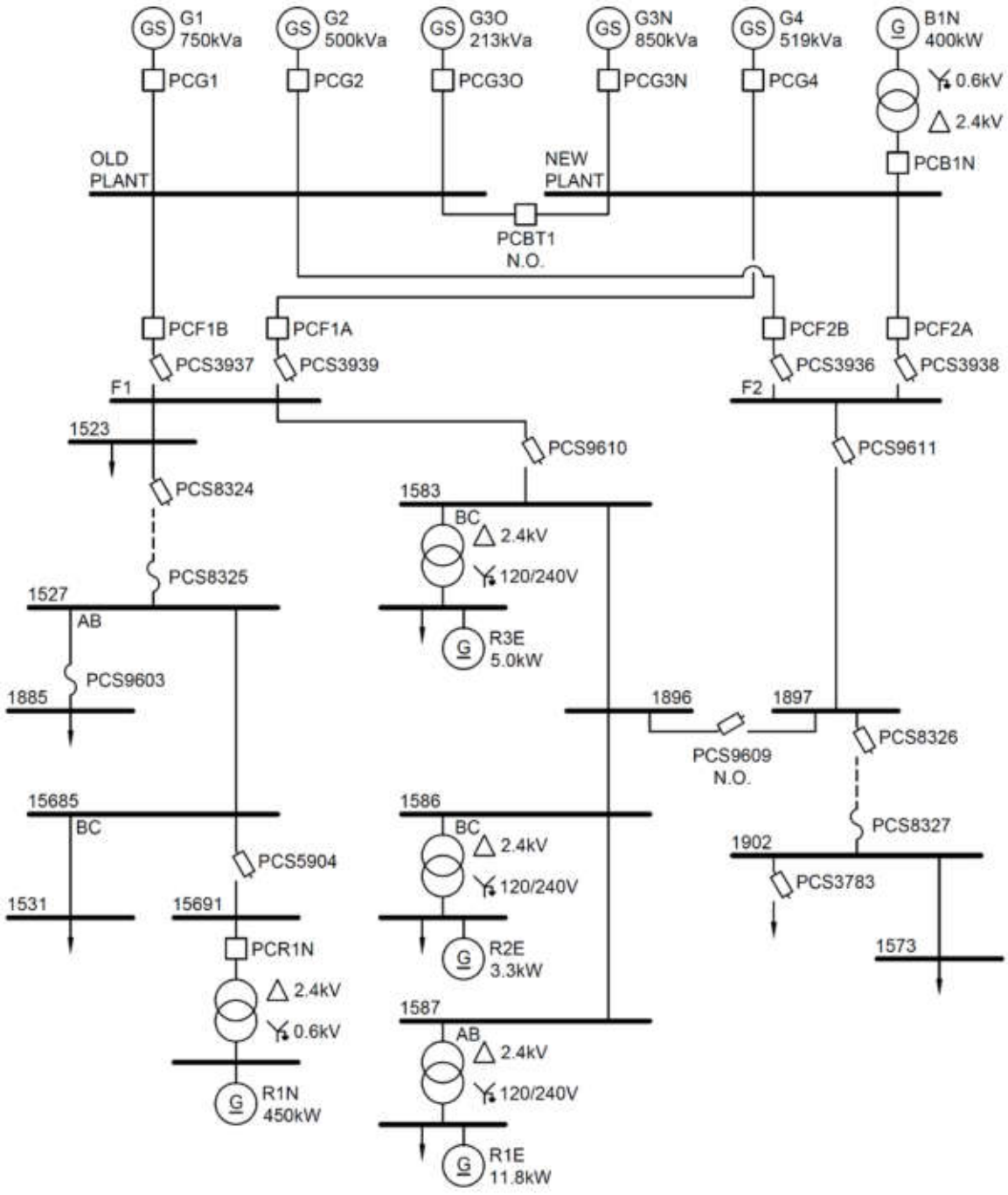

Figure 1: Single Line Diagram of the Old Crow System.

Notes:

1. *Only relevant buses are shown.*
2. *Loads between buses are not shown.*

2 METHODOLOGY

The three major sections of the project, energy balance, protection coordination, and large-disturbance stability, use specific processes and models. The methodology of each experiment is discussed here, and descriptions of the specific models are explored further within the appendix. The methodology explores the general process of the experiment, the parameters of each study and the assumptions made within each model.

This study examines multiple facets of the Old Crow grid with the implementation of a renewable energy source. Depending on the scenario, the experiment analyzes the grid using MATLAB R2017a and Simulink over time spans of a few seconds to months. The results of these processes output estimations of the response of the grid with the examined configurations, and provide a predictive basis to the real response of the system.

2.1 ENERGY BALANCE

The energy analysis examines the steady-state generation and load balance of the Old Crow electrical grid. The analysis uses the IEEE Std. 2030.2-2015, which outlines the recommended method of connecting electrical energy storage to an electric power infrastructure and the different power system simulation models that should be performed to analyze theses parameters.

The steady-state model uses one-minute time steps over a period of a single year. At each time-step the energy balance is calculated to ensure a steady-state real power (P) and reactive power (Q) balance at the fundamental frequency of 60 Hz (if possible), with the resulting system voltages (V) and currents (I) analyzed. It is assumed that all electromagnetic, electrical control and mechanical variances have settled. The simulation uses the power flow model and load flow capabilities of Simulink to capture long term variances and challenges that may arise due to the implementation of the solar PV plant and energy storage system.

This analysis performs a parametric study based on four main aspects:

- Energy balance
- Line loading limits
- Voltage profile
- Battery capacity sizing

Several assumptions are required, which have a direct impact on the accuracy and validity of the results collected from the analysis. The assumptions are as follows:

- The load data provided by ATCO are accurate and representative of a typical year.
- The irradiance, load, power supplied by generator etc. are constant over each time-step
- The system can be accurately modelled in the phasor domain for a balanced network
- A smooth transition between diesel and battery is possible

Furthermore, the following assumptions are made regarding the equipment to be installed:

- A grid following Solar PV system is installed at bus 15691 with a maximum capacity of 450 kW
- A lithium-ion grid forming (i.e., ability to operate in isochronous control mode) energy storage system (ESS) with capacity to meet peak demand of the community (400kW) for one hour (400 kWh) and a round-trip efficiency of 89% is connected at the new plant bus
- There is a single control system for Solar, ESS and diesel generators that has access to system measurements and can control the operating parameters of all generating resources

2.1.1 Energy Balance Data

The data pertaining to the energy balance simulations are provided for both the load and the solar power produced as per the specific plant design. Both the power and load data are provided in ten-minute time-steps. Due to the variability in the energy balance these data are required on a one-minute time-step scale for the simulation. The data have no accompanying standard deviation nor maximum and minimum values; therefore, the data are assumed to be linear between the data points. The linear assumption allows for the addition of data points to provide the required one-minute time step. Figure 2 shows the load and solar power profiles used for the simulation. The load profile is based on the estimated load growth provided by VGG.

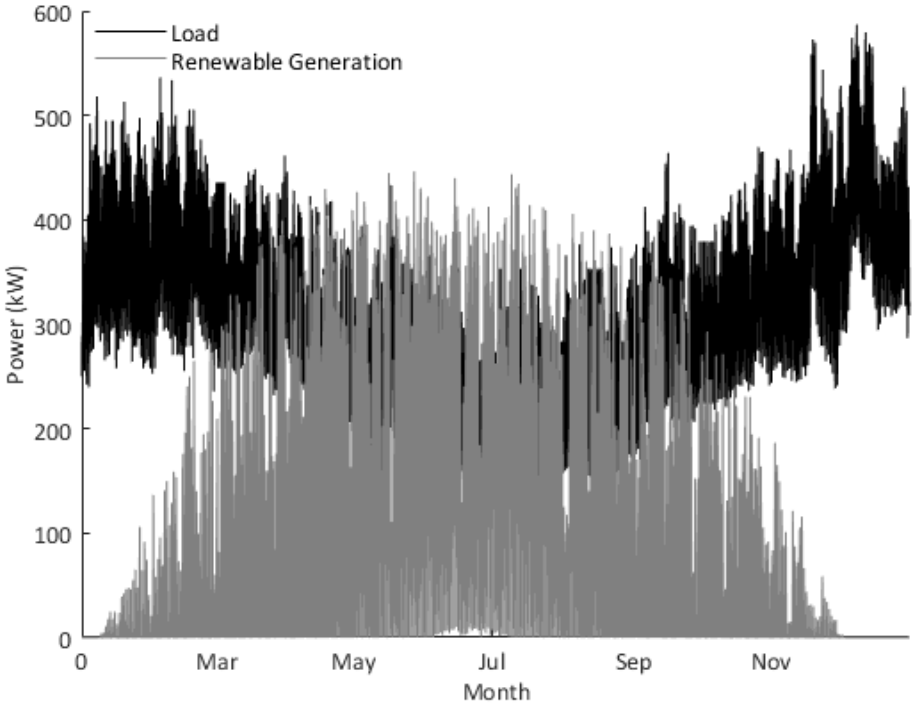

Figure 2: 2020 Load and Solar Power Profile

It is recommended that the simulations be performed with data at a smaller time step should they become available. The linear assumption and the ten-minute time-step data may not pick up the variations within the power of both the solar resource and the Old Crow load that occur on a smaller time scale. The changes within the smaller time frame may affect the results of the battery capacity study, the energy balance, voltage profiling, and the line loading limits.

Furthermore, due to the nature of the model and the use of memory delays, large gradients of load or solar produce errors within the model. Most notably, the battery working with data from the previous time step forces the three-phase source to provide the under or over power at the current time step. Smaller time steps keep this gradient to a minimum, and reduce the reliance on the three-phase source. The errors that arise with the data provided are of the magnitude of the change in required power over the largest of which is approximately 25 kW.

The expected solar power and the load is categorized using the energy analysis initialization code. This allows for both data sets to be fed into the Simulink simulation through one-dimensional look-up tables where the real power of the solar generation and the load are converted to three-phase voltage and current.

2.1.1.1 Line Loading Limits

The line loading study determines whether the system operates within the pre-determined limits of the existing infrastructure with the addition of the solar generation, or energy storage system and the solar generation. The study tests the voltage drop limits and the thermal loading limits of the lines.

The power flow that corresponds to the maximum allowable decrease in voltage magnitude is called the line's voltage drop limit. It is common for voltage to decrease across a line with distance when there isn't reactive power support or voltage regulating devices. This voltage drop is due to loading and losses within the lines from the series impedance. The voltage magnitude is examined throughout the distribution system. The generally accepted limits for allowable voltage drop in transmission lines is set between 5% and 10% of the sending end bus voltage [3]; however, this analysis uses a voltage variation limit of ±5% from nominal system voltage to reflect Canadian standards [4].

The thermal loading limits, given as current ratings, are intended to constrain the temperature attained by the energized conductors. An increase in temperature on transmission lines results in line sag and loss in tensile strength, which can lead to faults or line failures. The thermal rating for summer, winter and emergencies, as retrieved from the transmission line parameters in the CYME model, is shown in Table 16 in Appendix A.4. Within the simulation, a flag is sent to the results from a measurement block that reports an error in the transmission lines when this thermal loading limit is exceeded. Parameters used in the line loading study are provided in Table 1.

Table 1: Variables and descriptors used within line loading limit analysis

Block Parameter	Units	Description	Variable Name
Rated Amperage	A	The rated amperage is dependent on the type of conductor used in the distribution system. These values are determined from the transmission line parameters in the CYME model.	I_rated
Voltage Variation Limit	%	The voltage variation limit is the percent that the voltage in the system can vary from the base voltage. For this system, a value of 1.0pu ± 0.05pu was used.	V_limit
Base Voltage	V	This is the nominal voltage of the system. For Old Crow the base voltage used was 2400V.	BaseVoltage

2.1.1.2 Energy Storage System

The energy storage system in the Simulink model determines the control of the system and is based on the logic proposed by VGG. The storage logic flows between three states: “discharge”, “charge” and “idle”. The logic within each state will be discussed within this section. The logic used within this analysis is as per the request of VGG with additions to recognize errors and increase system stability.

The battery dispatch logic is contained within its own subsystem which can be deployed at the substation, along a feeder or as a focused system [5]. Table 2 provides a description of the battery dispatch logic input and output parameters. The input parameters are required by the logical process, while the output parameters are used within the simulation and for post processing analysis of the results.

The battery dispatch logic, shown in Figure 3, examines the current parameters of the system and controls the battery accordingly. The logical process uses a circular path to switch between discharge, idle and charge states. Each state contains a unique set of controls that dictate the power flow in and out of the battery. The battery switches between these states based on parameters focused around the power available at the time step, the state of charge of the battery, and the time spent outside each state. Further conditions are applied for system stability.

The initial state of the battery is set to idle. In the idle state the battery does not charge or discharge. While the battery is in this state, the PV solar generation may exceed the demand of the community with the generator at minute capacity. In this case, solar power is curtailed (P_spill) and recorded for post processing (it should be noted that the online diesel generator will not be operated below 30% of its rated power output; excess solar energy is curtailed to maintain this condition). The idle state is entered when the state of charge is below the set point for discharge and there is no solar energy

present to induce charging. The state therefore acts as an intermediary between the charge and the discharge states.

The discharge state is entered only when specific conditions are met. If any of the conditions are not met, the battery switches back into the idle state. The conditions are as follows:

1. The state of charge is greater than the user defined maximum. In this analysis, a maximum state of charge of 90% is used to limit full charge discharge cycles, and provide the ability to charge should excess power be made available.
2. The battery cannot enter the discharge state until one hour has elapsed since the last entry into this state. This is designed to prevent the generators from entering rapid start up and shut down cycles. This requirement of the dispatch logic is defined by ATCO with the purpose of extending generator lifespan.
3. The number of discharge cycles per day is less than the user defined maximum. This analysis sets this number to infinity, however the number of charge discharge cycles per day can be controlled using this feature. By controlling the number of cycles the battery undergoes per day the effects of battery aging and loss of capacity can be limited.
4. The load must not be larger than 80% of the battery's rated power output. This is set to encourage stability in the grid, and to prevent the rapid entry and subsequent exit from the discharge state. The use of this condition prevents any potential energy balance failures that may occur when the load cannot be provided by the battery.

While in the discharge state, the battery can charge with the excess solar power generation when the generation exceeds the demand. Should the battery reach a state of charge greater than 99.9% then the excess solar is curtailed. If the demand of the grid exceeds the maximum battery output a flag is output. However, the system can exit from the discharge state if the load exceeds 90% of the rated discharge power. The system waits for two minutes before leaving to represent the time required to bring a generator online.

By implementing these safety factors into the battery logic, the stability of the system is increased. Without them, the load could overdraw power from the battery tipping the energy balance such that a significant system disturbance is likely to occur. This safety factor will reduce the amount of renewable power put into the grid, however the system reliability will be increased.

Egress from the discharge state occurs if one of two conditions is met:

1. The state of charge drops below the user defined minimum state of charge, e.g. $SOC_{min} < 25\%$ for the 400 kWh battery. This minimum is set such that the battery can provide emergency power to the community for 15 minutes at 400 kW. Upon leaving the discharge state a clock is reset to ensure that the battery does not re-enter this state for one hour as mentioned previously. If the battery is within the discharge state for less than one hour, a flag is raised to indicate that the generator start-shutdown cycle is in error.

2. The load exceeds 90% of the rated discharge power of the battery. The system waits for two minutes before exiting the discharge state to represent the time required to bring a generator online.

The charge state is entered when the state of charge of the battery is less than or equal to the user defined maximum, SOCmax <= 90%, and the solar generation is greater than zero, P_solar > 0. While charging, the battery uses all the available solar power generated. The battery will not use diesel energy to charge, it is explicitly limited to charging with the available solar power. If the solar generation is greater than the maximum power input to the battery, the excess solar is sent into the grid while the battery charges at the maximum power rating, P_rated.

The charge state is exited if the solar generation, P_solar, is equal to zero or the state of charge of the battery exceeds the maximum state of charge, SOCmax >= 90%. If these conditions are met the battery switches into the idle state to determine the next state the battery will enter.

Table 2: Inputs and outputs of the battery dispatch logic system with short description of each parameter

Data Type	Parameter	Description	Variable Name	Units
Input	Solar Power	The solar power generation for the specific time step from the data provided to YRC.	P_solar	W
	Power Load	The Old Crow power demand, measured from the voltage and current at feeder 1 and 2	P_load	W
	Minimum Generation	The minimum loading of the diesel generator.	min_diesel	W
	Range of Operation	The maximum and minimum state of charge the battery can reach before discharging and charging respectively.	SOC max/min	%
	Efficiency	The efficiency of the battery. Designated as a charge and discharge, resulting in a round trip efficiency.	eff_	NA
	Rated Power Output	The maximum power battery can provide or consume during charge and discharge.	P_rated	W
	Capacity	The maximum energy storage capacity.	kWh_rated	kWh
	State of Charge	State of charge from the previous time-step.	SOCprev	%

	Cycling Limit	The maximum number of cycles the battery can undergo per day.	countMax	NA
Output	Output Power	The power exiting the battery. During charging this value becomes negative.	P_out	W
	State of Charge	The state of charge of the battery. This data is used to provide the SOCprev input.	SOC	%
	Flag	Count of the number of times that the battery discharges for less than one hour.	size_err	NA
	Solar Curtailment	The amount of solar energy that is spilled to meet energy balance.	P_spill	W

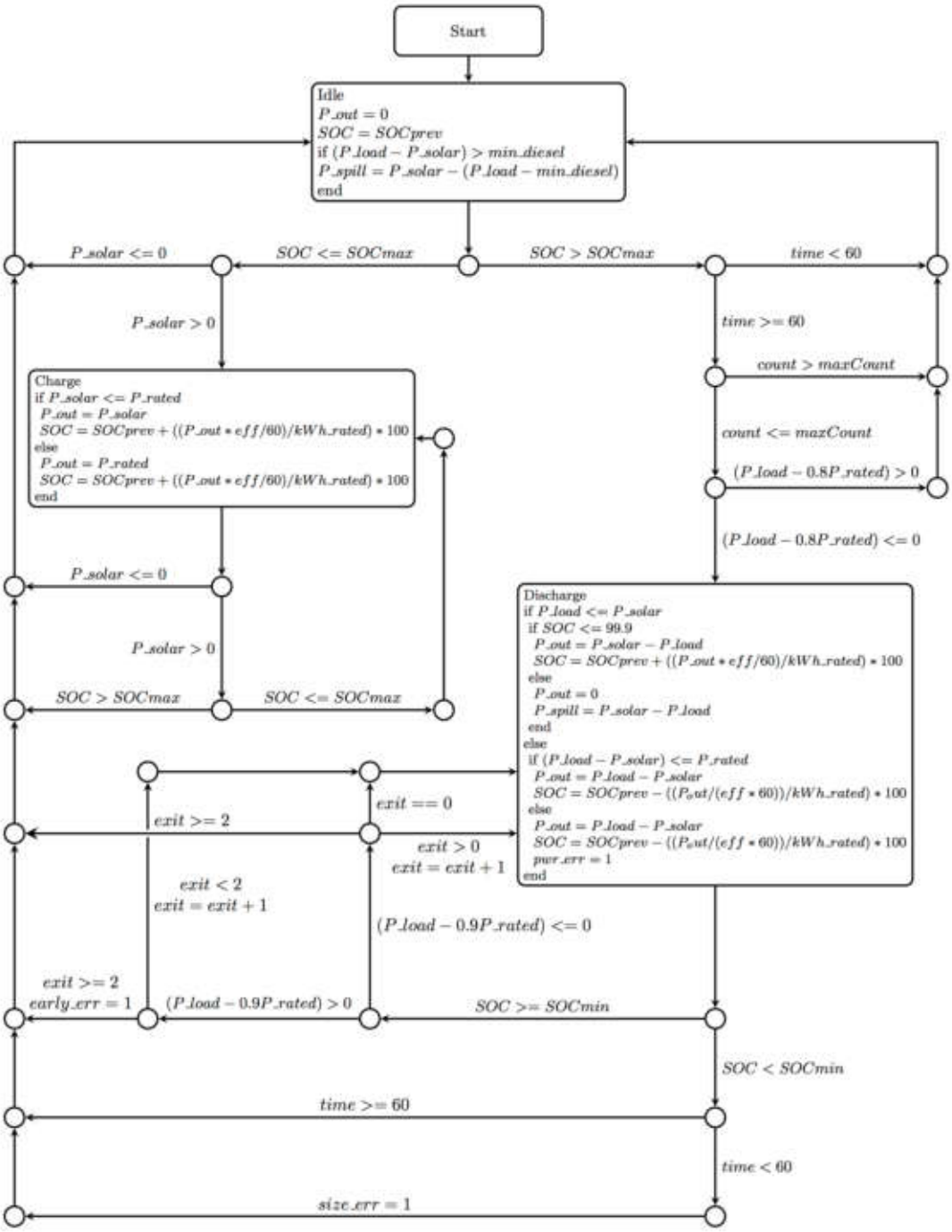

Figure 3: Flowchart depicting battery dispatch logic with error flags

2.1.2 Energy Capacity Capabilities

The energy capacity of the storage system is varied to examine the effect of energy storage capacity on total time of diesel off, charge discharge cycling, the feasibility of going diesel off for 2, 4, 6, 8, 12 and 24 hours at a time, and the total renewable energy input into the grid. This analysis provides the necessary information to find the energy capacity that best suits the demands of the Old Crow grid.

The battery capacities examined are displayed in Table 3. Each battery is set to have a maximum charge capacity of 90% and a minimum capacity that allows for 15 minutes of emergency power to the grid, assumed to be 400 kW. For 15 minutes the minimum energy required is 100 kWh. The minimum state of charge of the battery is set to provide this energy, if emergency capacity is less than 10% the total state of charge the minimum is set to 10%.

The energy capacity capability study uses the same model as the energy balance study, using the data provided for load and expected solar power production over the course of one year. The broad time scale provides a detailed picture of how the energy storage system will react to the grid.

Table 3: Energy storage capacities tested for cycling, total time diesel generator off and feasibility of long term diesel off phases

Capacity	200 kWh	400 kWh	600 kWh	800 kWh	1000 kWh	1200 kWh
Minimum State of Charge	50%	25%	16.67%	12.5%	10%	10%

The six battery capacities are determined based on the power requirements of the grid, and the feasibility of capacity. The power requirements of the Old Crow grid range between approximately 200 and 550 kW. The capacities are chosen to provide this power for a minimum of one hour. Larger capacities introduced to find the feasibility of long term diesel off phases.

At 550 kW, the winter power requirement, the Old Crow grid would require an energy storage system capable of storing approximately 14.4 MWh to provide 24 hours of power. A system of this size is considered infeasible due to financial as well as logistic constraints. Even using the summer months' 200 kW, load a storage of approximately 5.7 MWh would be required, which is also considered to be infeasible for the project. At maximum capacity, 450 kW, the solar plant could fill these batteries in 32 and 12.7 hours respectively. This time frame does not account for the sun setting and assumes peak solar generation for the specified time. For a larger capacity energy storage system to be implemented, a larger solar generation plant is required. Furthermore, the implementation of storage systems of this size is not likely to be economically feasible.

2.2 PROTECTION COORDINATION

The protection system acts to mitigate the impact of abnormal conditions on the power system. It comprises a compilation of protective relays, circuit breakers, solid barrel fuses (i.e. manual switches) and fuses. The purpose of protection systems is to disconnect and isolate faulted parts of the system to protect equipment while reducing the frequency and duration of outages to customers. The protection equipment must first observe and identify an abnormal or dangerous condition, which is a combination of both measurement and logic. It must then automatically apply the appropriate controlling action, such as opening a circuit breaker. Protective devices are intended to operate in a very short time period; they measure quickly, apply the protection logic with any associated delays, and then operate.

Protection controls throughout the system are coordinated to ensure that the appropriate devices operate to disconnect as little of the system as necessary while still isolating the abnormal or dangerous condition. The protection coordination is designed with the purpose of being sufficiently sensitive to detect and trip in a faulted scenario (i.e., eliminate non-detection zones), but remain dormant in normal and transient operating conditions that will not affect system integrity nor have negative effects (i.e., eliminate nuisance tripping). The protection coordination study is performed to ensure that only the appropriate protection devices operate when they are supposed to do so, and within the standard operation time limits.

The classical methodology to perform a protection coordination study is to calculate the fault current at each point in the system; however, an alternative method is used here. The analysis of protection coordination is conducted on a case by case basis, where each case, or scenario, requires a unique simulation and analysis. The maximum fault current and the clearing time for each relay or fuse that trips is recorded for each simulation. The main concerns are a potential increase in maximum fault current, non-detection zones caused by fault shadowing, nuisance tripping, and reverse power flow. The maximum fault current and clearing times are used to assess whether the protection system correctly operates for each fault applied to the system with the newly installed resources. It is important to note that the analysis keeps the existing equipment, logic, and coordination that is currently implemented. The advantage to using a case by case assessment with full simulations, is that the dynamics of multiple protective devices can also be assessed.

A discussion of the generation (diesel-electric generator, solar PV array), line, load, and protective relay models and parameters is provided in Appendix B, and are modelled based on the existing devices and settings. It is important to note that the generation models of existing equipment have not yet been validated due to an unavailability of applicable system data.

Fault Type

Shunt faults were assumed to be line-line (LL) or three-phase (3ϕ). Single-line-ground (SLG), double-line-ground (2LG), and triple-line-ground (3LG) faults were not simulated. Ground faults are not

simulated because the system is an ungrounded delta system. In an ungrounded delta system, a SLG fault causes negligible ground currents since there is no other connection to ground that would create a closed path for the ground current to flow (it is common practice to assume that zero sequence fault currents are non-existent in an ungrounded system). If two lines fault to ground (i.e. a 2LG fault), the result is a LL fault. Faults with a low fault impedance (i.e. LL, 3ϕ, 2LG, 3LG) were assumed to have an impedance of $1\times10^{-7}\Omega$. Additionally, all faults are assumed to be persistent faults.

Series faults were not explicitly simulated. The exception to this was the simulation of one line open (1LO) or two line open (2LO) faults that occurred as a result of blown fuses caused by a prior shunt fault.

Fault Location

Faults were simulated at buses 1531, 15691, 1885, 1902, F1, and F2. Figure 1 shows the locations of each fault within the system and with respect to each protective device. Three-phase sections were simulated with LL and 3ϕ faults. Two-phase sections of the system were simulated with LL faults only.

Note that faults were not simulated at every location in the system, due to the inherently time intensive nature of the simulations performed. However, the fault locations that were simulated provides a decent representation of faults that can occur throughout the system.

2.2.1 Generator G2

One set of scenarios was run with Generator G2 and the renewable energy systems R1N, R1E, R2E, and R3E connected. All other sources (G3O, G3N, G4, and B1N) were disconnected. R1N was connected at bus 15691. Each scenario is comprised of a parameter set and a test case. A single parameter set was used, as follows:

1. The system load (Psys) was held constant at 400kW. 400kW is the maximum active power (under continuous operation) of G2. All loads were assumed to have a constant load impedance.
2. The capacity (Pn) of R1N was held constant at 260kW. 260kW is the difference between the maximum active power (under continuous operation) and the minimum active power (assuming a 30% loading) of G2, minus the existing PV capacity already installed on the system.

The parameter set was run for each of the faults, where each fault is a test case. The result was a set of 11 scenarios.

2.2.2 Generator G4

One set of scenarios was run with Generator G4 and the renewable energy systems R1N, R1E, R2E, and R3E connected. All other sources (G2, G3O, G3N, and B1N) were disconnected. R1N was

connected at bus 15691. Each scenario is comprised of a parameter set and a test case. A single parameter set was used, as follows:

1. The system load (Psys) was held constant at 415kW. 415kW is the maximum active power (under continuous operation) of G4. All loads were assumed to have a constant load impedance.
2. The capacity (Pn) of R1N was held constant at 270kW. 270kW is the difference between the maximum active power (under continuous operation) and the minimum active power (assuming a 30% loading) of G4, minus the existing PV capacity already installed on the system.

The parameter set was run for each of the faults, where each fault is a test case. The result was a set of 11 scenarios.

2.2.3 Battery B1N

One set of scenarios was run with Battery B1N and the renewable energy systems R1N, R1E, R2E, and R3E connected. All other sources (G2, G3O, G3N, and G4) were disconnected. R1N was connected at bus 15691. Each scenario is comprised of a parameter set and a test case. A single parameter set was used, as follows:

1. The system load (Psys) was held constant at 420.1kW. 420.1kW is the set capacity of B1N + R1E + R2E + R3E. All loads were assumed to have a constant load impedance.
2. The capacity (Pn) of R1N was held constant at 400kW. 400kW is the maximum active power of B1N.

The parameter set was run for each of the faults, where each fault is a test case. The result was a set of 11 scenarios.

2.3 LARGE-DISTURBANCE STABILITY

Large-disturbance stability concerns the ability of the power system, when subjected to large disturbances, to maintain stability. More formally, power system stability can be defined as “the ability of an electric power system, for a given initial operating condition, to regain a state of operating equilibrium after being subjected to a physical disturbance, with most system variables bounded so that practically the entire system remains intact” [6]. Power system stability is classified according to the main system variable in which instability is observed, the size of the disturbance, and the time span which must be considered. There are three main system variables in which instability may be observed: frequency, voltage, and rotor-angle. The classical concern of large-disturbance stability is that of rotor-angle stability (often called transient stability). However, in remote power systems, the concern is largely frequency stability and voltage stability. Due to the scale of remote power systems, the time frame of concern is restricted to the short term.

The analysis of large-disturbance stability is conducted on a case by case basis, where each case, or scenario, requires a unique simulation and analysis. Monte-Carlo Filtering is used to determine whether each simulation is behavioural or non-behavioural, wherein non-behaviour is ascribed to exceeding upper or lower thresholds on frequency, voltage, or rotor-angle. The threshold must be exceeded for 4ms (~1/4cycle), which prevents erroneous flagging of non-behaviour caused by spikes in variables during discontinuities in the simulation (i.e., the inception of the large disturbance). An inner and outer set of thresholds is considered for both frequency and voltage. The inner thresholds are the desired conditions under normal operation, whereas the outer thresholds are determined from the protective relay settings. The thresholds are provided in Table 4. The applicable thresholds are checked for each synchronous generator (i.e. diesel-electric generator), renewable energy system (i.e. battery energy storage system, and solar PV array), and bus in the system.

Table 4: System Variable Threshold Boundaries for Large-Disturbance Stability

Variable	Bounds	
	Inner	*Outer*
Frequency	59.3Hz ≤ f ≤ 60.5Hz,	58.0Hz ≤ f ≤ 66.0Hz
Voltage	0.95pu ≤ V ≤ 1.04pu,	0.90pu ≤ V ≤ 1.10pu
Rotor-Angle		0.00° ≤ δ ≤ 90.0°

A discussion of the generation (diesel-electric generator, solar PV array, and battery energy storage system), line, and load models is provided in Appendix B. Protective relay models are not included in the large-disturbance simulations. It is important to note that the generation models of existing equipment have not yet been validated due an unavailability of applicable system data. Validation of system models is important, as it ensures that models accurately reproduce real system disturbances.

Three distinct groups of case studies were conducted, which are discussed in the following subsections.

2.3.1 Generator G2 Scenarios

Three sets of scenarios were run with Generator G2 and the renewable energy systems R1N (the proposed solar PV array), R1E (the existing 11.8kW solar PV array), R2E (the existing 3.3kW solar PV array), and R3E (the existing 5.0kW solar PV array) connected. All other diesel generators (G3O, G3N, and G4) and the battery energy storage system (B1N) were disconnected. The first set of scenarios was run with the R1N connected at bus 15691. The second set scenarios were run with R1N connected at the new plant bus.

Each scenario is comprised of a parameter set and a test case. A total of 12 parameter sets were generated from the parameter distributions using a Latin Hypercube sampling method. The parameter distributions are as follows:

1. The system load (Psys) was held constant at 400kW. 400kW is the maximum active power (under continuous operation) of G2. All loads were assumed to have a constant load impedance.
2. The capacity (Pn) of R1N was varied from 10kW to 260kW in a uniform distribution. 260kW is the difference between the maximum active power (under continuous operation) and the minimum active power (assuming a 30% loading) of G2, minus the existing PV capacity already installed on the system.
3. The maximum rate of change of active power (dPmax) of R1N was varied from 0.2pu/s to 1pu/s (90% of the cumulative distribution function (CDF)) to 10000 pu/s (10% of the CDF) in a piecewise linear distribution. This parameter limits the rate at which R1N connects to the system.

The 12 parameter sets were run for each of the three following test cases:

1. Instantaneous disconnection of R1N at 0.1s into the scenario simulation.
2. Loss of full capacity of R1N, over 5s, at 0.1s into the scenario simulation.
3. Connection of R1N at 0.1s into the scenario simulation.

The result is a set of 36 scenarios, for a total of 72 scenarios.

2.3.2 Generator G4 Scenarios

Three sets of scenarios were run with Generator G4 and the renewable energy systems R1N, R1E, R2E, and R3E connected. All other diesel generators (G2, G3O, and G3N) and the battery energy storage system (B1N) were disconnected. The first set of scenarios was run with the R1N connected at bus 15691. The second set of scenarios were run with R1N connected at the new plant bus.

Each scenario is comprised of a parameter set and a test case. A total of 12 parameter sets were generated from the parameter distributions using a Latin Hypercube sampling method. The parameter distributions are as follows:

1. The system load (Psys) was held constant at 415kW. 415kW is the maximum active power (under continuous operation) of G4. All loads were assumed to have a constant load impedance.
2. The capacity (Pn) of R1N was varied from 10kW to 270kW in a uniform distribution. 270kW is the difference between the maximum active power (under continuous operation) and the minimum active power (assuming a 30% loading) of G4, minus the existing PV capacity already installed on the system.
3. The maximum rate of change of active power (dPmax) of R1N was varied from 0.2pu/s to 1pu/s (90% of the CDF) to 10000 pu/s (10% of the CDF) in a piecewise linear distribution. This parameter limits the rate at which R1N connects to the system.

The 12 parameter sets were run for each of the three following test cases:

1. Instantaneous disconnection of R1N at 0.1s into the scenario simulation.
2. Loss of full capacity of R1N, over 5s, at 0.1s into the scenario simulation.
3. Connection of R1N at 0.1s into the scenario simulation.

The result is a set of 36 scenarios, for a total of 72 scenarios.

2.3.3 Battery B1N Scenarios

Four scenarios were run with battery energy storage system B1N and the renewable energy systems R1N, R1E, R2E, and R3E connected. All other diesel generators (G2, G3O, G3N, and G4) were disconnected. The first set of scenarios was run with R1N connected at bus 15691. The second set of scenarios were run with R1N connected at the new plant bus.

Each scenario is comprised of a parameter set and a test case. One parameter set was used, with the following:

1. The battery energy storage system B1N was connected at the new plant bus. The capacity of B1N was set to 400kW, and operated and controlled-frequency mode.
2. The capacity of R1N was set to 400kW.
3. The total system load was set at 400kW. All loads were assumed to have a constant load impedance.

The parameter set was run for each of the two following test cases:

1. Instantaneous disconnection of R1N at 0.1s into the scenario simulation.
2. Loss of full capacity of R1N, over 5s, at 0.1s into the scenario simulation.

The result is a set of 2 scenarios, for a total of 4 scenarios.

An additional, 5th scenario was run with battery energy storage system B1N connected with the same simulation parameters as the G4 scenario with the largest R1N capacity. The following parameter set was used:

1. The capacity of B1N was set to 400kW, and operated in controlled-current mode.
2. In the REPC_A model of B1N, the frequency down and up regulation gains were set to 30pu/pu, with a frequency error deadband of 0.0117pu to -0.0083pu (a frequency deadband of 59.3Hz to 60.5Hz). These settings are intended to allow B1N to provide frequency support for transient events.

3 RESULTS

The following section includes the results and analyses for energy balance, protection coordination, large-disturbance stability, and battery capacity sizing.

3.1 ENERGY BALANCE

The energy balance examines the impacts of the assumed solar panel and energy storage system with the rest of the system remaining "as is". The load and solar data are analyzed to assess the validity of these installations. The results for expected solar production and consumption are shown in Sections 3.1.1 and 3.1.2. This provides the basis for an analysis on the potential impacts on the system with regards to power flow and the expected voltage variation throughout a full year on the Old Crow grid.

To form a complete analysis, various times throughout the year are assessed. A full year of data are used to consider a variety of potential issues in the system. The results shown within this section demonstrate the operation of the planned PV plant, the diesel generator, the existing PV arrays, the energy storage system, and the distributed loads. Each time interval presents potential energy balance issues due to the implementation of solar and energy storage system.

Solar Spill: Should the solar production exceed the demand of the grid when the battery is at maximum capacity in discharge and the diesel generator is off, the excess solar power is spilled and quantified. Furthermore, should the PV production exceed the load when the diesel is at 10% above the minimum capacity (120 kW) the excess solar is spilled and quantified.

Under Time of Diesel Off: If the battery energy capacity is insufficient to provide one hour power to the grid, a flag is output marking this event. The number of times this occurs is added up to show the total number of occurrences within a year.

Early Exit: If the battery approaches 90% of its maximum power rating it will initiate an exit sequence taking a total of three minutes. This time is representative of the time required to bring a diesel generator online. If this exit sequence is entered a flag is raised and the total number summed at the end of the simulation.

Under Power Rating: If the battery cannot supply enough power to supply the grid the discharge state is left and the diesel generator is brought back online. This event is flagged and recorded.

Negative Loading of Diesel Generators: Due to the reactive nature of the solar array and the battery in the models, occasionally these systems do not react fast enough to changes in the system load. In these cases, the diesel generator model picks up these variations since it is modelled as a three-phase voltage source/slack bus. This can result in negative loading of the generator, and the total negative energy picked up by the generator is recorded and documented. The slow reaction of the PV and battery models is under review and several solutions have been proposed.

3.1.1 Voltage Profile

The voltage profile from the generation plant to the solar plant and the generation plant to bus 1573, is averaged over every quarter of the examined year. The voltage profile to the solar plant shows a voltage rise as the voltage is controlled at the generation plant. The other path is the longest run of transmission line, which shows a drastic voltage drop along its length.

Figure 4 shows the voltage profile from the generation plant to the end of the transmission line at bus 1573. The lines depict average voltage through each quarter of the year as well as the maximum and minimum of that quarter. It can be observed that the voltage in extreme cases can fall below 0.88 pu. Figure 4 also shows the voltage on line A of the three-phase system, however due to the model being built as a balanced system lines B and C have identical profiles.

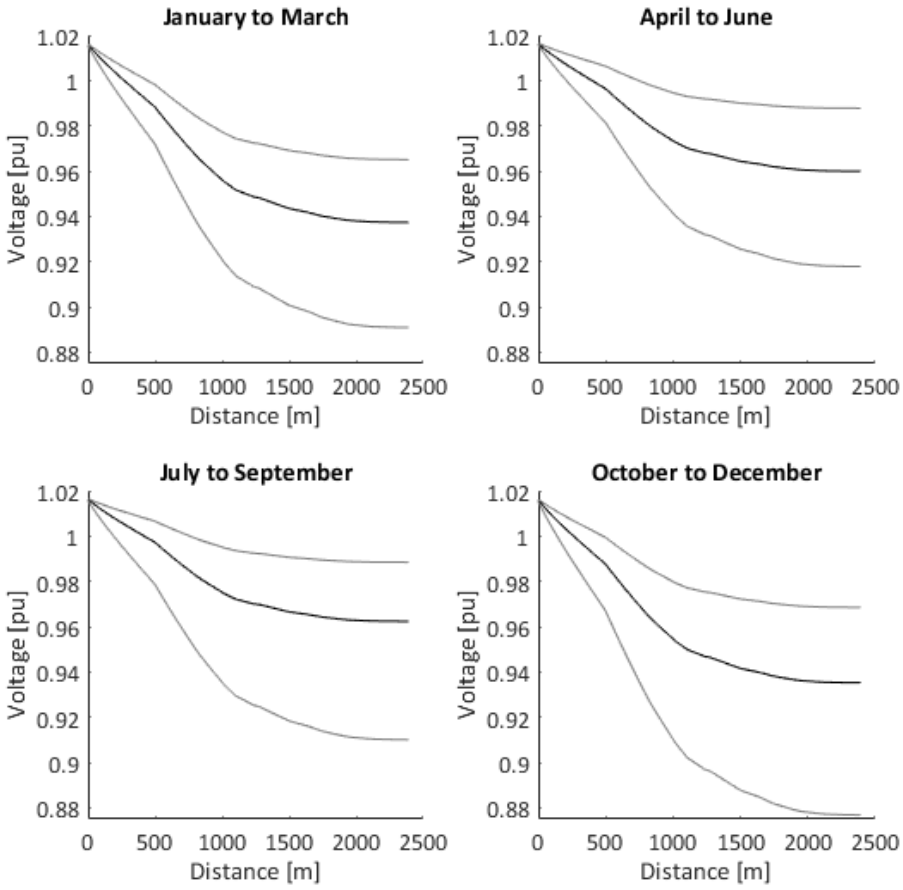

Figure 4: Voltage Profile From the Point of Generation to Bus 1573

Alternatively, the transmission line path from the generation station to the PV plant for line A, Figure 5, shows opposite trends. The voltage profile increases from the generation station to the PV plant

due to the voltage regulation occurring at the generation bus. In some extreme cases this voltage can rise as high 1.09 pu.

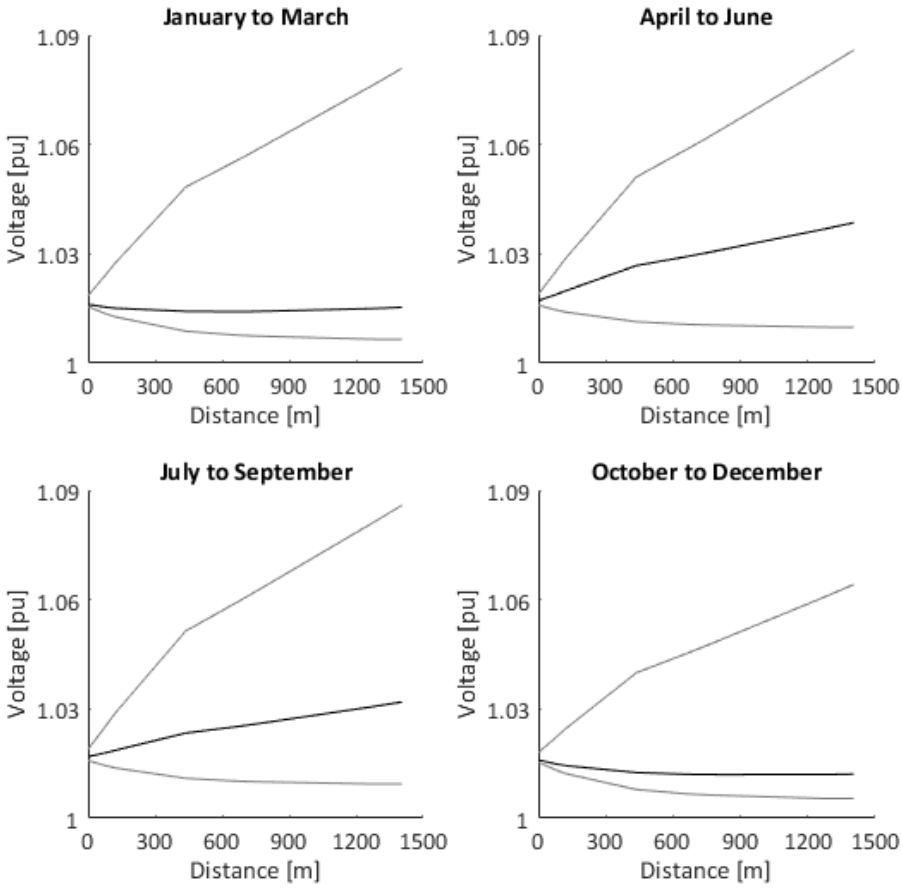

Figure 5: Voltage Profile From Point of Generation to PV Plant at Bus 15691

The transmission lines are given maximum and minimum voltage limits, which are set to ±5% in this simulation. The end of line and the point at which these limits are crossed are expressed in Figure 6 and Figure 7. Where the voltage at each time is shown in black, while the limit is expressed with a grey dashed line.

From the generation plant to bus 1573, the voltage is seen to drop below the limitations set forward in this simulation. The voltage at the end of the line and at the first bus to experience under-voltages is shown in Figure 6. The under-voltages appear to be in agreement with the voltage profiles provided by ATCO from the CYME model. It can be noted that the minimums are only exceeded during the winter months when load demand is high and solar production is low.

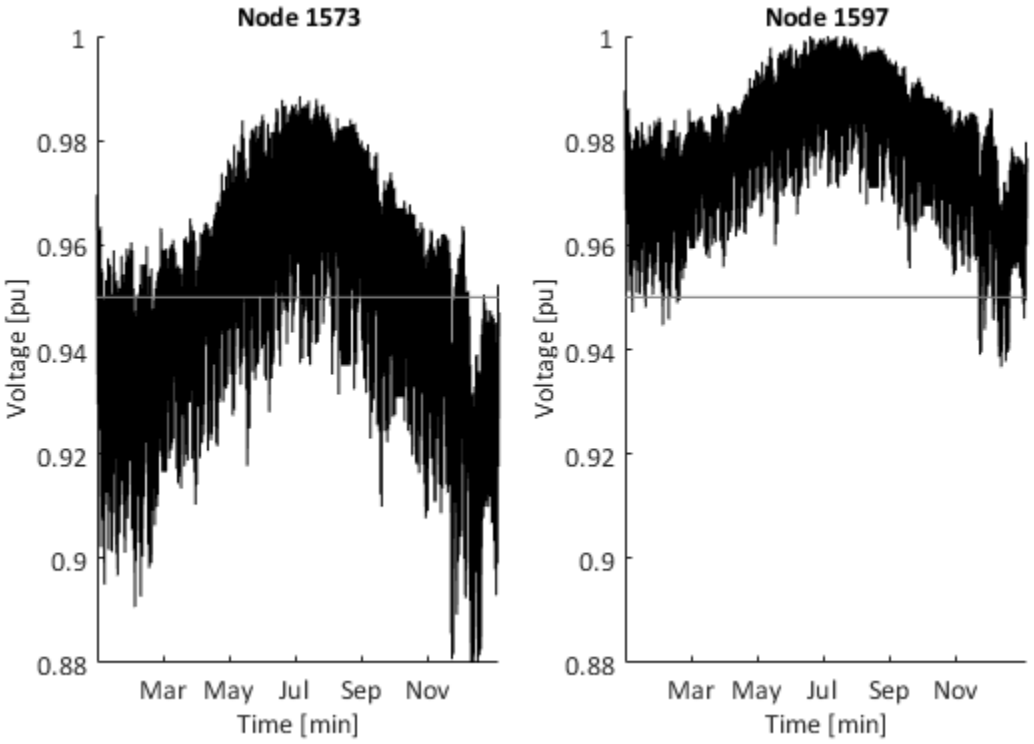

Figure 6: Voltage at Select Buses Experiencing Under-Voltage

Note: Bus 15709 is the First Bus to Experience Under-Voltage on the Transmission Path Between The New Plant Bus and Bus 1597 Which Is At the End of the Transmission Line.

From the generation plant to the PV plant the voltage is seen to rise. The voltage at the end of the line and at the first bus from the generation plant to experience over-voltages are shown in Figure 7. The voltage rise at bus 15691 can be seen to be as large as ~0.06pu over the threshold of 1.05pu. The voltage profile follows a similar shape to the irradiance or PV power output curve, and rises above the common threshold of 1.1pu that is used for over-voltage protection. Note that this simulation used a unity power factor setting at the PV plant. The PV plant can be controlled to use a constant power factor so as to consume reactive power in proportion to generation of active power, which should reduce the magnitude of the voltage rise.

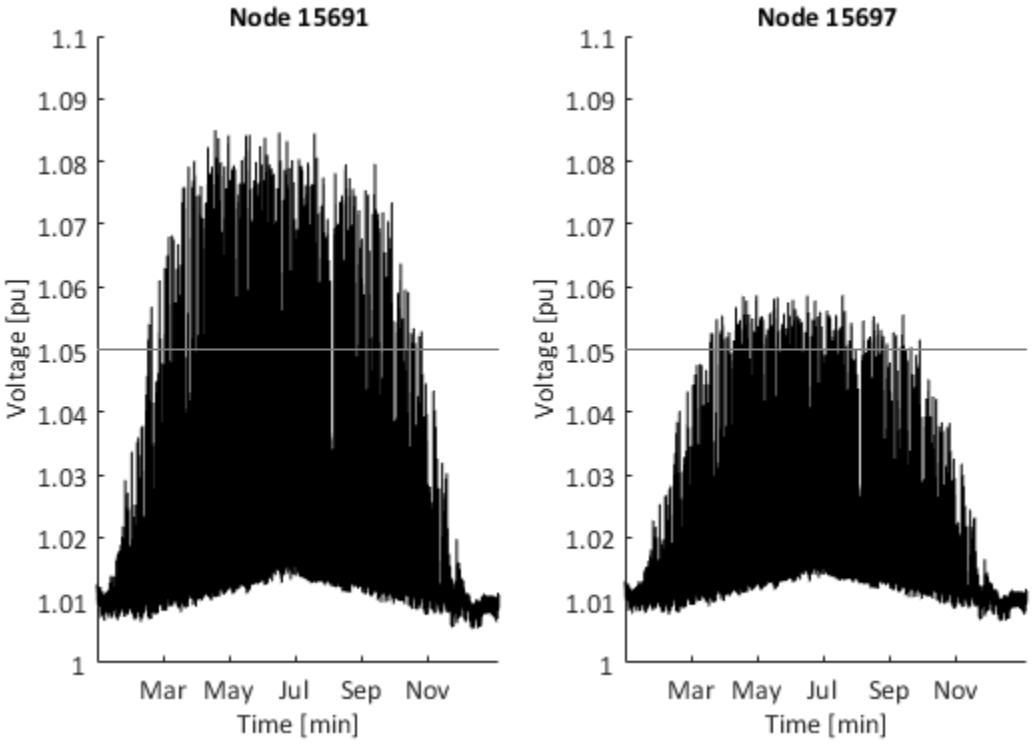

Figure 7: Voltage at Select Buses Experiencing Over-Voltage

Note: Bus 1890 is the first bus to experience over-voltage on the transmission path between the new plant bus and bus 15691 which is at the proposed solar PV array.

The voltage profile along two paths, from the generation bus to the PV pant and from the bus to the northern most point of the grid, both exceed the voltage limits set forth by the simulation. The voltage profile to bus 1573 is expected to drop as that is observed from past models. The voltage rise to the PV plant is expected due to the large input of power to this line. However, the model provides quantitative predictive values to what this voltage rise will be.

3.1.2 Line Loading Limits

Analysis over one year with the PV plant connected at bus 15691 shows that at no point does the current exceed the thermal loading limits for the estimated 2020 load data. The observations made from these results show that the existing transmission lines will not encounter over currents.

3.1.3 Battery Capacity Sizing

Each capacity produced from this estimation is examined within an energy balance model described in the energy balance section of this report. Each battery is tested throughout the entirety of one year beginning January 1st and ending December 31st. The battery is set such that the minimum state of

charge can provide 15 minutes of emergency backup power or is 10% of the total capacity, whichever is higher. The initial state of charge of each battery is set to 90%.

The simulated load is set to the estimated 2020 load as provided to the study. The PV plant power profile is the profile provided to the study based on 450 kW of solar facing east and west. The battery discharge and charge power rating is set to $400\ \mathrm{kW}$, and held constant through all simulations. Figure 8, shows the number of times the diesel generator is off for the allotted times.

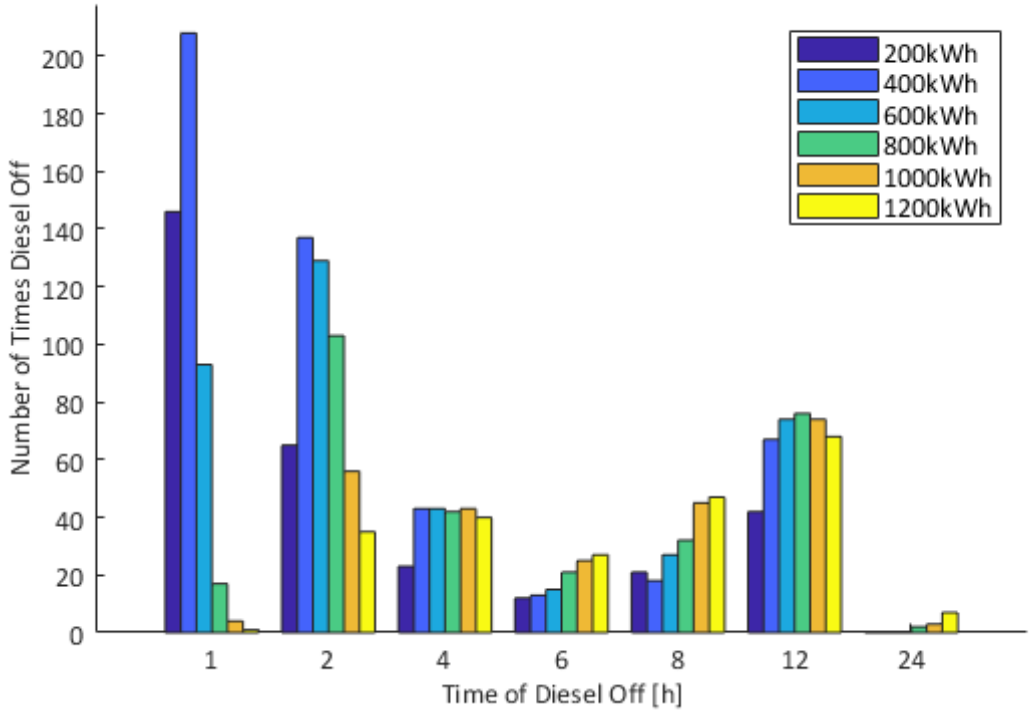

Figure 8: Number of Diesel Off Cycles for the Allotted 1, 2, 4, 6, 8, 12 and 24 Hours Per Battery Capacity.

The results shown in Figure 8 show the smaller battery sizes more capable of discharging for the lower allotted times, and the larger capacities the longer time spans. Less than one hour is not shown because it makes the results illegible due to a very high number of less than one hour discharges from the 200kWh battery (see Table 5, as discussed later). This is a consequence of the battery not containing enough stored energy to meet its discharge capacity under the discharge logic. Most notably the 600 kWh battery can discharge 129 times over 2 hours, nearly 3 times a day. An interesting trend to the data is that every size produces more discharge times at 8 and 12 hours than at 6 hours.

Examining the total number of diesel off hours shows that the 200 kWh capacity has the lowest number of hours of diesel off, approximately 86 days in total. With the increase in energy storage

capacity the number of hours of diesel off increases to approximately 104 days. Indicating that larger sizes are a better solution for increasing the diesel off hours.

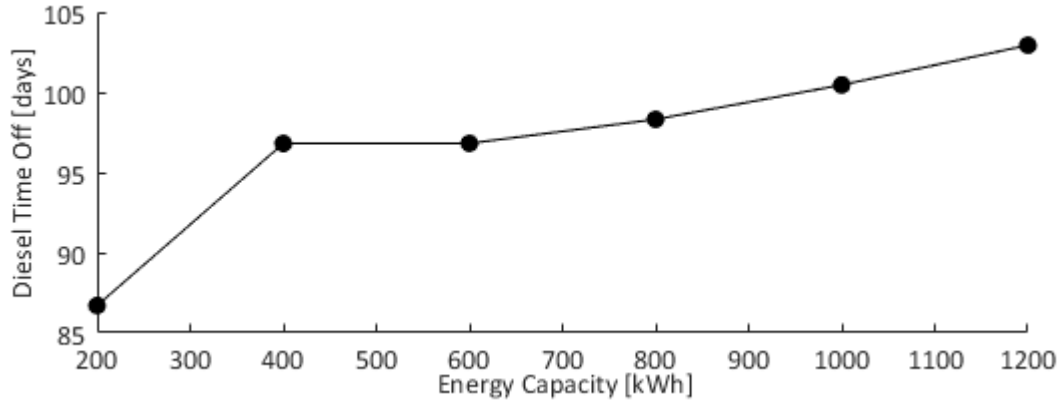

Figure 9: Total Amount of Time of Diesel Off Over a Full Year

Despite the lower number of diesel hours off the smaller battery capacity also performs more cycles. The lower capacities of 200 kWh and 400 kWh are incapable of meeting the minimum diesel off time of 1 hour. Furthermore, the lower energy capacity of the system increases the number of charge discharge cycles of the system.

High charge discharge cycling of batteries may decrease the life span of the battery. Examining the number of discharges that occur throughout the year provides an understanding of whether the energy capacity of the battery is indicative of high cycling levels. Figure 10 shows the number of partial discharges the battery experiences throughout the year. As expected, the smaller capacities experience higher levels of cycling.

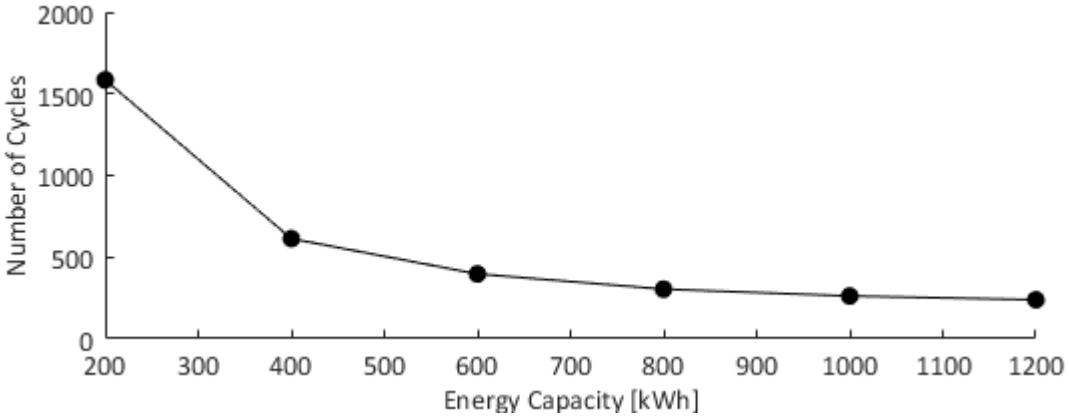

Figure 10: The Total Number of Partial Charge Discharge Cycles with Respect to the Capacity of the Battery Throughout the Year

However, due to the limitations placed on each battery for the purpose of emergency power, not every charge discharge cycle is a complete one. Figure 11 shows the total number of full charge discharge cycles of the energy storage system relative to a complete 0% to 100% state of charge. Each of the energy capacities examined is seen to reduce the total number of cycles experienced.

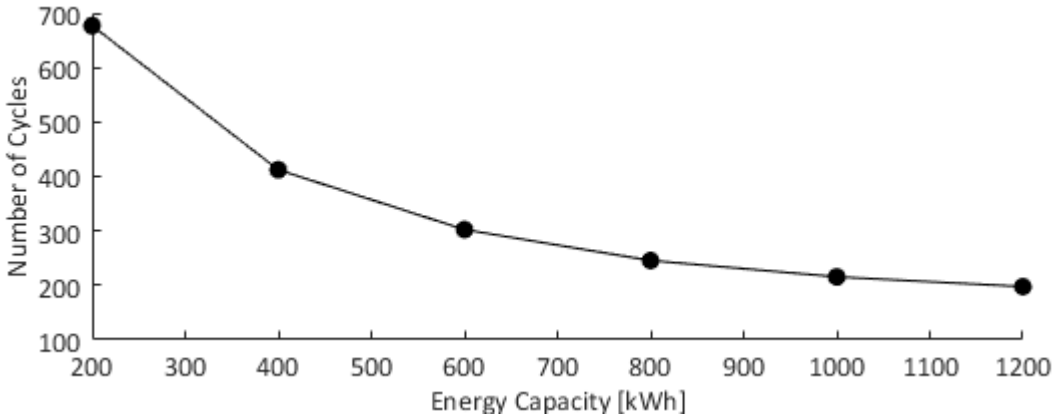

Figure 11: The Total Number of Full Cycles of Each Battery Energy Capacity

Cycling a battery through charging and discharging speeds up the aging process. Saft, a battery manufacturer, states that lithium ion batteries decay to approximately 80% their original capacity within 6000 cycles, and estimate the end of life at 70% the original capacity [7]. Saft also states that with a charge cycle ranging from 80% to 10%, a total of 10,000 cycles can be achieved before the end of life is met. Using these estimates, the 200 kWh battery is estimated to reach 6000 cycles after 8.78 years and provide 14.65 years of service before reaching 10,000 cycles on the Old Crow grid under this logic scheme, assuming no other degradation effects are experienced. While the 1200 kWh battery can be estimated to have a life span of 50.7 years using these limitations. The estimated service lives provided here do not account for battery degradation.

As mentioned earlier, other parameters exist that limits the capacity of the battery used, such as the ability of the energy system to provide one hour of power, provide sufficient power to the system, and reduce the amount of solar power spilled to maintain energy balance. Table 5 shows that smaller capacities are more likely to be incapable of providing the necessary power to remain diesel-off for one hour. It is noted that the storage systems of larger capacities are more likely to exit the discharge state before its state of charge reaches the lower limit due to the load exceeding the battery's dispatch threshold setting.

Examining this information shows that a medium or larger sized battery capacity is better suited to provide diesel-off for more than one hour at a time while decreasing the cycling experienced by the battery. The one hour off limitation set forth by ATCO is an important consideration, therefore it should be noted that the 200 kWh and 400 kWh are likely undersized for the Old Crow grid using the provided energy management system logic.

Table 5: Parameters With Regards to Sizing and Energy Balance

Capacity	Under 1 hour	Early Exit from Discharge
200 kWh	1136	4
400 kWh	51	22
600 kWh	0	17
800 kWh	0	25
1000 kWh	0	25
1200 kWh	0	36

Furthermore, the early exit from the discharge state indicates the number of times the demand of the grid began to approach the limit of the battery's rated power output. The rated power output used in these simulations is set to 400 kW. Increasing this value will decrease the number of early exits, however allowing the battery to input more power into the grid may increase the number of discharges that are under one hour in length. This is a relationship that should be examined further.

The amount of energy that is curtailed in order maintain energy balance is also quantified within the simulations. It is shown that increasing the energy capacity of the battery decreases the amount of curtailed energy, Figure 12. This indicates that a larger energy capacity is better suited to the old crow grid under the current dispatch logic.

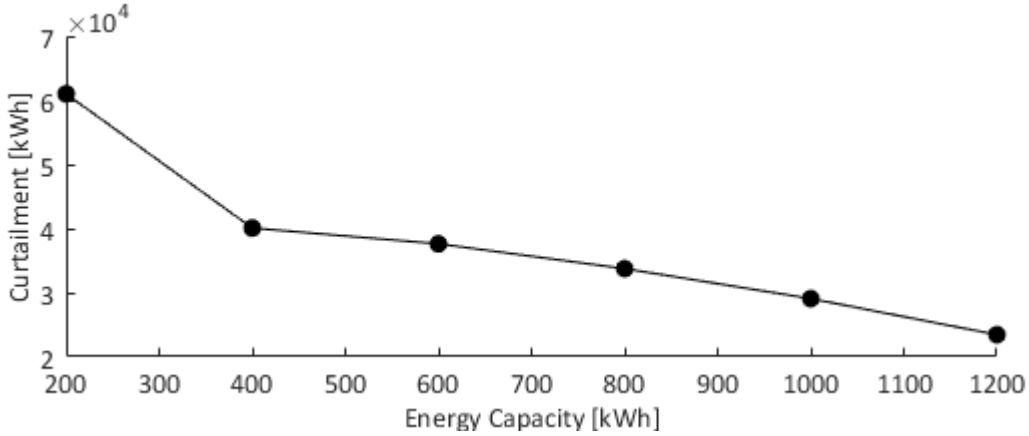

Figure 12: Total Energy Curtailed Throughout One Year Per a Range of Battery Energy Capacities

Finally, a flag was raised in the simulations for times when the power required from the battery is greater than the maximum rated power. Within this analysis, this flag was never raised for any of the examined sizes. This is likely due to the dispatch logic preventing the battery from entering the discharge state when the demand is high, as well as the early exit option within the logic allowing the battery to exit the discharge state before the demand reaches the limit of the battery.

3.2 PROTECTION COORDINATION

The results of the protection coordination studies are outlined in the following subsections.

3.2.1 Generator G2 Scenarios

The results of the G2 scenarios are provided in Table 6 and Table 7. It is clear that the instantaneous time delays applied to device no. 27 (under-voltage) and 59 (over-voltage) on the feeder relays (PCF1B and PCF2B) caused the relays to trip in every scenario, even those where it is desirable for one or more of the fuses (PCS8325, PCS8327, and PCS9603) to blow. This indicates a conflict in the coordination of the fuses and the feeder relays; however, no scenario with a fault resulted in a no-trip condition. It is recommended that the feeder under- and over-voltage relays be set appropriately so as to coordinate the relays with the fuses. From comparison of Table 6 and Table 7 it can be observed that:

1. R1N has a small impact (<20%) on the observed maximum current
2. Feeder relays have comparable clearing times.

Table 6: Results for G2 Fault Scenarios with Existing PV Only

Scenario	Fault Location	Fault Type	Observed Maximum Current (A)	Device: Clearing Time @ Trip Time (Device No.)
1	NA	No Fault	88	
2	1531	LL	521	PCF1B: 0.0010s @ 0.1083s (27) PCF2B: 0.0010s @ 0.1083s (27)
3	15691	LL	511	PCF1B: 0.0010s @ 0.1065s (27) PCF2B: 0.0010s @ 0.1065s (27)
4	15691	3L	571	PCF1B: 0.0010s @ 0.1067s (27) PCF2B: 0.0010s @ 0.1067s (27)
5	1885	LL	670	PCF1B: 0.0010s @ 0.1061s (27) PCF2B: 0.0010s @ 0.1061s (27)
6	1902	LL	332	PCF1B: 0.0010s @ 0.1100s (59) PCF2B: 0.0010s @ 0.1100s (59)
7	1902	3L	437	PCF1B: 0.0013s @ 0.1097s (27) PCF2B: 0.0013s @ 0.1097s (27)
8	F1A	LL	900	PCF1B: 0.0010s @ 0.1060s (27) PCF2B: 0.0010s @ 0.1060s (27)
9	F1A	3L	1057	PCF1B: 0.0010s @ 0.1042s (27)

				PCF2B: 0.0010s @ 0.1042s (27)
10	F2A	LL	901	PCF1B: 0.0010s @ 0.1060s (27) PCF2B: 0.0010s @ 0.1060s (27)
11	F2A	3L	1057	PCF1B: 0.0010s @ 0.1042s (27) PCF2B: 0.0010s @ 0.1042s (27)

To understand how the data provided in Table 6, and the other tables, can be interpreted, scenario 2 will be used as an example. In scenario 2, we are applying a line-line fault at bus 1531, which can be found in Figure 1. During this scenario, a maximum current of 521A was observed during the fault. We also observe that the feeder relays, PCF1B and PCF2B, took 0.0010s to clear from the system for under-voltage (Function 27), and tripped at 0.1042s into the scenario. Since the fault occurs at 0.1000s, it is clear that there is a delay from when the fault first occurs, when the relay first observes an issue in the system, and when the relay actually trips.

Table 7: Results for G2 Fault Scenarios with R1N Capacity of 260kW

Scenario	Fault Location	Fault Type	Observed Maximum Current (A)	Device: Clearing Time @ Trip Time (Device No.)
1	NA	No Fault	62	
2	1531	LL	466	PCF1B: 0.0010s @ 0.1084s (27) PCF2B: 0.0010s @ 0.1084 (27) PCR1N: 0.5148s @ 0.6207s (27)
3	15691	LL	470	PCF1B: 0.0015s @ 0.1057s (27) PCF2B: 0.0015s @ 0.1057s (27) PCR1N: 0.5132s @ 0.6167s (27)
4	15691	3L	516	PCF1B: 0.0014s @ 0.1056s (27) PCF2B: 0.0014s @ 0.1056s (27) PCR1N: 0.5132s @ 0.6167s (27)
5	1885	LL	654	PCF1B: 0.0017s @ 0.1057s (27) PCF2B: 0.0017s @ 0.1057s (27) PCR1N: 0.5162s @ 0.6247s (59)
6	1902	LL	391	PCF1B: 0.0010s @ 0.1101s (59) PCF2B: 0.0010s @ 0.1101s (59) PCR1N: 0.5162s @ 0.6247s (59)
7	1902	3L	398	PCF1B: 0.0015s @ 0.1097s (27) PCF2B: 0.0015s @ 0.1097s (27) PCR1N: 0.5145s @ 0.6287s (59)
8	F1A	LL	880	PCF1B: 0.0018s @ 0.1057s (27) PCF2B: 0.0018s @ 0.1057s (27) PCR1N: 0.5132s @ 0.6167s (27)
9	F1A	3L	975	PCF1B: 0.0018s @ 0.1057s (27) PCF2B: 0.0018s @ 0.1057s (27) PCR1N: 0.5132s @ 0.6167s (27)
10	F2A	LL	879	PCF1B: 0.0018s @ 0.1057s (27) PCF2B: 0.0018s @ 0.1057s (27) PCR1N: 0.5132s @ 0.6167s (59)
11	F2A	3L	975	PCF1B: 0.0018s @ 0.1057s (27) PCF2B: 0.0018s @ 0.1057s (27) PCR1N: 0.5127s @ 0.6167s (59)

3.2.2 Generator G4 Scenarios

The results of the G4 scenarios are provided in Table 8 and Table 9. It is apparent that the installation of R1N does not alter the coordination of the fuses, feeder relays, and generation relays. Under no scenario was a non-detection zone observed, nor did any nuisance tripping or tripping due to reverse power occur. From comparison of Table 8 and Table 9 it can be observed that:

1. R1N has a minimal impact (<10%) on the observed maximum current
2. Fuses have slightly faster (order of ~100-200ms) clearing times.
3. Feeder relays have comparable clearing times.

Table 8: Results for G4 Fault Scenarios with Existing PV Only

Scenario	Fault Location	Fault Type	Observed Maximum Current (A)	Device: Clearing Time @ Trip Time (Device No.)
1	NA	No Fault	91	
2	1531	LL	589	PCS8325: 0.6781s @ 0.7801s (Fuse B)
3	15691	LL	649	PCS8325: 0.7306s @ 0.8343s (Fuse A)
4	15691	3L	661	PCS8325: 1.4044s @ 1.5063s (Fuse C) 1.4131s @ 1.5154s (Fuse B)
5	1885	LL	871	PCS9603: 0.1536s @ 0.2561s (Fuse A) 0.1536s @ 0.2561s (Fuse B)
6[1]	1902	LL	453	PCS8327: 0.9723s @ 1.0765s (Fuse A) PCF1A: 3.0146s @ 3.3887s (81) PCF2A: 3.0146s @ 3.3887s (81) PCG4: 2.0037s @ 5.5847s (59)
7[1]	1902	3L	482	PCS8327: 1.6745s @ 1.7771s (Fuse B) 1.7160s @ 1.8213s (Fuse A) 1.7330s @ 1.8352s (Fuse C) PCF1A: 3.0140s @ 3.3167s (81) PCF2A: 3.0140s @ 3.3167s (81)
8	F1A	LL	1121	PCF1A: 2.0165s @ 2.1207s (27) PCF2A: 2.0165s @ 2.1207s (27)
9	F1A	3L	1140	PCF1A: 2.0144s @ 2.1167s (27) PCF2A: 2.0144s @ 2.1167s (27)
10	F2A	LL	1121	PCF1A: 2.0165s @ 2.1207s (27) PCF2A: 2.0165s @ 2.1207s (27)
11	F2A	3L	1140	PCF1A: 2.0144s @ 2.1167s (27) PCF2A: 2.0144s @ 2.1167s (27)

Notes:

1. *Scenario 6 & 7 results must be rejected, due to frequency falling below the range wherein the speed-governor and excitation system models can be expected to provide reasonable accuracy.*

Table 9: Results for G4 Fault Scenarios with R1N Capacity of 270kW

Scenario	Fault Location	Fault Type	Observed Maximum Current (A)	Device: Clearing Time @ Trip Time (Device No.)
1	NA	No Fault	64	
2	1531	LL	577	PCR1N: 0.5142s @ 20.6208s (27) PCS8325: 0.5219s @ 20.6239s (Fuse C)
3	15691	LL	603	PCR1N: 0.5136s @ 20.6167s (27) PCS8325: 0.5618s @ 20.664s (Fuse B)
4	15691	3L	713	PCR1N: 0.5136s @ 20.6167s (27) PCS8325: 1.2894s @ 21.3914s (Fuse B) 1.3034s @ 21.4067s (Fuse A)
5	1885	LL	819	PCS9603: 0.1062s @ 0.2077s (Fuse A) 0.1062s @ 0.2077s (Fuse B) PCR1N: 0.5147s @ 0.9067s (27)
6[1]	1902	LL	436	PCR1N: 0.5153s @ 20.6247s (F27), PCS8327: 0.7393s @ 20.8421s (Fuse A) PCF1A: 3.0127s @ 23.3407s (81) PCF2A: 3.0127s @ 23.407s (81), PCG4: 1.996s @ 25.5132s (59)
7[1]	1902	3L	482	PCR1N: 0.51295s @ 20.6207s (27) PCS8327: 1.3627s @ 21.4648 (Fuse B) 1.3985s @ 21.5021s (Fuse A) PCF1A: 3.013s @ 23.2567s (81) PCF2A: 3.013s @ 23.2567s (81) PCG4: 2.0049s @ 25.3727s (59)
8	F1A	LL	1042	PCR1N: 0.5136s @ 20.6167s (27) PCF1A: 2.0139s @ 22.1167s (27) PCF2A: 2.0139s @ 22.1167s (27)
9	F1A	3L	1247	PCR1N: 0.5136s @ 20.6167s (27) PCF1A: 2.0139s @ 22.1167s (27) PCF2A: 2.0139s @ 22.1167s (27)
10	F2A	LL	1064	PCR1N: 0.5136s @ 20.6167s (27) PCF1A: 2.0139s @ 22.1167s (27) PCF2A: 2.0139s @ 22.1167s (27)
11	F2A	3L	1260	PCR1N: 0.5136s @ 20.6167s (27) PCF1A: 2.0139s @ 22.1167s (27) PCF2A: 2.0139s @ 22.1167s (27)

Notes:

1. *Scenario 6 & 7 results must be rejected, due to frequency falling below the range wherein the speed-governor and excitation system models can be expected to provide reasonable accuracy.*

3.2.3 Battery B1N Scenarios

It was found that an R1N capacity of 400kW, when connected at bus 15691, caused a large enough voltage rise to trip the over-voltage protection at R1N. Figure 13 shows the voltage at the new plant bus and bus 15691 during the initialization portion of the simulation; the relay (PCR1N) is enabled at 1s, and it trips at ~1.5s, after the time delay. The New Plant bus voltage is ~0.008pu higher than 1.038pu (2.49kV), which is likely due to a voltage rise through the transformer connecting B1N to the system, and may contribute to the tripping of the over-voltage relay; however, this is a marginal increase, and should not be mistaken as the cause of the issue. The over-voltage is corroborated by the voltage profile results in section 3.1.1.

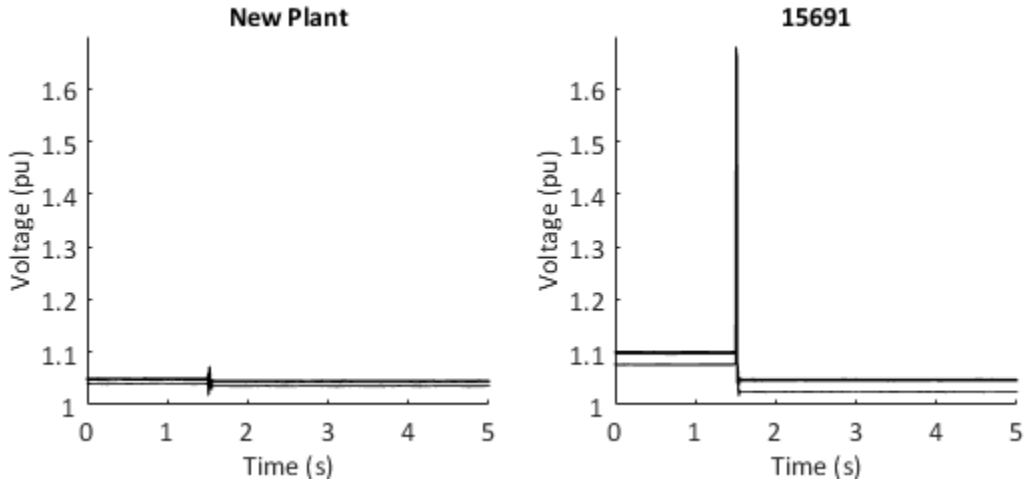

Figure 13: New Plant & Bus 15691 RMS Voltage with R1N Capacity of 400kW.

Due to the erroneous tripping of PCR1N during the simulation initialization, the remainder of the scenario is not given here.

3.3 LARGE-DISTURBANCE STABILITY

The results of Monte-Carlo Filtering for the scenarios are described in each of the following subsections. A summary of the cause(s) of non-behaviour and the point at which they begin to occur is provided in each subsection, along with figures of key system variables for specific cases. Table 4,

given in the methodology, provides the thresholds used within this study. It is important to note that exceeding the inner frequency threshold may cause disconnection of the existing solar PV arrays (R1E, R2E, and R3E), which can exacerbate any frequency or voltage variations. Exceedance of outer frequency and voltage thresholds may cause operation of protective relays, and constitute unacceptable system operation.

While simulations were run with R1N connected at both the new plant bus and bus 15691, the results were reasonably similar. As such, the following subsections focus on the results of the simulations performed with R1N connected at bus 15691.

3.3.1 Generator G2 Scenarios

In every case, the inner voltage thresholds were exceeded. This is likely due to the voltage drop on feeder 2.

After instantaneous disconnection of R1N, the following can be observed:

1. The inner frequency thresholds begin to be exceeded for R1N capacities of greater than approximately 70kW.
2. The outer frequency thresholds begin to be exceeded for R1N capacities of greater than 225kW.
3. The outer voltage thresholds begin to be exceeded for R1N capacities of greater than 160kW.

After loss of full capacity of R1N over 5s, the following can be observed:

1. Only the inner voltage thresholds are exceeded.

After connection of R1N, the following can be observed:

1. The limitation on the maximum rate of change of active power plays a significant role in preventing the exceedance of the frequency thresholds. A limitation on the maximum rate of change of active power of between 0.2 and 1.0 pu/s prevented the exceedance of outer frequency and voltage thresholds for each scenario.

Figure 14 shows the frequency and voltage of G2 for scenario 11 (a capacity of 157kW of solar PV).

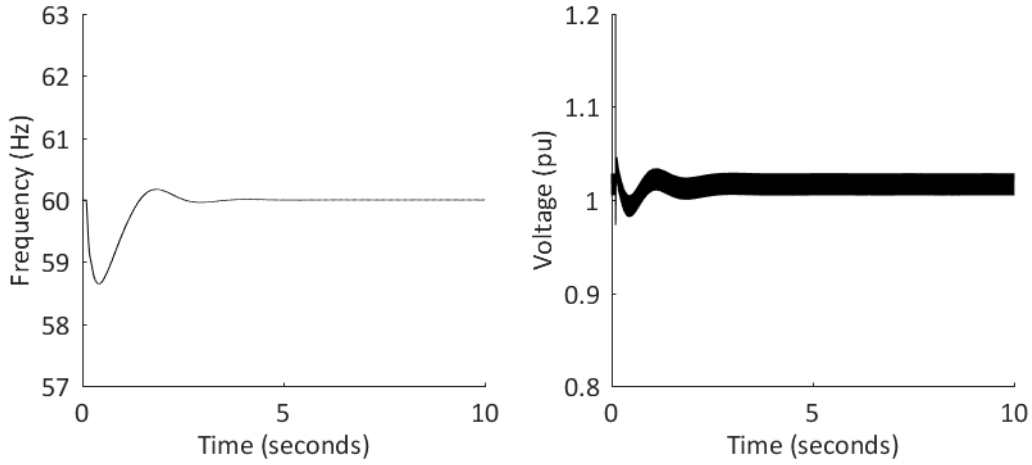

Figure 14: Generator G2 Frequency and Voltage after Instantaneous Loss of 157kW of Solar PV

Figure 15 to Figure 17 showcase the frequency and voltage of generator G2 for scenarios 8, 20, and 32 (instantaneous disconnection, full loss over 5s, and connection of 256kW of solar PV, respectively). For the case of the PV connection, the maximum rate of change of active power was set to 0.4726pu/s.

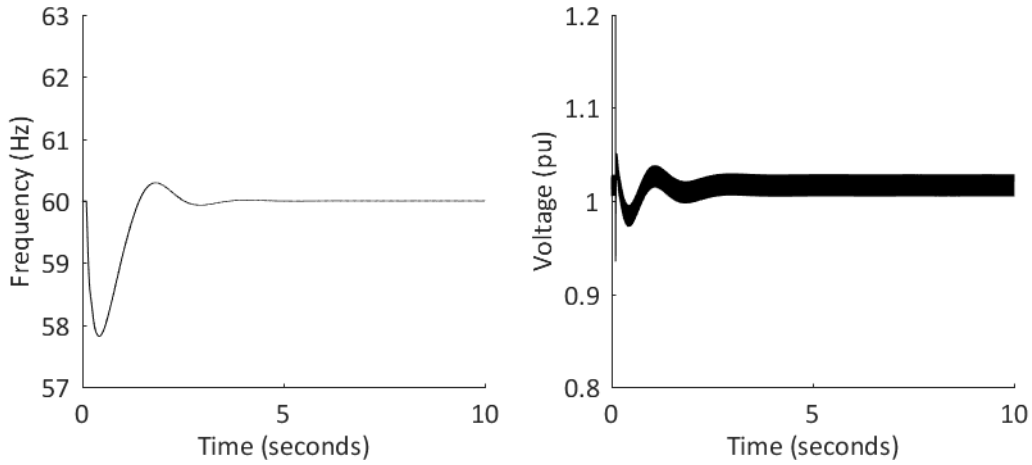

Figure 15: Generator G2 Frequency and Voltage after Instantaneous Loss of 256kW of Solar PV

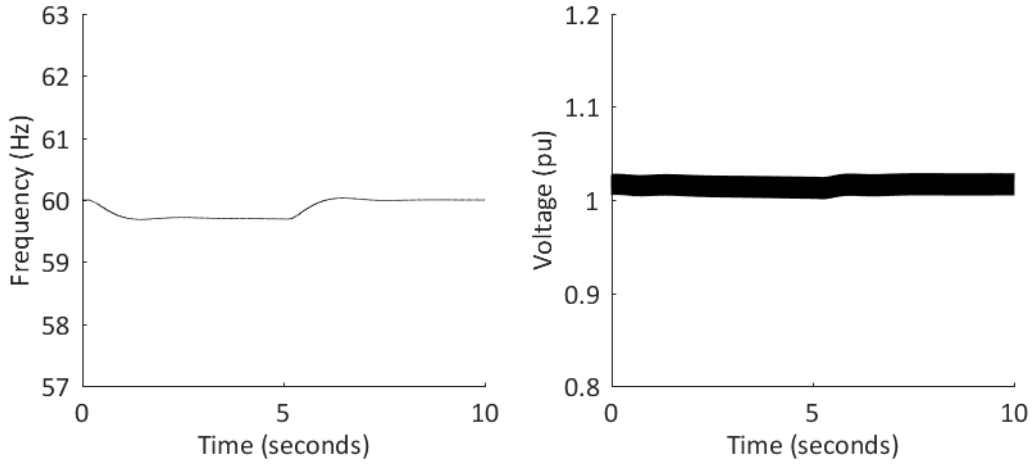

Figure 16: Generator G2 Frequency and Voltage after Loss of 256kW of Solar PV over 5s

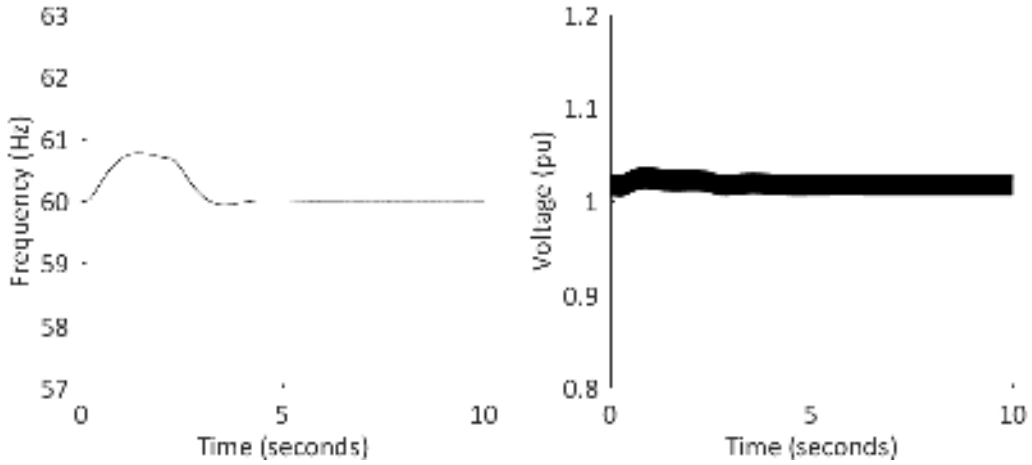

Figure 17: Generator G2 Frequency and Voltage after Connection of 256kW of Solar PV over 2.12s

3.3.2 Generator G4 Scenarios

Regardless of the connection location of R1N (i.e., at bus 15961 or the diesel plant bus), the results of both scenario sets are very similar. In every case, the inner voltage thresholds were exceeded. This is likely due to the voltage drop on feeder 2.

After instantaneous disconnection of R1N, the following can be observed:

1. The inner frequency thresholds begin to be exceeded for R1N capacities of greater than approximately 55kW.
2. The outer frequency thresholds begin to be exceeded for R1N capacities of greater than approximately 175kW.

3. The outer voltage thresholds begin to be exceeded for R1N capacities of greater than approximately 100kW.

After loss of full capacity of R1N over 5s, the following can be observed:

1. Only the inner voltage thresholds are exceeded.

After connection of R1N, the following can be observed:

1. The limitation on the maximum rate of change of active power plays a significant role in preventing the exceedance of the frequency thresholds. A limitation on the maximum rate of change of active power of between 0.2 and 1.0 pu/s prevented the exceedance of outer frequency and voltage thresholds for each scenario.

Figure 18 shows the frequency and voltage of G2 for scenario 10 (a capacity of 173kW of solar PV), with R1N connected at bus 15961.

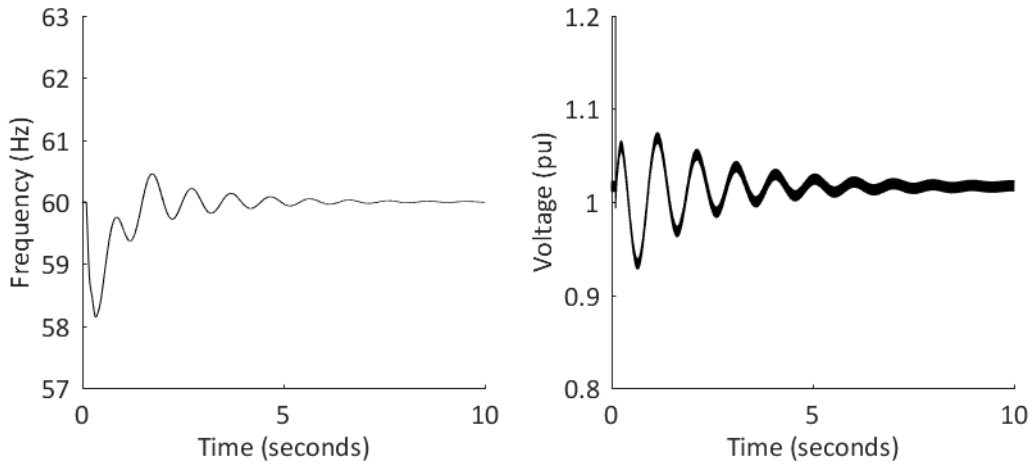

Figure 18: Generator G4 Frequency and Voltage after Instantaneous Loss of 173kW of Solar PV

***Note: Outer voltage thresholds were exceeded at several buses during this scenario.**

Figure 19 to Figure 21 showcase the frequency and voltage of G4 for scenarios 5, 17, and 29 (instantaneous disconnection, full loss over 5s, and connection of 263kW of solar PV, respectively), with R1N connected at bus 15961. For the case of the PV connection, the maximum rate of change of active power was set to 0.3453pu/s.

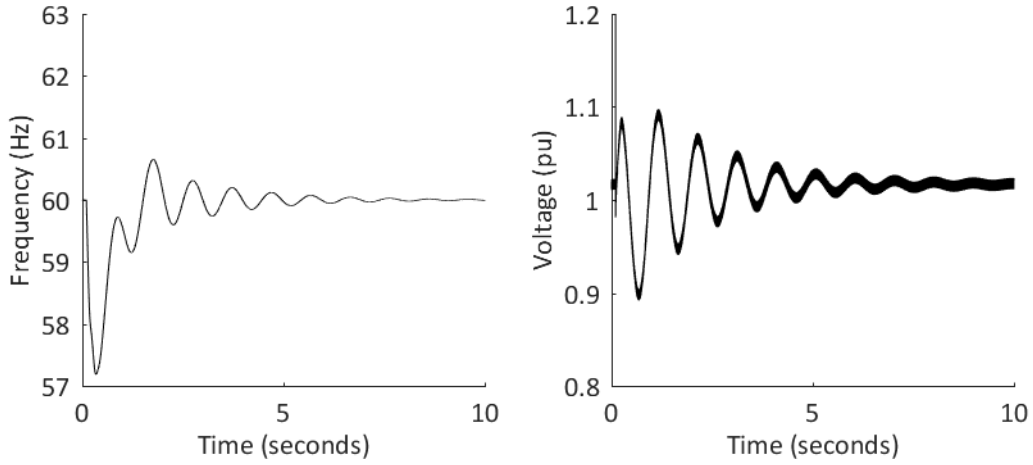

Figure 19: Generator G4 Frequency and Voltage after Instantaneous Loss of 263kW of Solar PV

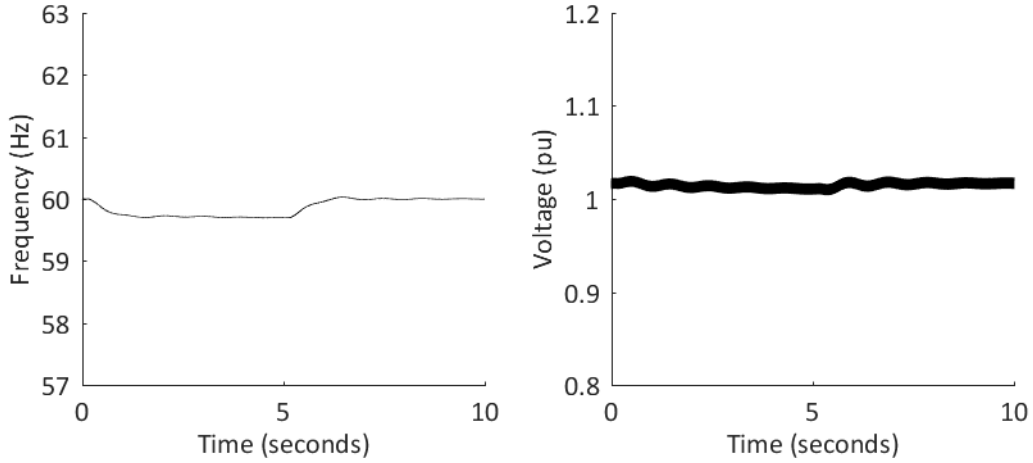

Figure 20: Generator G4 Frequency and Voltage after Loss of 263kW of Solar PV over 5s

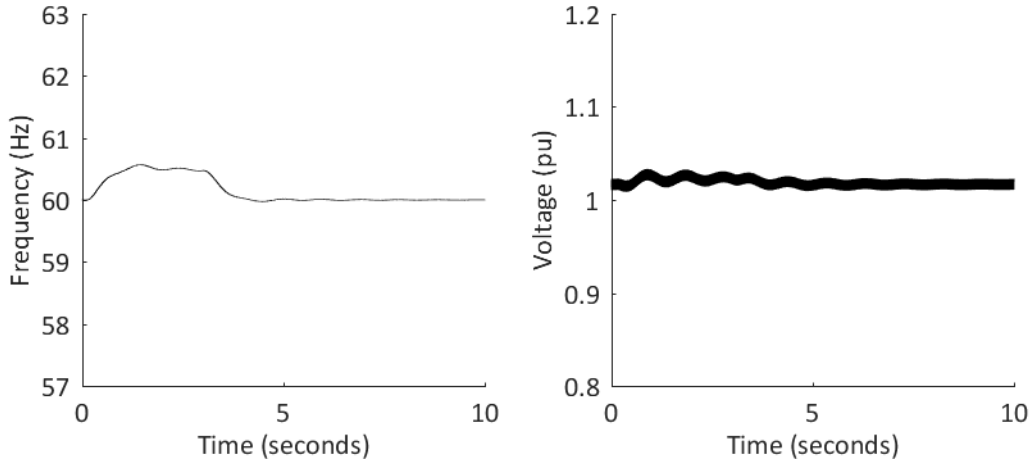

Figure 21: Generator G4 Frequency and Voltage after Connection of 263kW of Solar PV over 2.9s

3.3.3 Battery B1N Scenarios

In every case, the inner voltage thresholds were exceeded. This is likely due to the voltage drop on feeder 2.

After instantaneous disconnection of R1N, the following can be observed:

1. There is no visible change in the frequency measured at B1N. Frequency thresholds are not exceeded at any points in the system.
2. There is a very short transient in the terminal voltage measured at B1N that exceeds the outer voltage threshold for less than the 4ms required to flag the threshold in the Monte-Carlo Filtering.
3. The outer voltage threshold was exceeded when R1N was connected at bus 15691; however, it was not exceeded when R1N was connected at the new plant bus.

After loss of full capacity of R1N over 5s, the following can be observed:

1. There is no visible change in the frequency or voltage at the B1N terminals. Frequency thresholds are not exceeded at any points in the system.
2. There is no visible change in the terminal voltage measured at B1N.
3. The outer voltage threshold was exceeded when R1N was connected at bus 15691; however, it was not exceeded when R1N was connected at the new plant bus.

Figure 22 and Figure 23 showcase the frequency and voltage of B1N for scenarios 1 and 2 (instantaneous disconnection and full loss over 5s, respectively), with R1N connected at bus 15691.

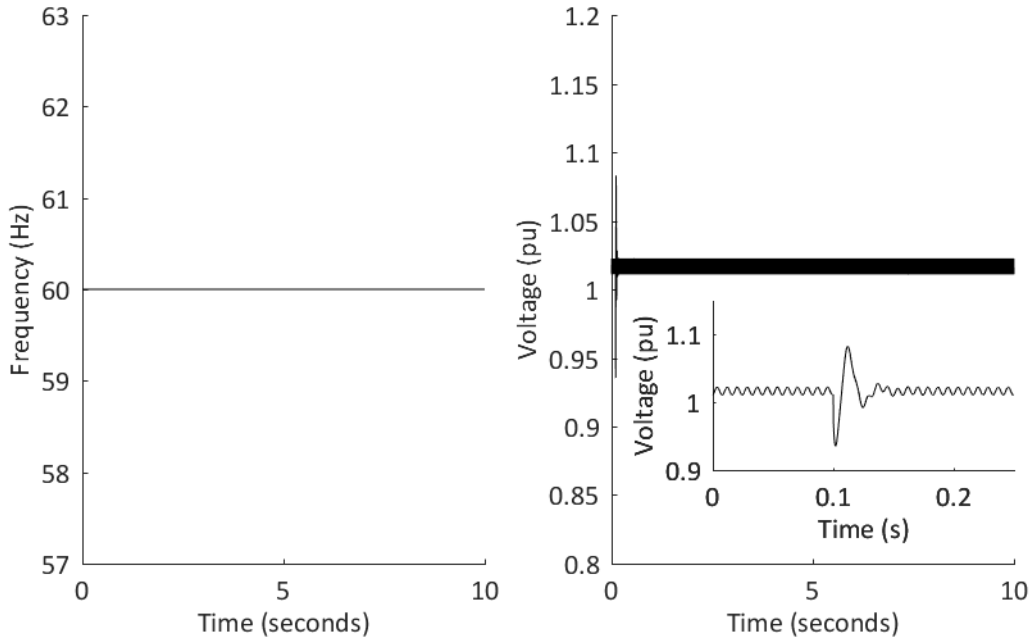

Figure 22: BESS B1N Frequency and Voltage after Instantaneous Loss of 400kW of Solar PV

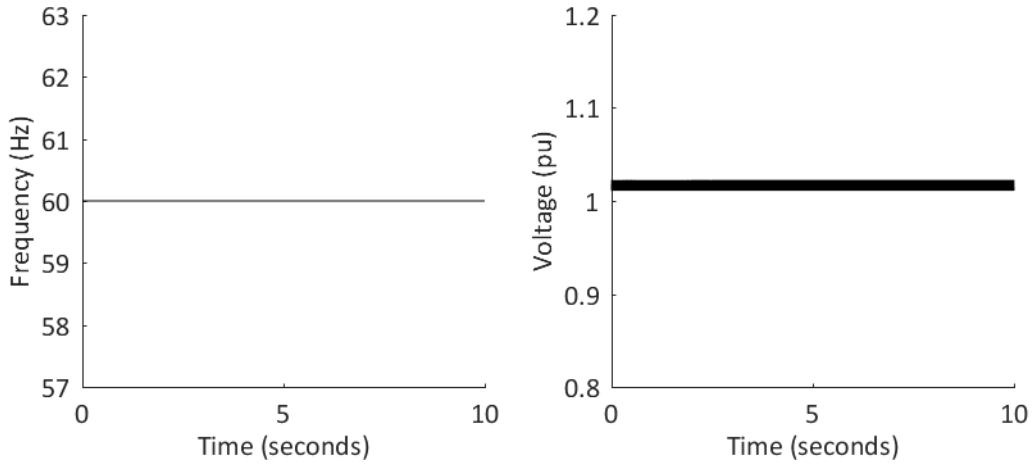

Figure 23: BESS B1N Frequency and Voltage after Loss of 400kW of Solar PV over 5s

The frequency of B1N does not vary when operating in controlled-frequency mode because it is set to a value of 60Hz by the phase-locked loop. Consequently, the system response to disturbances occurs mainly in terms of voltage; however, small variations in frequency can still be observed in the measurements obtained by the phase-locked loops of the existing PV arrays.

The cause of exceeding the outer voltage threshold is not apparent from the voltage of B1N; however, it is likely due to the control methodology used in the model of B1N. The control method uses the dq-frame (direct quadrature frame), which transforms the sinusoidal three-phase voltages and currents

from the abc-frame (i.e., the power system time-domain three-phase reference frame) into dc signals in a rotating reference frame. The resulting dq-frame measurements are, in essence, a representation of the three phase rms signals. The controller acts on these non-sinusoidal signals to produce a dq-frame modulating signal, which is then transformed back to the abc-frame. The modulating signal is then used to control the switching of the voltage-sourced converter. Consequently, the abc-frame voltages are not directly controlled, and can deviate from the desired voltage so long as the positive sequence of the three voltages is equivalent to the desired voltage. Figure 24 and Figure 25 showcase the three-phase line-line voltages measured at the new plant bus for the four scenarios.

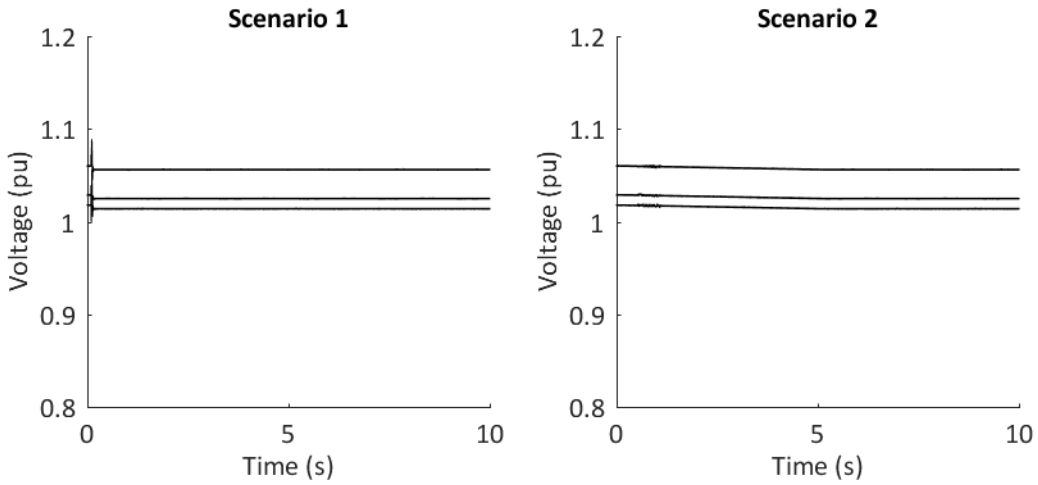

Figure 24: New Plant Bus RMS Voltage with R1N Connected at the New Plant Bus

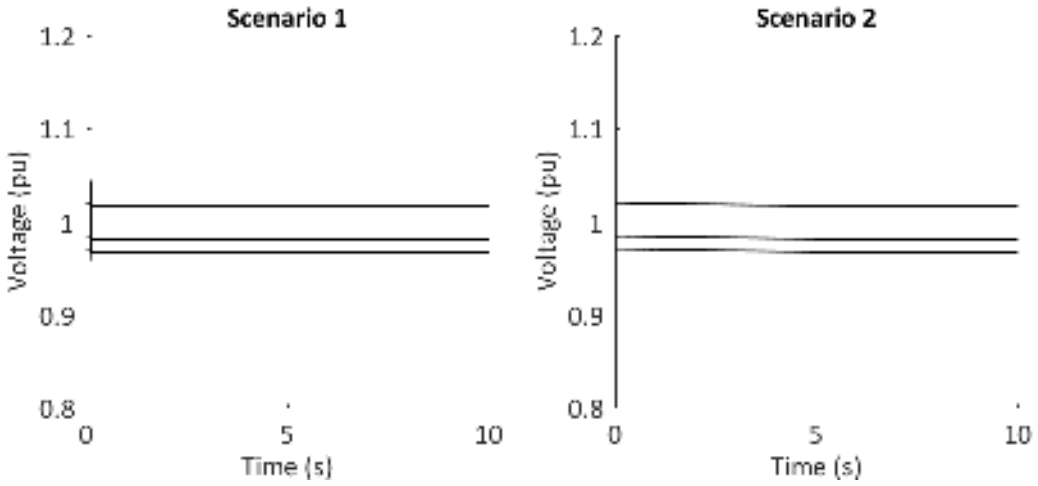

Figure 25: New Plant Bus RMS Voltage with R1N Connected at the Bus 15691

The 5th scenario was set to run the generator G4 scenario 5 settings for R1N connected at bus 15691. Figure 26 and Figure 27 show the frequency and voltage at G4 and B1N, respectively.

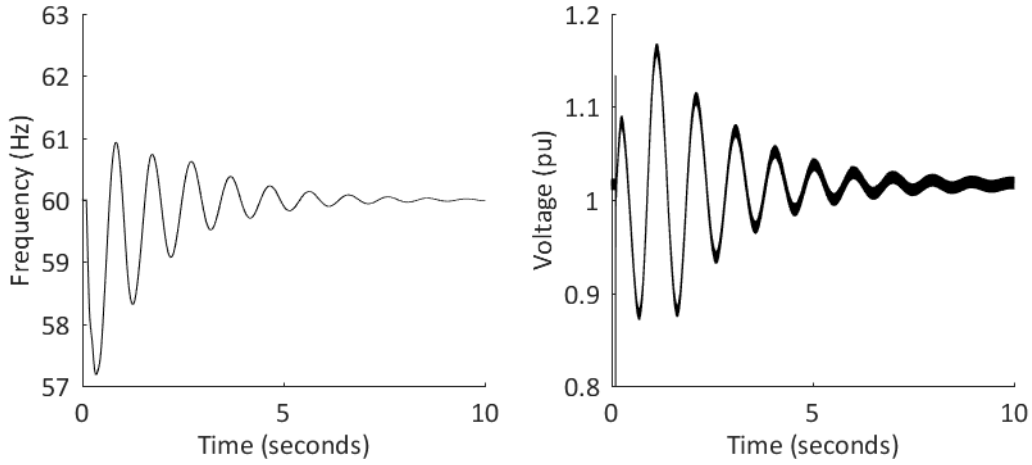

Figure 26: G4 Frequency and Voltage with B1N after Instantaneous Loss of 263kW of Solar PV

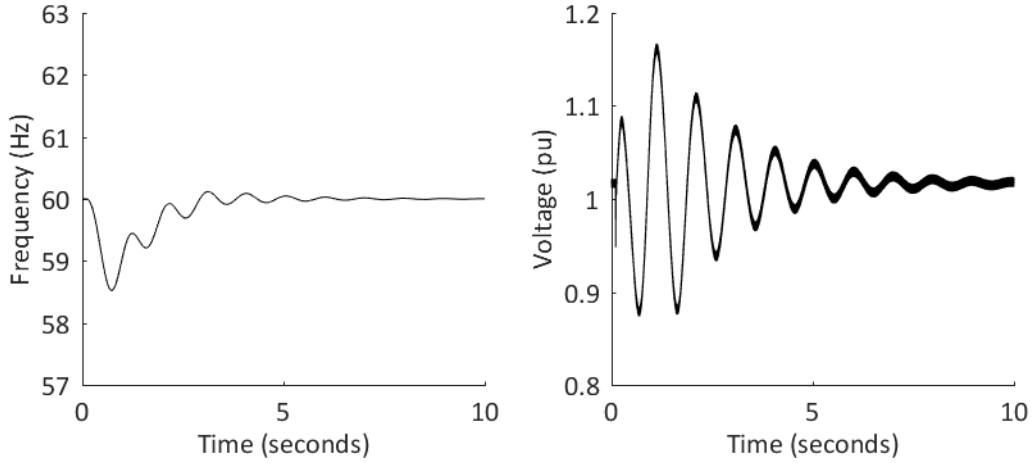

Figure 27: B1N Frequency and Voltage with G4 after Instantaneous Loss of 263kW of Solar PV

The frequency of B1N, as measured by the phase-locked loop, shows a considerable lag in its response to changes in the system frequency. By comparing Figure 26 and Figure 27 with Figure 19, it is observed that B1N does not affect the frequency nadir, as the frequency measured by the phase-locked loop does not exceed the deadband settings before the nadir is reached. The delayed response of the phase-locked loop causes B1N to output power at a point when G4 is already starting to recover, which results in much larger oscillations in frequency and voltage.

It is clear that this is an example of poor coordination of the generator and battery storage system controls; however, this scenario serves to show that the response of the phase-locked loop must be sufficiently fast to allow B1N to provide frequency support when in controlled-current mode, if this type of control is desired.

This scenario serves to show a negative impact that can occur if B1N is intended to provide frequency support for any of the diesel generators. If so, it is important to ensure the response time of the phase-locked loop will be sufficiently small to respond to the event, but also sufficiently large to not overcompensate any other minor disturbances in the system.

4 ADDITIONAL STUDIES (METHODOLOGY AND RESULTS)

The following additional studies have been performed to supplement the results previously provided in section 3, either at the request of VGG and/or ATCO or due to continued improvement of the study methodology and tools.

4.1 ENERGY BALANCE – VARIED SOLAR PLANT POWER FACTOR

A voltage rise, from the diesel generation plant to the point of interconnection, is expected and observed within the simulations for the interconnection of the proposed solar plant. A method of addressing this is through varying the power factor at the solar plant, such that it consumes reactive power in unison with producing active power. The power factor is ranged from unity to 0.90 in steps of 0.025 creating a sweep of 5 values. The energy storage capacity is also examined from 200 kWh to 1200 kWh in steps of 200 kWh, adding 6 test cases. The minimum battery energy storage capacity is set to 5 minutes of reserve power at a load of 550 kW or 10%, whichever is larger. The scenario set examines each power factor angle for each energy storage capacity. The results of the simulations explore the effect that the power factor has on the voltage profile, days of diesel off (non-continuous), and amount of curtailed resource.

The implementation of a leading power factor (consuming reactive power) is shown to decrease the total voltage rise within the transmission line. Figure 28 shows the maximum voltage profile from the diesel generation plant to the solar plant for each quarter of the year. It is observable that reducing the power factor of the solar photovoltaic plant decreases the maximum voltage rise experienced by the transmission line throughout the year.

Decreasing the power factor is also shown to reduce the amount of energy curtailed within the system. Figure 29 shows the total energy curtailed from a 450 kW solar plant over the course of one year with respect to the energy capacity of the battery. The total energy curtailed is decreased with respect to the size of the battery. However it also shown to decrease with respect to the power factor.

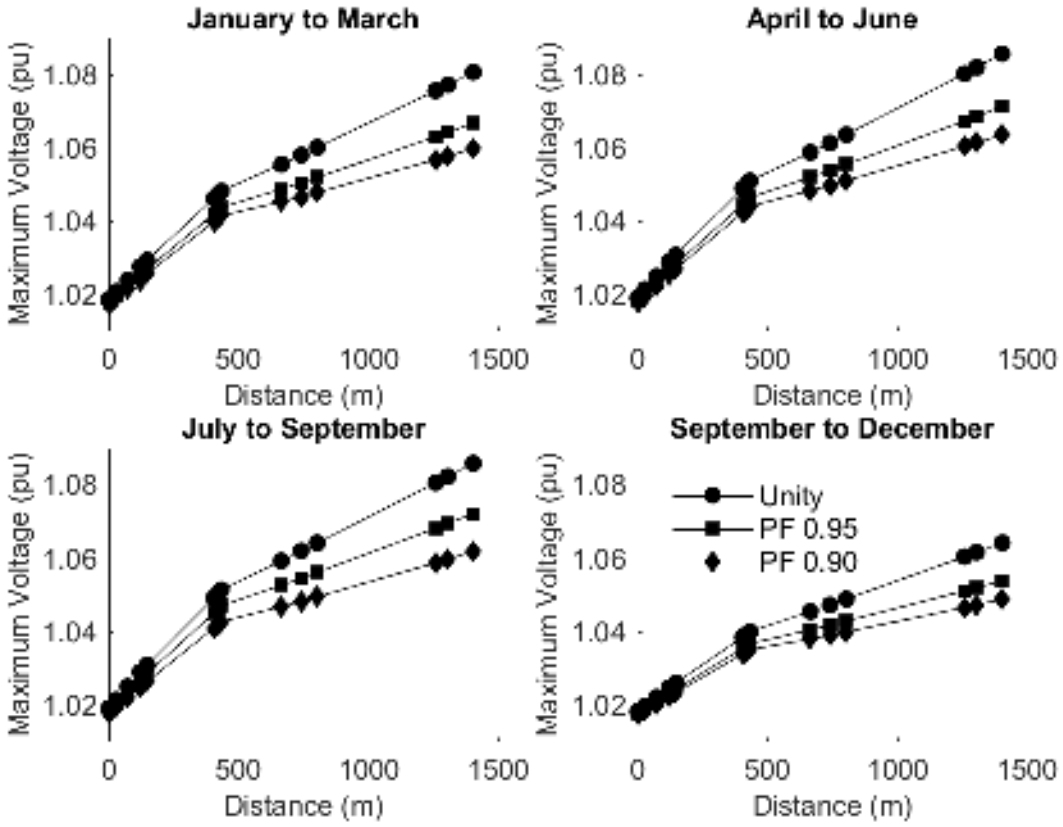

Figure 28: Maximum Voltage Rise from Generation Plant to Solar Plant Shown for Each Quarter of the Year and for Unity 0.95 and 0.90 Leading Power Factor [8].

It is observable in Figure 30 that the energy capacity is directly related to the number of days the diesel generator spends off. Increasing size increasing the time off. It is also observable that the power factor angle decreases the time off as it decreases. It may be desirable to increase the number of hours the diesel generator spends off, however, it may also desirable to decrease the total resource curtailed. It is likely a power factor exists that is the best fit to reduce curtailment while increasing the amount of time the generator is off.

It should be noted that the maximum consumption of reactive power by the solar plant may need to be limited to ensure that both the diesel generators and the battery energy storage system are capable of providing the system reactive load and the solar plant reactive demand.

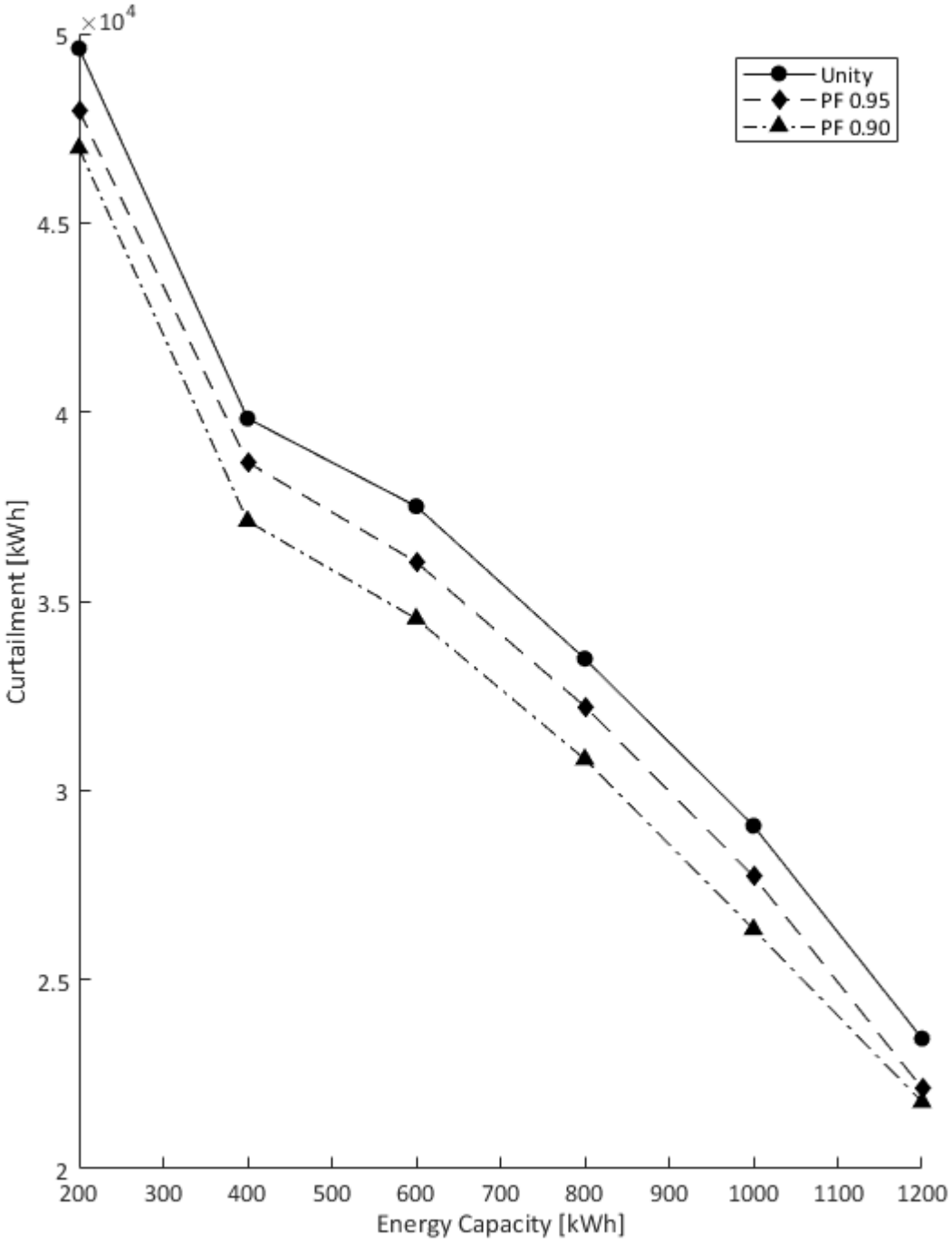

Figure 29: Total Energy Curtailed for a Range of Energy Storage Capacities and Leading Power Factors

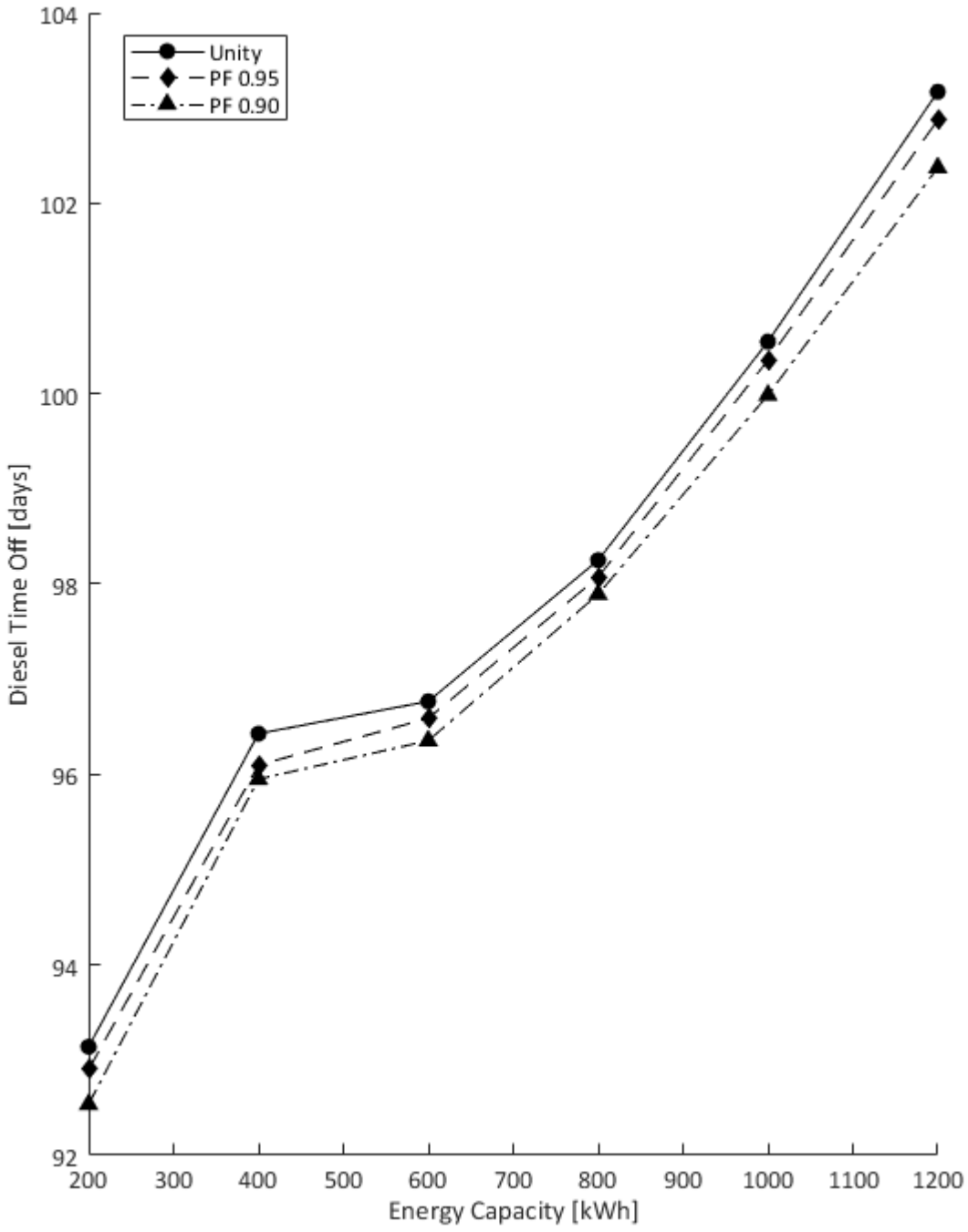

Figure 30: Total Diesel Time Off in Days With Respect to Energy Capacity

4.2 ENERGY BALANCE – VARIED SOLAR PLANT CAPACITY, NO STORAGE

The existing Old Crow system was tested with for a parameter sweep of solar photovoltaic plant capacity. The plant sizes where ranged from 20 kW to 260 kW in 10 kW increments, using scaled versions the proposed east-west facing solar plant. The simulations examined a time frame of one year, from January 1st to December 31st. The battery energy storage system was removed and replaced with a logical process that calculates the level of curtailment required to maintain energy balance while preventing the diesel generator from dipping below the minimum loading limit.

The analysis calculates the fraction of the curtailed energy to the produced energy plus curtailed energy. It is found that little to no curtailment occurs for solar plant capacities of 100 kW or less, Figure 31. This result is dependent on the solar plant configuration, and may vary substantially with other configurations, such as a south facing solar plant. Increasing the size of the solar plant beyond 100 kW increases the fraction curtailed energy.

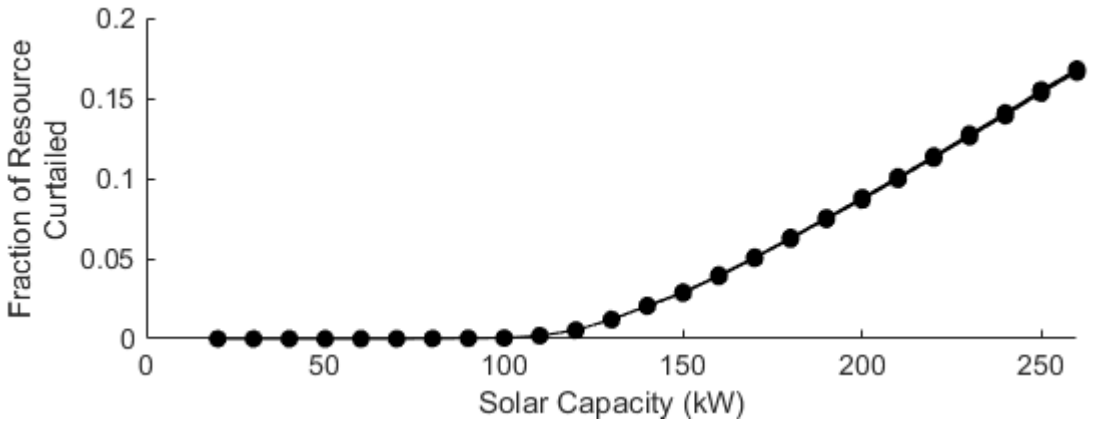

Figure 31: Fraction of Curtailed Resource to Total Renewable Energy Produced Relative to the Solar Photovoltaic Plant Size. Figure Reproduced From [8]

4.3 ENERGY BALANCE – 500KW/400KWH BATTERY STORAGE SYSTEM

As shown in section 3, a battery energy storage system with a power capacity of 400 kW occasionally requires the battery to leave the discharge state before it has completely discharged its available energy. This is due to the dispatch logic containing a clause that dispatches a diesel generator when the battery reaches 90% of its rated active power capacity. A simulation is performed where the power capacity is increased to 500 kW to observe the effects of a higher power capacity on the system.

The simulation is compared to a power capacity of 400 kW for a control. The energy capacities are held constant at 400 kWh with the minimum energy capacity set to 46 kWh or 11.5%. Which is equivalent to 5 minutes of power supplied to a 550 kW demand. Table 10 displays the notable changes in behaviour with the change in power capacity.

Table 10: 500 kW power capacity vs 400 kW power capacity

Power Capacity	Early Exit from Discharge State	Under one Hour discharge
400 kW	18	0
500 kW	2	25

The number of exits from the discharge state due to approaching the maximum power capacity is decreased significantly. However, it can also be noted that the number of discharges under 1 hour increases almost equally. The minor difference between the two power capacities indicates that increasing the power capacity without also altering the energy capacity has little benefit to the system based on the goal of maintaining 1 hour of diesel off.

4.4 LARGE-DISTURBANCE STABILITY – GRIDDED SOLAR PLANT CAPACITY

A set of scenarios was run with Generator G2 and the renewable energy systems R1N (the proposed solar PV array), R1E (the existing 11.8kW solar PV array), R2E (the existing 3.3kW solar PV array), and R3E (the existing 5.0kW solar PV array) connected. All other diesel generators (G3O, G3N, and G4) and the battery energy storage system (B1N) were disconnected. In this scenario set, the R1N capacity was varied in a gridded parameter sweep from 10kW to 260kW in 10kW increments. The 260kW upper limit is the difference between the maximum active power (under continuous operation) and the minimum active power (assuming a 30% loading) of G2, minus the existing PV capacity already installed on the system.

A second set of scenarios was run with Generator G4 and the renewable energy systems R1N (the proposed solar PV array), R1E (the existing 11.8kW solar PV array), R2E (the existing 3.3kW solar PV array), and R3E (the existing 5.0kW solar PV array) connected. All other diesel generators (G2, G3O, and G3N) and the battery energy storage system (B1N) were disconnected. In this scenario set, the R1N capacity was varied in a gridded parameter sweep from 10kW to 270kW in 10kW increments. 270kW is the difference between the maximum active power (under continuous operation) and the minimum active power (assuming a 30% loading) of G4, minus the existing PV capacity already installed on the system.

In both scenario sets, the gridded parameter sweep was run for following test cases: 1) instantaneous disconnection of R1N occurring at 0.1s into the scenario simulation, and 2) loss of full capacity of R1N over 5s beginning at 0.1s into the scenario simulation. All of the scenarios assume a unity power factor at the solar plant.

The results of the Monte-Carlo Filtering were aggregated as a fraction of non-behavioural measurements for each of the thresholds, provided in Table 4 previously, and shown as a function of the solar plant capacity. Figure 32 and Figure 33 show the fraction of non-behaviour for frequency

and voltage for the G2 scenarios. Figure 34 and Figure 35 show the fraction of non-behaviour for frequency and voltage for the G4 scenarios. In both scenario sets, no frequency thresholds were exceeded after the loss of the solar plant over 5 seconds.

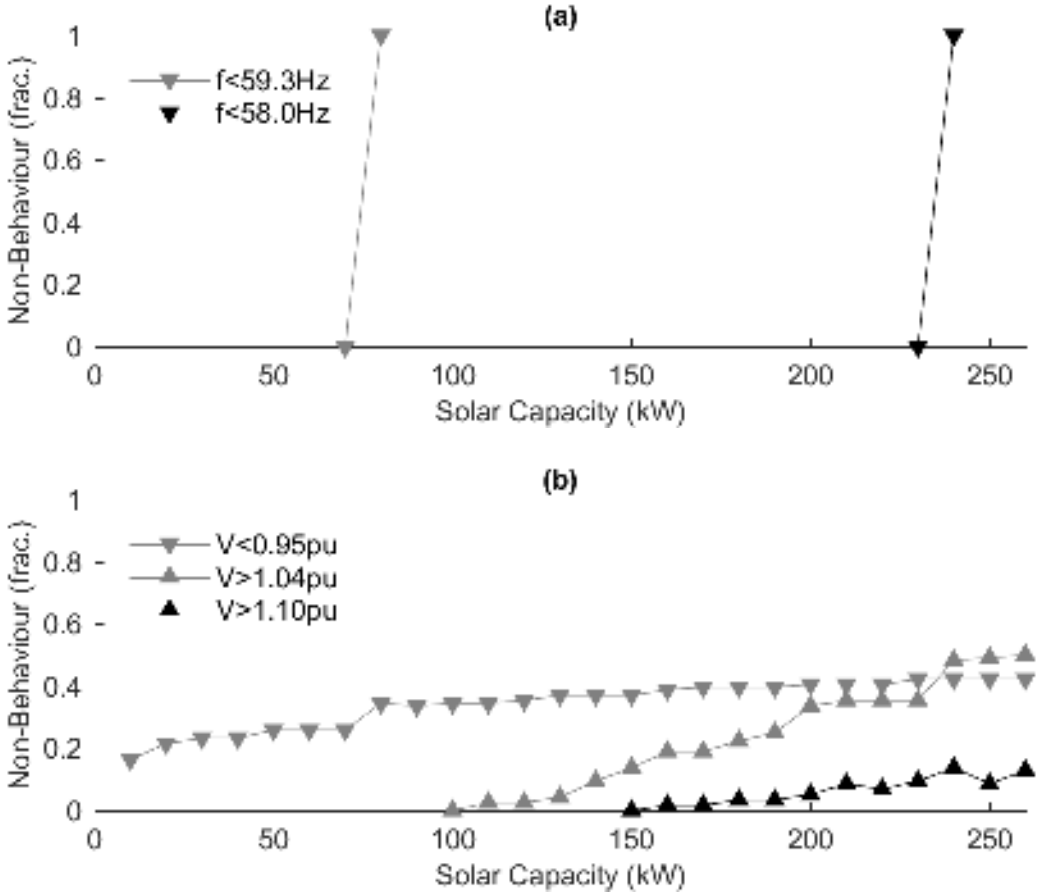

Figure 32: Fraction of Non-Behavioural Measurements After Instantaneous Loss of Solar Plant For (a) frequency, (b) voltage. Figure Reproduced from [8]

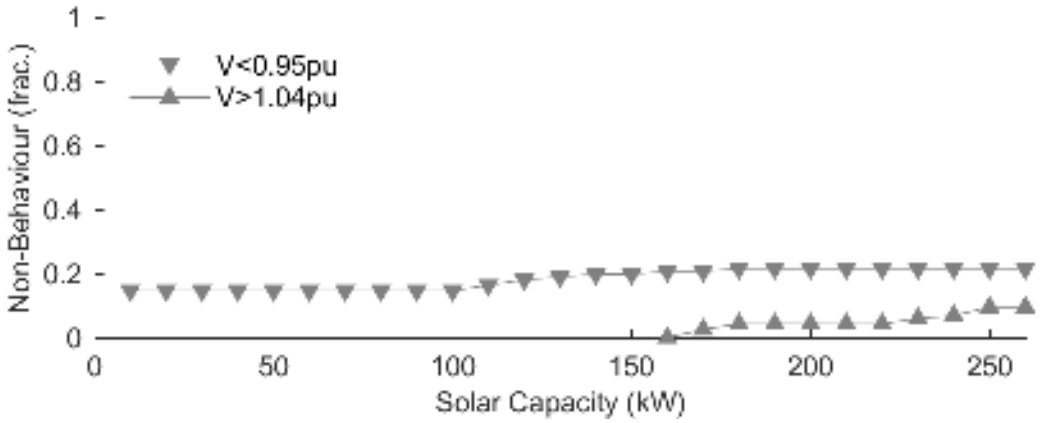

Figure 33: Fraction of Non-Behavioural Measurements After Loss of Solar Plant over 5 Seconds For voltage. Figure Reproduced from [8]

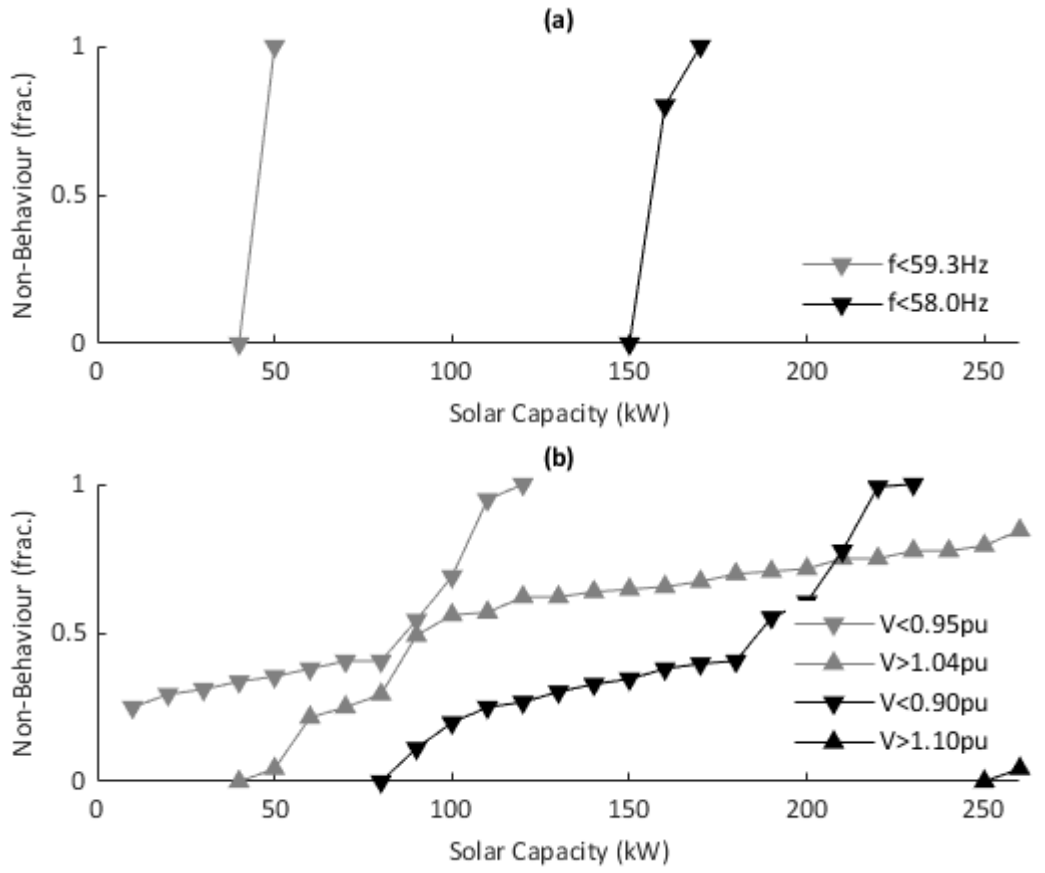

Figure 34: Fraction of Non-Behavioural Measurements After Instantaneous Loss of Solar Plant For (a) Frequency, (b) Voltage.

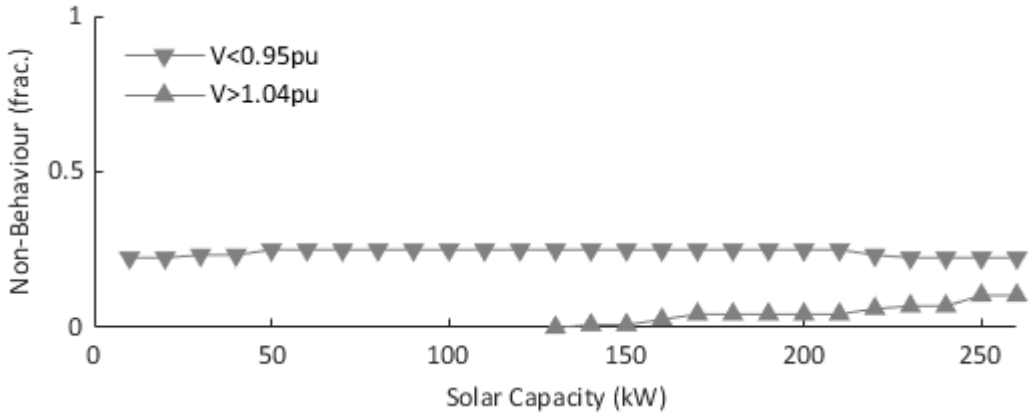

Figure 35: Fraction of Non-Behavioural Measurements After Loss of Solar Plant over 5 Seconds For Voltage.

The results shown in Figure 32 to Figure 35 are in agreement with the results presented previously in section 3.3.1 and 3.3.2. Under normal operation (i.e. loss of the solar plant over 5 seconds), the solar plant has a minimal impact on voltage and frequency. It is apparent from Figure 33 and Figure 35 that there is a pre-existing low voltage issue, which agrees with the results presented in section 3.1.1 and the system model in CYME.

4.5 SPECIFIED ESS BY ATCO

Additional studies have been requested by ATCO to examine the system according to the technical specifications for the procurement of the technology. The simulations are based from these specifications with ESS energy storage capacities of 500 and 550 kWh and power ratings of 500 and 550 kVA. The solar plant is held constant at a power of 450 kW and a power factor angle of -0.318 radians. The results of these simulations are compared on the basis of: curtailment, fuel savings, ESS cycling, insufficient generator off time, insufficient power events. Furthermore, the amount of time each generator spends at a specific level of loading is used for comparison as well.

The fuel consumed by the diesel generators is estimated to be approximately 667,400 litres for the 550 kWh ESS. This is reduced by approximately 30 litres for an ESS of 500 kWh. The slight change in energy capacity and power rating of the storage systems results in minimal changes in total diesel fuel consumed. Furthermore the amount of time the generation plan remains in shut down is shown to be nearly identical at 2165 non-consecutive hours.

The two examined energy capacities show little variation across a variety of parameters, including: curtailment and the number of both full and partial discharge cycles. While displaying some variation in the number of discharges under 1 hour in length as well as the number of early exits from discharge. Furthermore, the fuel consumed by the generators is shown to be equal across both simulations,

indicating that the energy capacity and power rating of the ESS is not strongly correlated to the fuel consumed by the generator plant. These parameters are summarized in the following table.

Table 11: Summary of parameters for the examined energy storage systems.

Parameter	500 kWh & 500 kVA	550 kWh & 550 kVA
Curtailment	27.92 MWh	27.91 MWh
Partial Discharge Cycles	487 Cycles	488 Cycles
Full Discharge Cycles	395 Cycles	397 Cycles
Discharges Under 1 Hour	0	8
Fuel Consumption	666,230 liters	666,230 liters
Early Exit from Discharge	5	0

These energy storage systems are operated between 10% and 90% state of charge. The minimum state of charge of 10% provides emergency backup power, while the 90% can act as a dispatchable load. Both of these limitations also allow the energy storage system to operate outside of the exponential voltage regions for a lithium-ion battery. It must also be noted that these simulations operate with an improved curtailment method using a PI controller as opposed to the previous method of estimation according to the last timestep. This method reduces the amount of error in the simulations and increases the accuracy of the amount of curtailment.

A new analysis of the simulations examines the number of hours each generator runs at a specific load. This not only shows which generators are used most often as well as at what loading level each generators are operating, Figure 36. The simulations show that G4 is in operation the most, while G3 is operated the least. Furthermore, G2 is observed to operate below 50% of its rated loading, while the remainder of the generators operate above this level. Furthermore, it is observed that for a few hours throughout the year both generator G3 and G2 are operating together at 50% load.

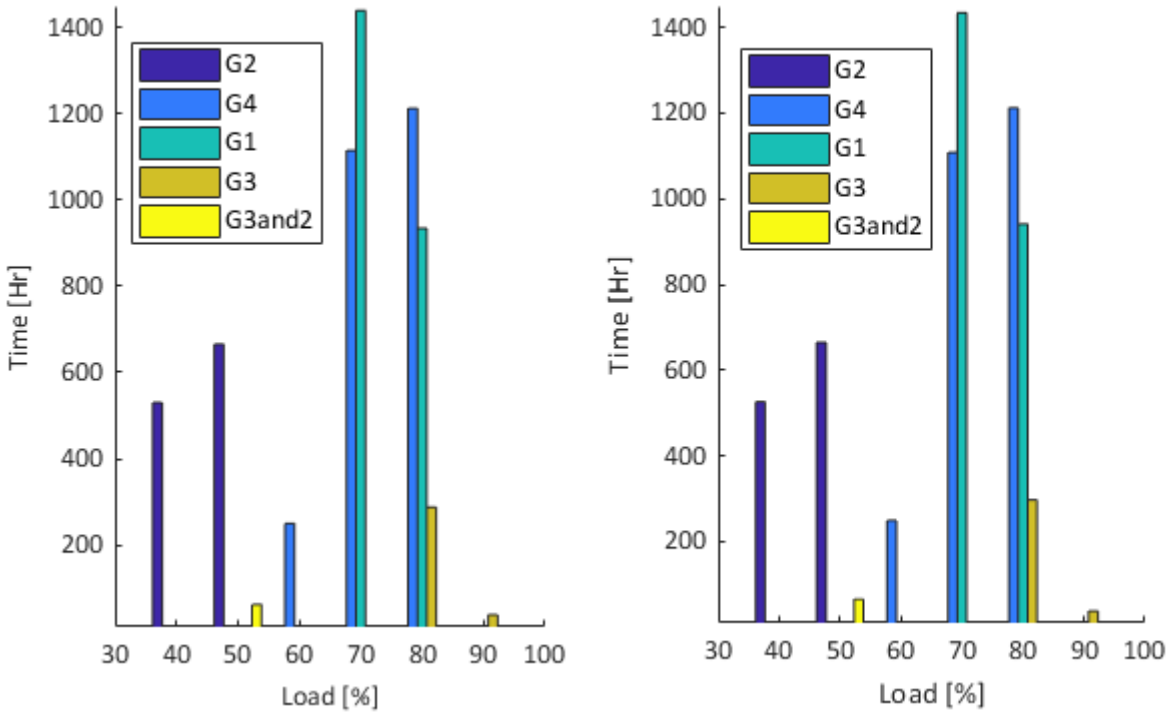

Figure 36: Hours spent at each level of loading. Left 500 kWh 500 kVA. Right 550 kWh 550 kVA.

With the newly reconfigured system the voltage profile from the generation plant to the end of line is expected to vary from previous simulations. The same voltage rise is observed from the generation plant to the renewable generation plant followed by a decrease in voltage out to the end of the line (node 1573), **Figure *37***. The figure shows the maximum and minimum voltage profiles for the specified time periods in grey, and the average voltage profile over the quarter is represented in black. The high voltage approximately the same as observed in previous simulations, this is thought to be due to the implementation of capacitance in the underground transmission line models.

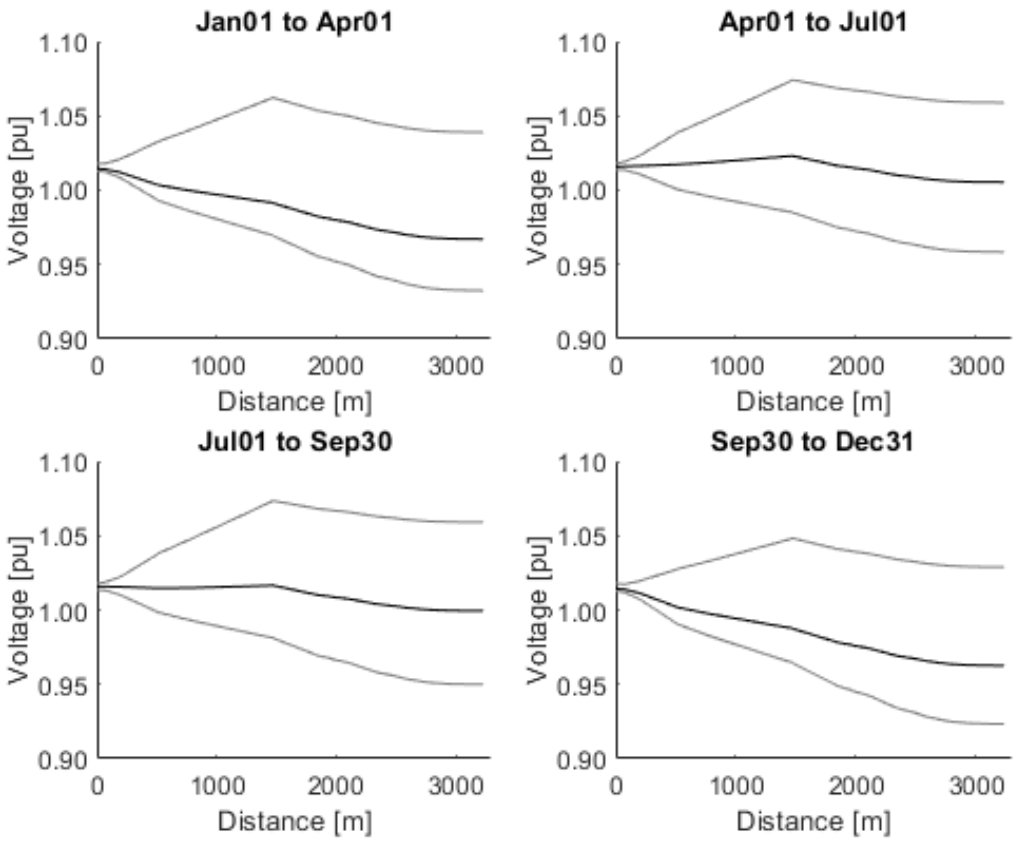

Figure 37: Voltage profile from generator plant to end of line, node 1573. Grey shows the maximum and minimum voltages for the specified time periods, black represents the average.

4.6 SINGLE FEEDER EXAMINATIONS

The energy balance simulations solver is used to complete these simulations examining the energy consumption and production of Old Crow over the entirety of one year. The first simulation opens the switches on Feeder 2 and switch S9609 is closed routing all of the power through Feeder 1. The second simulation keeps switch S9609 closed while opening the switches on Feeder 1, allowing for all of the power to be routed through Feeder 2. Through both these simulations, the maximum, minimum and average voltage profiles are observed, as well as the line loading limits to ensure that over currents in the lines are not experienced.

4.6.1 Entire Load on Feeder 1

The voltage profile from the generator plant to node 1573, shown in **Figure *38***. The voltage rise to the solar plant is shown as expected, as well as the voltage drop from the generator plant to the end of the line that occurs at times of zero renewable resource generation. Placing all of the load on Feeder

1 may be feasible with minor high and low voltages. This configuration splits the load while also maintaining the same length of line as the load spread across both Feeders.

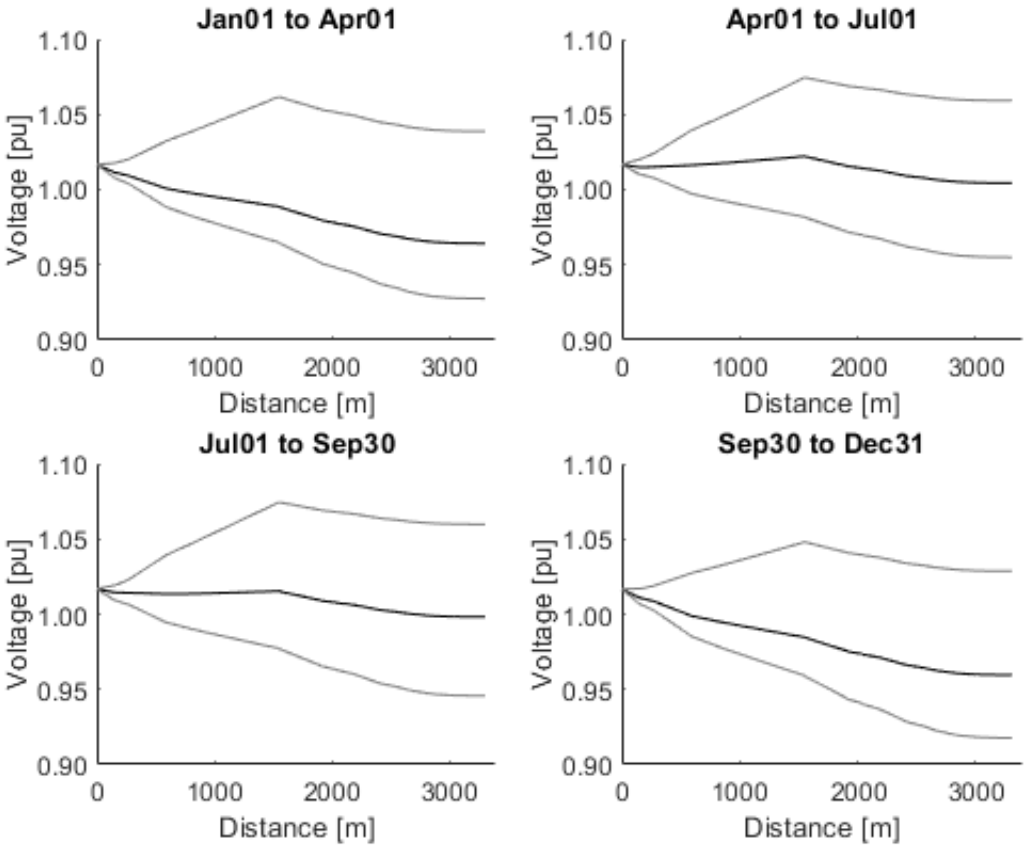

Figure 38: Voltage profile on Feeder 1 for phase to phase voltage AB, from generation plant to node 1573.

4.6.2 Entire Load on Feeder 2

With the entirety of the load placed on Feeder 2 both the voltage rise and the voltage drop are exemplified. This is likely due to the large distance of over 4000 meters required to distribute the power to the end of line, **Figure *39***. Both high and low voltage scenarios in these cases would likely result in failure and disconnection of the renewable resource. Placing the entirety of the load on Feeder 2 is likely infeasible.

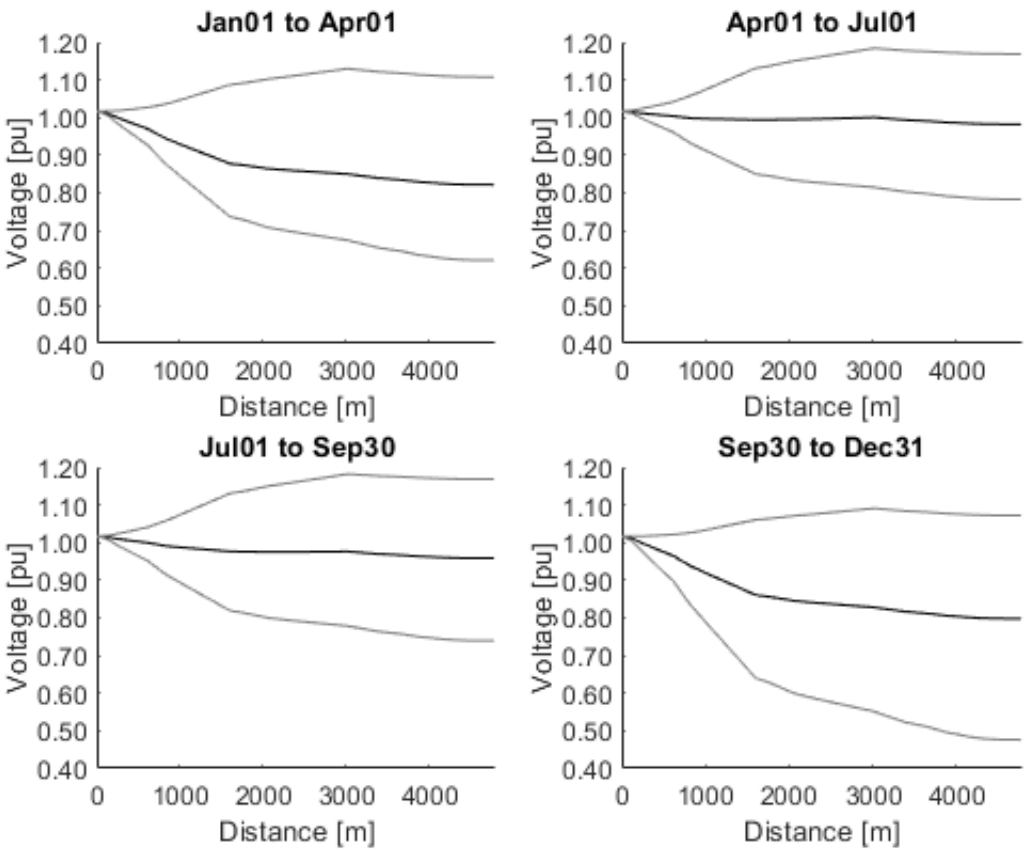

Figure 39: Voltage profile from generation plant to node 1573 for phase to phase voltage AB from January to December.

4.6.3 Imbalance on Existing and Proposed Reconfiguration

Using the energy balance simulations on an, imbalanced model, over the course of one year, the maximum imbalance is found throughout the system. The line to line voltages are compared to the average voltage on all three lines and divided by the base line to line voltage. This provides a fractional value of the imbalance from which the maximum is found.

Examining the imbalance on the existing system shows that there is a maximum imbalance of 0.139, as shown in Table 12. The maximum imbalance at the generator terminals and ESS terminals is also observed. It is shown that the generator maintains a minimal equal imbalance across all phases while the ESS manages to maintain a low imbalance albeit unequal.

Table 12: Imbalance observed at the generator terminals, ESS terminals and maximum imbalance on the existing system.

	Vab	Vbc	Vca
Generator Terminals	0.0164	0.0164	0.0164
ESS Terminals	0.0174	0.0162	0.0163
Maximum Imbalance	0.139	0.094	0.064

The reconfigured system shows that the maximum imbalance across Vab and Vbc is reduced, while an increase in imbalance is observed on Vca, Table 13. At the generator terminals the imbalance is found to be the same as the existing system. At the ESS terminals the imbalance is seen to rise on phases Vbc and Vca, while Vab remains constant.

Table 13: Imbalance observed at the generator terminals, ESS terminals and maximum imbalance system with the north road access line.

	Vab	Vbc	Vca
Generator Terminals	0.0164	0.0164	0.0164
ESS Terminals	0.0174	0.0175	0.0173
Maximum Imbalance	0.0808	0.105	0.0867

It should be noted that this imbalance is found with load assumed to be proportional to the transformer rating, and may not be representative of the real system. Furthermore, the imbalance at the generator and ESS terminals is dependent on the models used and may also not be representative of existing or future equipment.

4.7 LARGE-DISTURBANCE STABILITY – LINE SWITCHING

Additional studies have been requested by ATCO to examine the effects of line switching on the large-disturbance stability of the system.

The test cases and line switching events are defined in Table 14. Each test case may define a baseline or a switching event. The switching events are indicated in underlined bold. Baselines are intended as

a comparison against switching events and show the number of thresholds exceeded during normal operation.

Table 14: Line Switching Test Cases

	Test Case	Switch						
		S6109	S3788	S9609	F1A	F1B	F2A	F2B
Alternate Configuration Switching	1	closed	open	open	closed	closed	closed	closed
	2	closed	**closing**	open	closed	closed	closed	closed
	3	**opening**	closed	open	closed	closed	closed	closed
	4	open	closed	open	closed	closed	closed	closed
	5	**closing**	closed	open	closed	closed	closed	closed
	6	closed	**opening**	open	closed	closed	closed	closed
100% Load on F1 or F2 Proposed Configuration	7	closed	open	**closing**	closed	closed	closed	closed
	8	closed	open	closed	**opening**	**opening**	closed	closed
	9	closed	open	closed	open	open	closed	closed
	10	closed	open	closed	closed	closed	**opening**	**opening**
	11	closed	open	closed	closed	closed	open	open
100% Load on F1 or F2 Existing Configuration	12	open	closed	**closing**	closed	closed	closed	closed
	13	open	closed	closed	**opening**	**opening**	closed	closed
	14	open	closed	closed	open	open	closed	closed
	15	open	closed	closed	closed	closed	**opening**	**opening**
	16	open	closed	closed	closed	closed	open	open

For the line switching test cases, the R1N capacity was varied in a gridded parameter sweep from 50kW to 250kW in 50kW increments for G2 and G4, and 50kW to 450kW in 50kW increments for G3N. In addition, the system demand was fixed at 400kW for G2, 680kW for G3N, and 415kW for G4. The following subsections discuss the results for each generator.

4.7.1 Generator G2

The results of the simulations performed for G2 are provided in Figure 40 to Figure 51. No voltage thresholds were exceeded for any scenarios for test cases 1, 2, 6, and 7 (test cases 1, 2, 6, and 7). These test cases essentially define the proposed system configuration, with S6109 closed; S3788

open, opening, or closing; and S9609 open or closing. Furthermore, no frequency thresholds were exceeded for any of the scenarios.

Figure 40 to Figure 42 (test cases 3-5) show that the opening or closing of S6109 has a minimal impact on the system stability. The exceeded thresholds are largely due to the low voltage issue observed in the existing system, as discussed in more detail in the results of the energy balance simulations.

Figure 43 and Figure 44 (test cases 8 and 9) show that a significant number of under voltage thresholds are exceeded for 100% load on feeder 2 in the proposed system configuration. The fraction of non-behaviour decreases as the solar plant capacity increases, due to the location of the solar plant reducing the power flow through the feeder to the furthest end of the feeder.

Figure 45 and Figure 46 (test cases 10 and 11) show that, while still significant, a reduced number of under voltage thresholds are exceeded for 100% load on feeder 1 in the proposed system configuration as compared to 100% load on feeder 2. The fraction of non-behaviour was found to be minimally affected by the solar plant capacity.

Figure 47 (test case 12) shows that the closing of S9609, while in the existing system configuration, has a minimal impact on the system stability. The exceeded thresholds are largely due to the low voltage issue observed in the existing system, as discussed in more detail in the results of the energy balance simulations.

Figure 48 and Figure 49 (test cases 13 and 14) show that a significant number of voltage thresholds are exceeded for 100% load on feeder 2 in the existing system configuration. The fraction of non-behaviour for under voltage decreases with increasing solar plant capacity; however, the fraction of non-behaviour for over voltage increases with increasing solar plant capacity.

Figure 50 and Figure 51 (test cases 15 and 16) show that a significant number of under voltage thresholds are exceeded for 100% load on feeder 1 in the existing system configuration. The fraction of non-behaviour for under voltage was found to be minimally affected by the solar plant capacity; however, high solar plant capacities led to a small fraction of non-behaviour for over voltage.

In all cases, system instability was not observed to be caused by line switching, as evidence by comparison of the steady-state and switching test cases. System frequency was not observed to be impacted by line switching; however, due to the magnitude of non-behavioural voltage measurements, the simulation of the system loads with voltage dependence may cause changes in demand during switching events that could lead to larger frequency swings in the system.

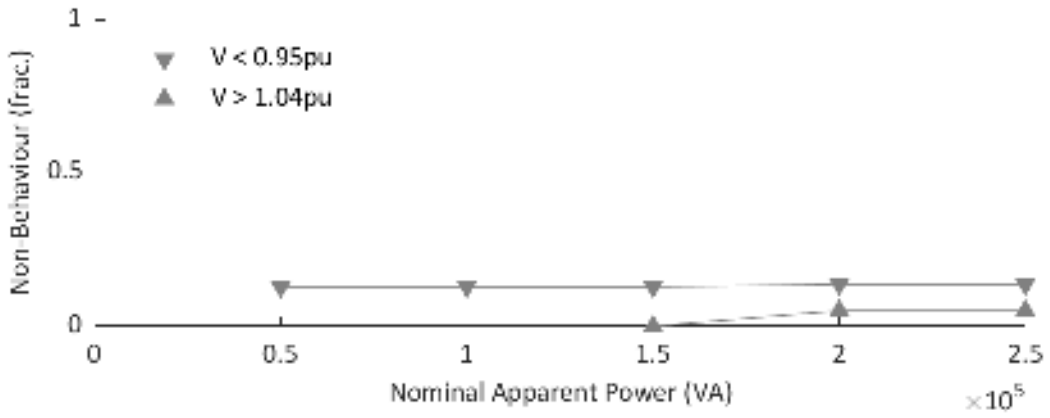

Figure 40: Fraction of Non-Behavioural Voltage Measurements for Line Switching Test Case 3

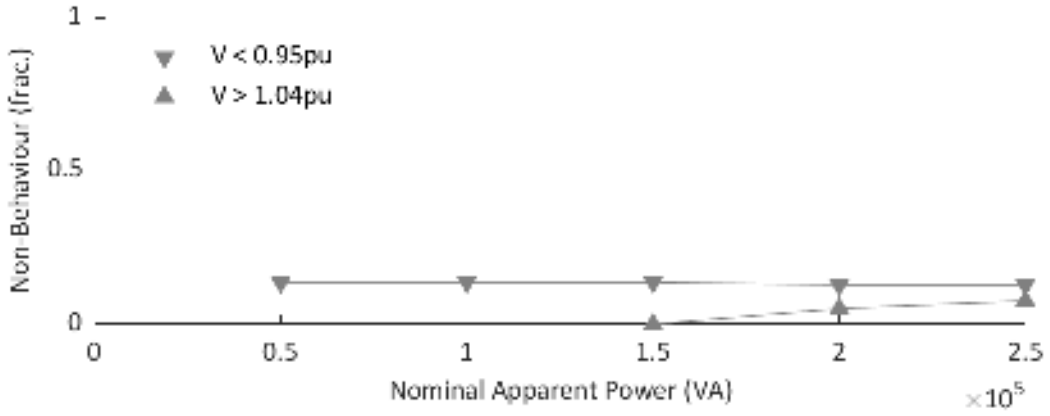

Figure 41: Fraction of Non-Behavioural Voltage Measurements for Line Switching Test Case 4

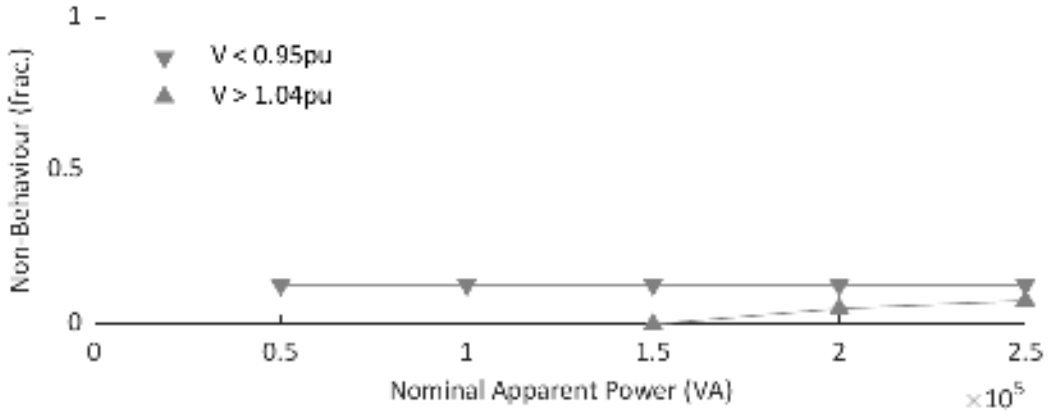

Figure 42: Fraction of Non-Behavioural Voltage Measurements for Line Switching Test Case 5

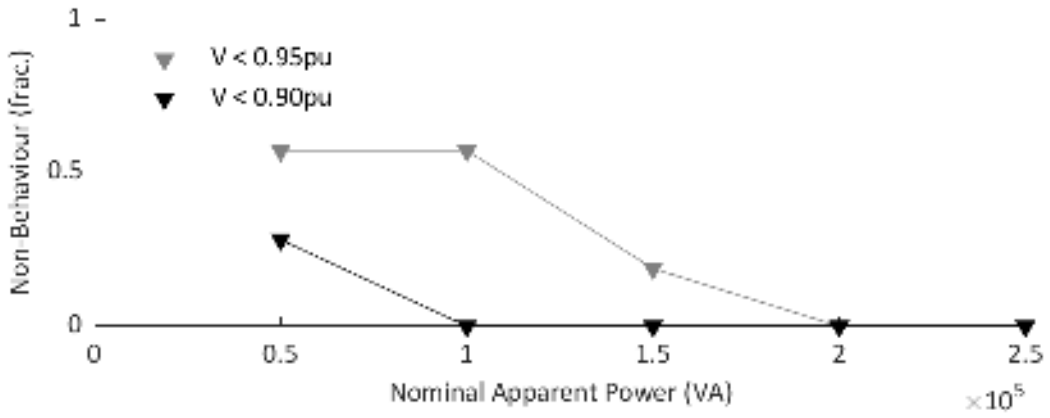

Figure 43: Fraction of Non-Behavioural Voltage Measurements for Line Switching Test Case 8

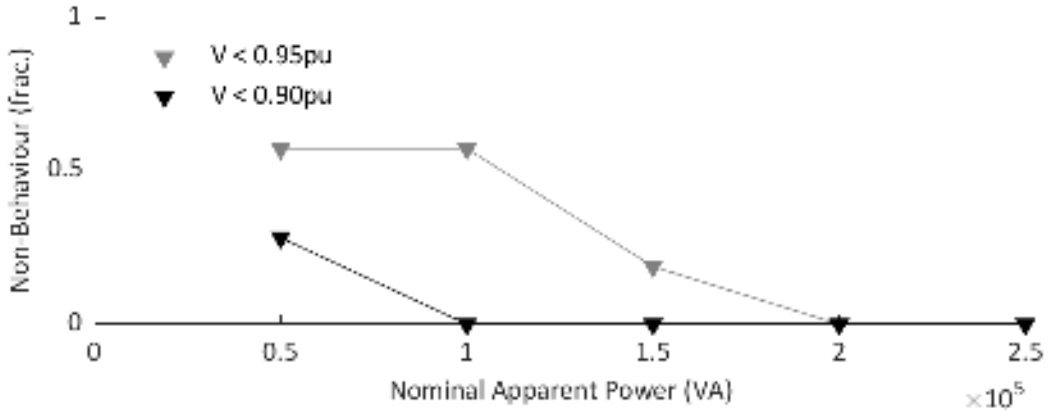

Figure 44: Fraction of Non-Behavioural Voltage Measurements for Line Switching Test Case 9

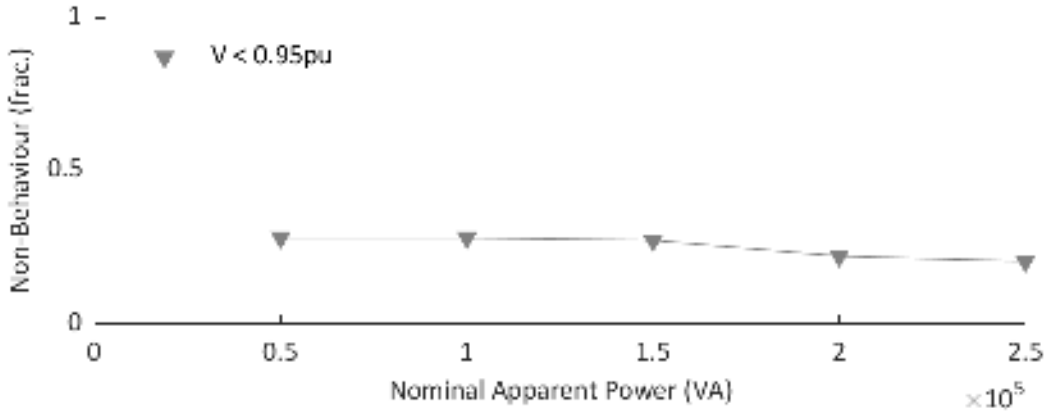

Figure 45: Fraction of Non-Behavioural Voltage Measurements for Line Switching Test Case 10

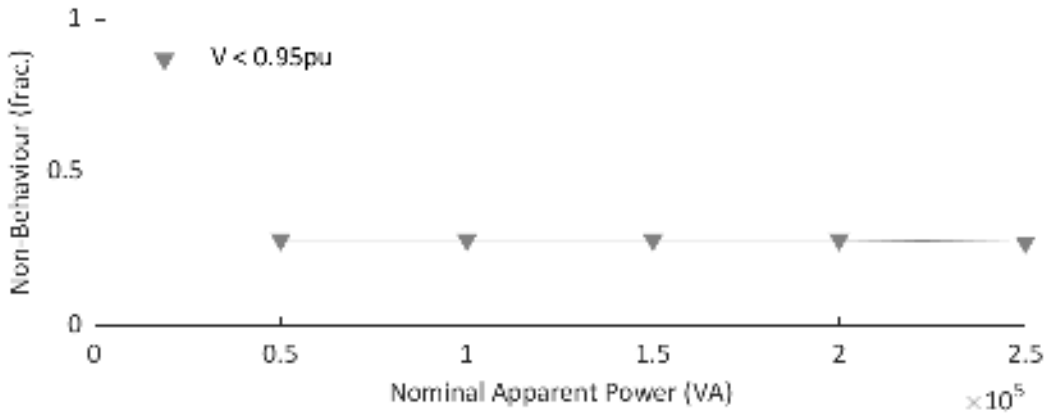

Figure 46: Fraction of Non-Behavioural Voltage Measurements for Line Switching Test Case 11

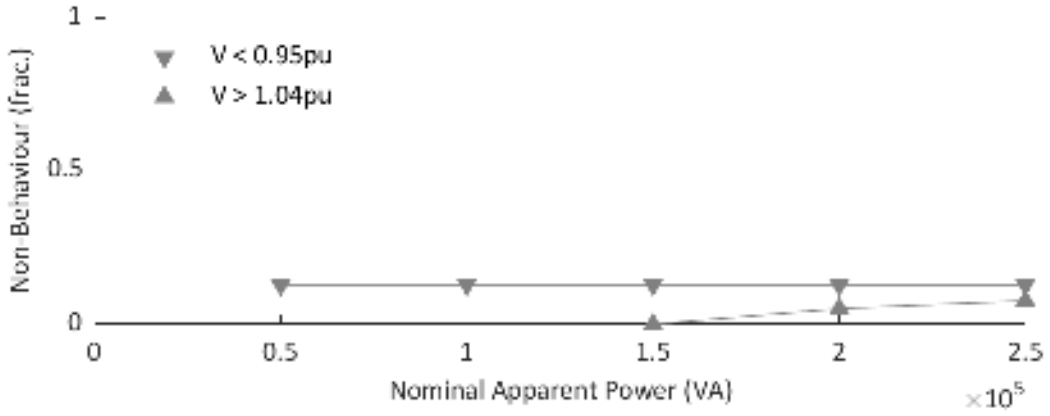

Figure 47: Fraction of Non-Behavioural Voltage Measurements for Line Switching Test Case 12

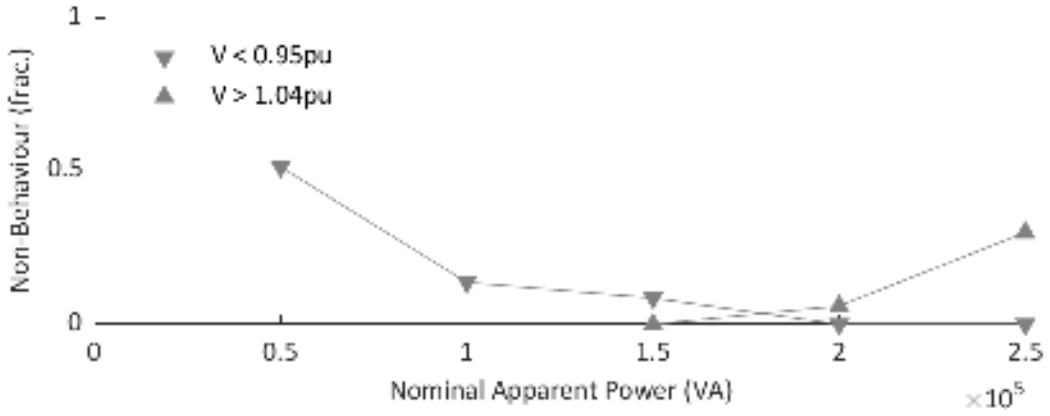

Figure 48: Fraction of Non-Behavioural Voltage Measurements for Line Switching Test Case 13

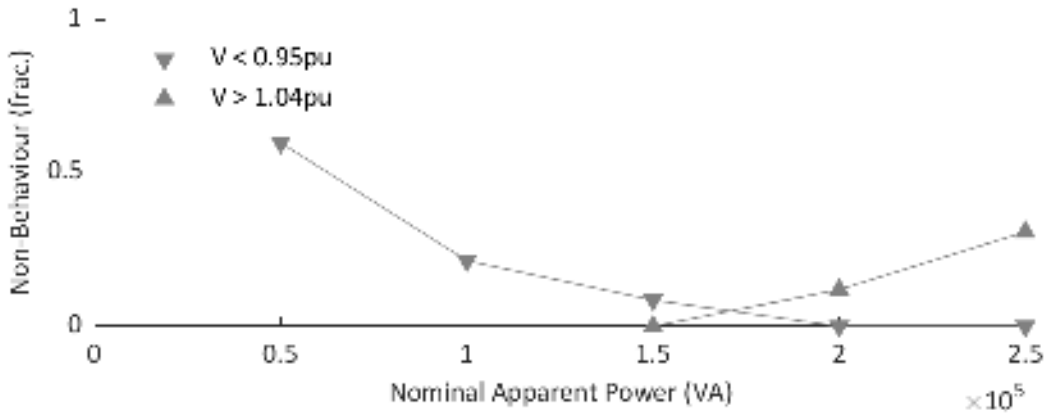

Figure 49: Fraction of Non-Behavioural Voltage Measurements for Line Switching Test Case 14

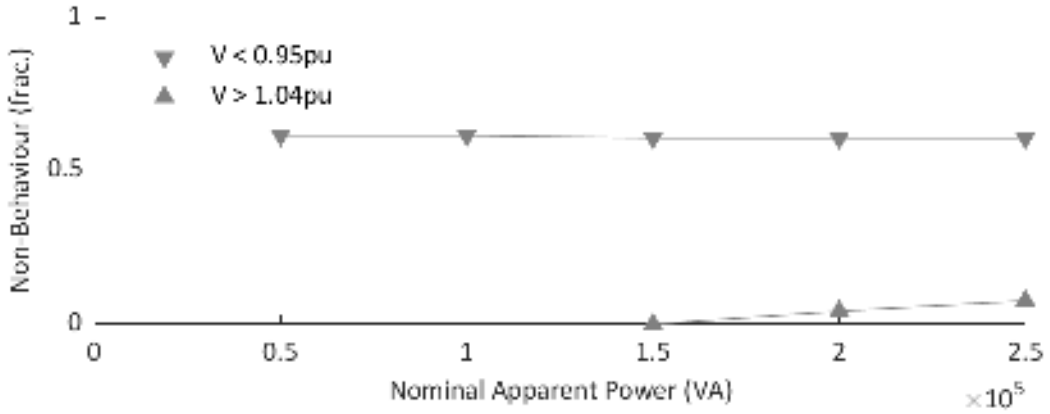

Figure 50: Fraction of Non-Behavioural Voltage Measurements for Line Switching Test Case 15

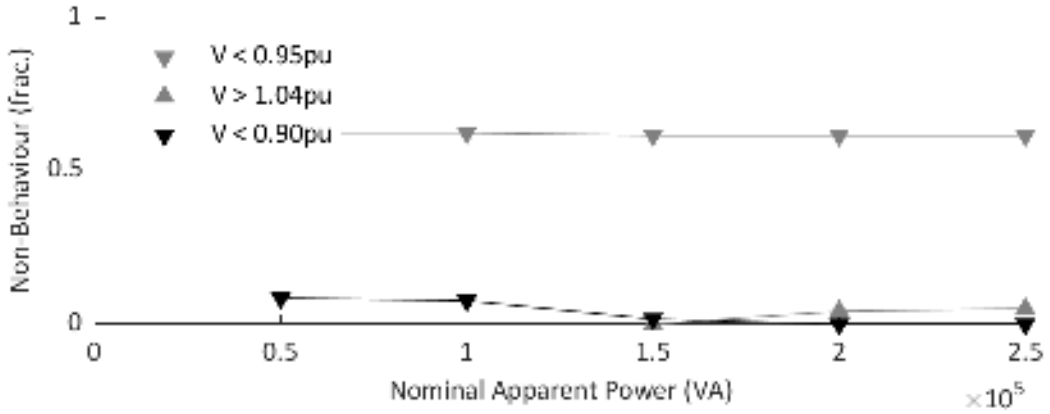

Figure 51: Fraction of Non-Behavioural Voltage Measurements for Line Switching Test Case 16

4.7.2 Generator G3N

This section to be completed pending results of the G3N simulations

The results of the simulations performed for G3N are provided in Figure 52 to Figure 67. No frequency thresholds were exceeded for any of the scenarios.

Figure 52, Figure 53, Figure 57 and Figure 58 (test cases 1, 2, 6, and 7) show that a minimal number of under voltage thresholds are exceeded for the proposed system configuration, with S6109 closed; S3788 open, opening, or closing; and S9609 open or closing. The under voltage thresholds exceeded in these scenarios differ from those of G2 (in the previous subsection) and G4 (in the following subsection), largely due to the increase system load (680kW vs 400-415kW).

Figure 54 to Figure 56 (test cases 3-5) show that the opening or closing of S6109 has a minimal impact on the system stability. The exceeded thresholds are largely due to the low voltage issue observed in the existing system, as discussed in more detail in the results of the energy balance simulations.

Figure 59 and Figure 60 (test cases 8 and 9) show that a significant number of under voltage thresholds are exceeded for 100% load on feeder 2 in the proposed system configuration. The fraction of non-behaviour decreases as the solar plant capacity increases, due to the location of the solar plant reducing the power flow through the feeder to the furthest end of the feeder.

Figure 61 and Figure 62 (test cases 10 and 11) show that, while still significant, a reduced number of under voltage thresholds are exceeded for 100% load on feeder 1 in the proposed system configuration as compared to 100% load on feeder 2. The fraction of non-behaviour was found to be minimally affected by the solar plant capacity.

Figure 63 shows that the closing of S9609 (test case 12), while in the existing system configuration, has a minimal impact on the system stability. The exceeded thresholds are largely due to the low voltage issue observed in the existing system, as discussed in more detail in the results of the energy balance simulations.

Figure 64 (test case 13) was inconsistent with Figure 65 (test case 14). Figure 65 showed that a significant number of voltage thresholds are exceeded for 100% load on feeder 2 in the existing system configuration. The fraction of non-behaviour for under voltage decreases with increasing solar plant capacity; however, the fraction of non-behaviour for over voltage increases with increasing solar plant capacity. The cause of the inconsistency is, as of yet, unexplained and requires further investigation.

Figure 66 and Figure 67 (test cases 15 and 16) show that a significant number of under voltage thresholds are exceeded for 100% load on feeder 1 in the existing system configuration. The fraction of non-behaviour for under voltage was found to be minimally affected by the solar plant capacity; however, high solar plant capacities led to a small fraction of non-behaviour for over voltage.

In all cases, system instability was not observed to be caused by line switching, as evidence by comparison of the steady-state and switching test cases. System frequency was not observed to be impacted by line switching; however, due to the magnitude of non-behavioural voltage

measurements, the simulation of the system loads with voltage dependence may cause changes in demand during switching events that could lead to larger frequency swings in the system.

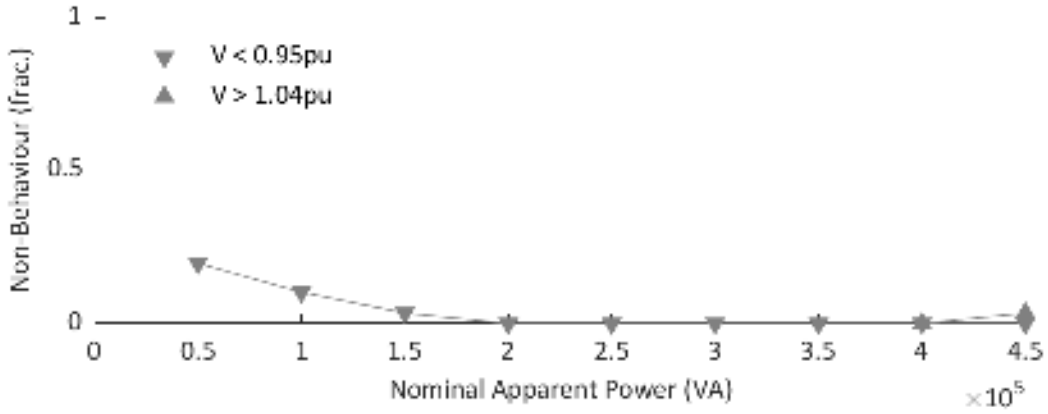

Figure 52: Fraction of Non-Behavioural Voltage Measurements for Line Switching Test Case 1

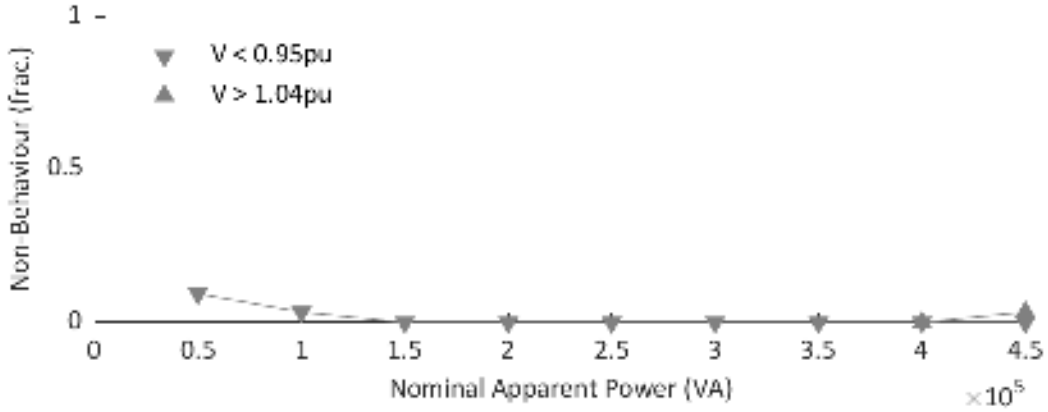

Figure 53: Fraction of Non-Behavioural Voltage Measurements for Line Switching Test Case 2

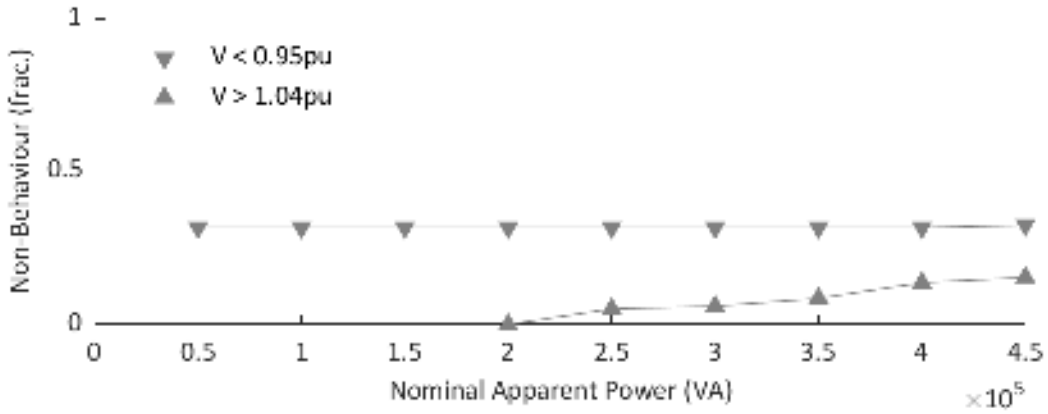

Figure 54: Fraction of Non-Behavioural Voltage Measurements for Line Switching Test Case 3

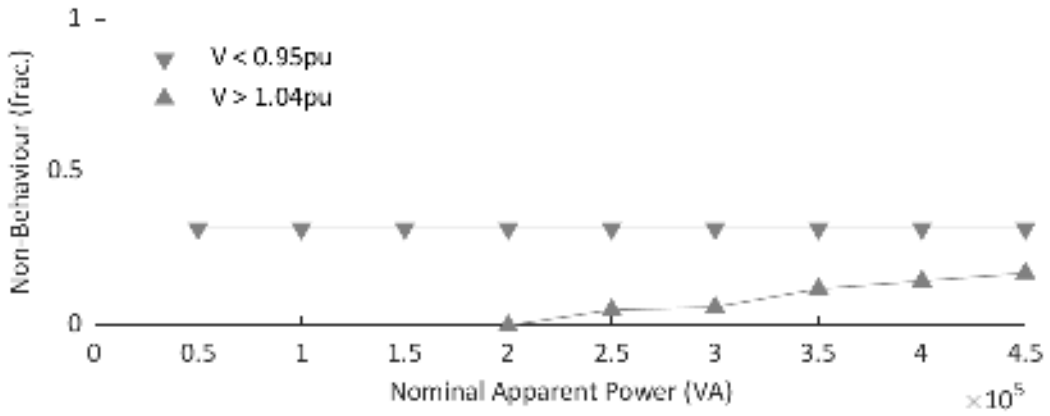

Figure 55: Fraction of Non-Behavioural Voltage Measurements for Line Switching Test Case 4

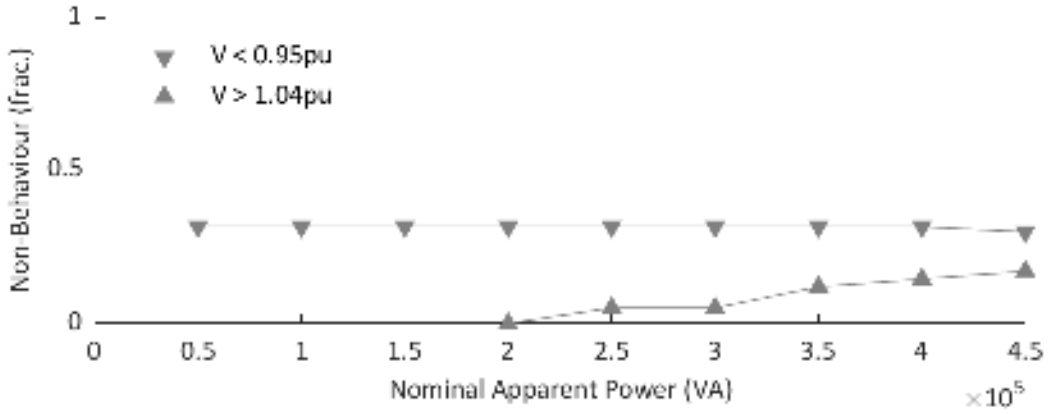

Figure 56: Fraction of Non-Behavioural Voltage Measurements for Line Switching Test Case 5

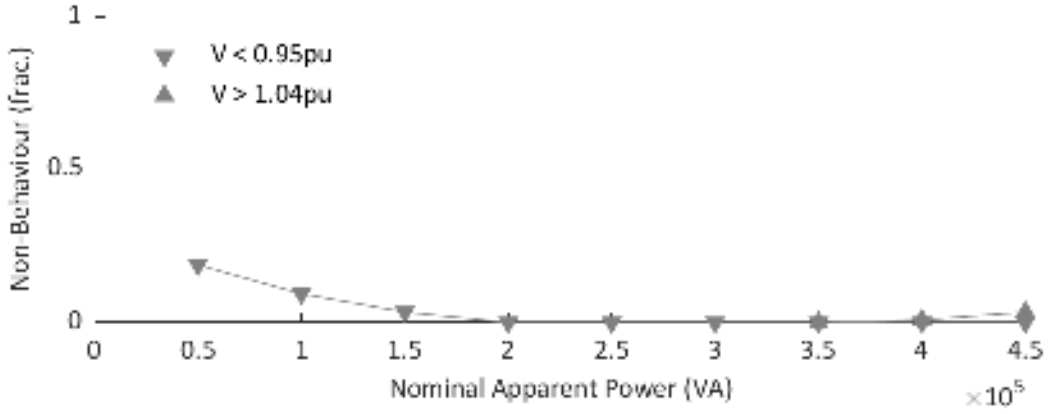

Figure 57: Fraction of Non-Behavioural Voltage Measurements for Line Switching Test Case 6

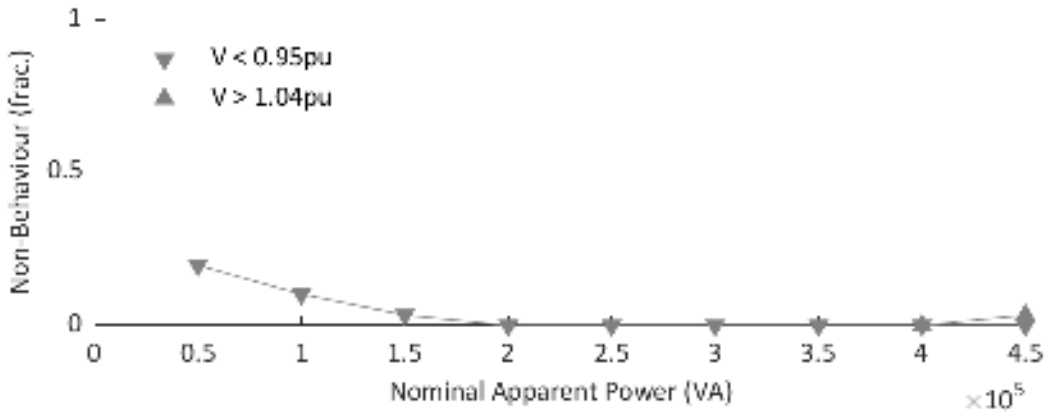

Figure 58: Fraction of Non-Behavioural Voltage Measurements for Line Switching Test Case 7

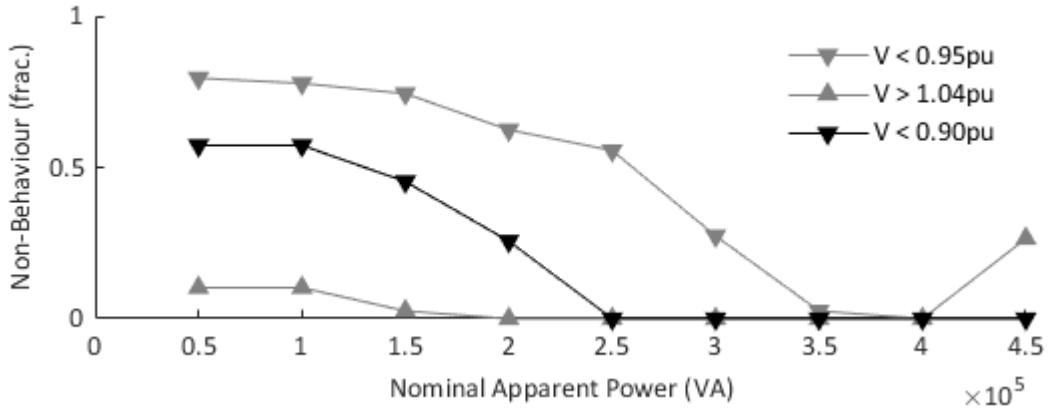

Figure 59: Fraction of Non-Behavioural Voltage Measurements for Line Switching Test Case 8

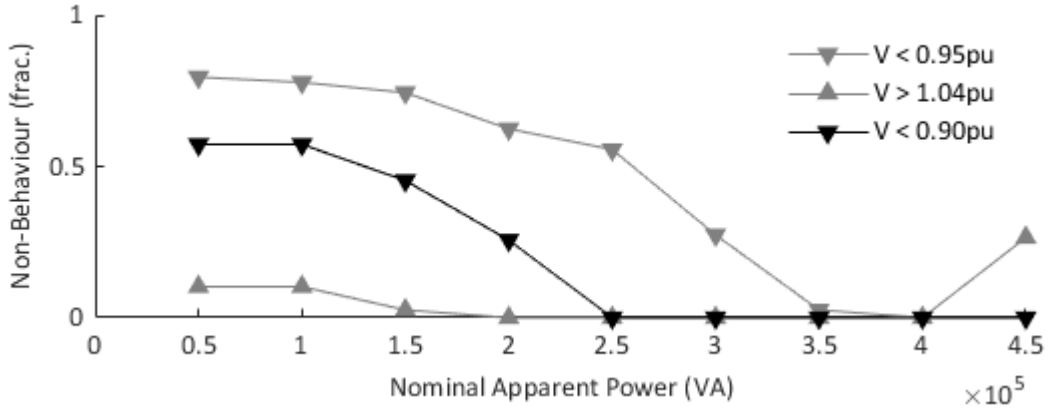

Figure 60: Fraction of Non-Behavioural Voltage Measurements for Line Switching Test Case 9

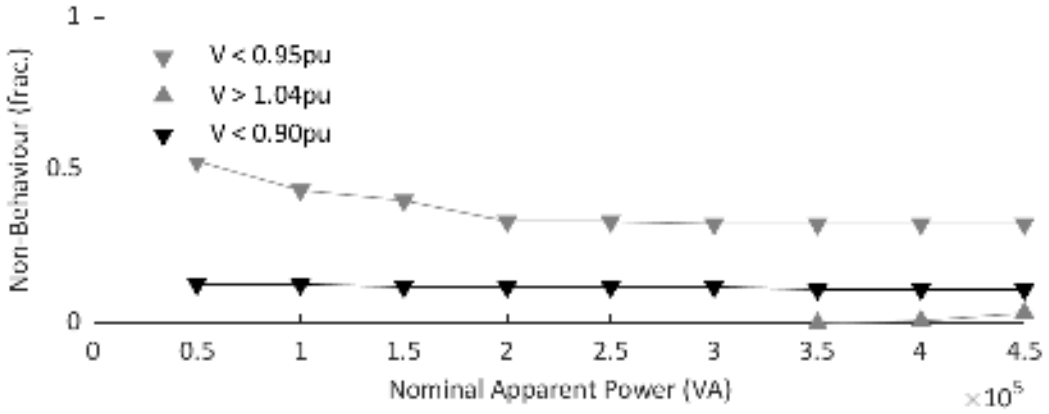

Figure 61: Fraction of Non-Behavioural Voltage Measurements for Line Switching Test Case 10

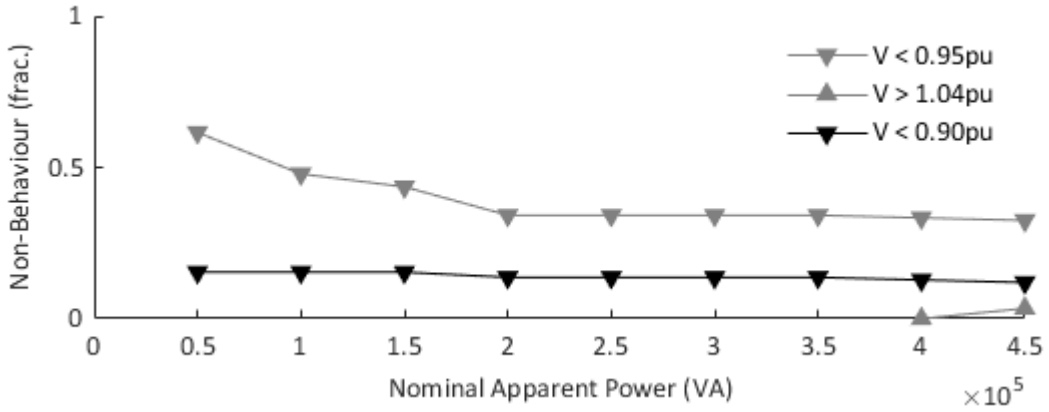

Figure 62: Fraction of Non-Behavioural Voltage Measurements for Line Switching Test Case 11

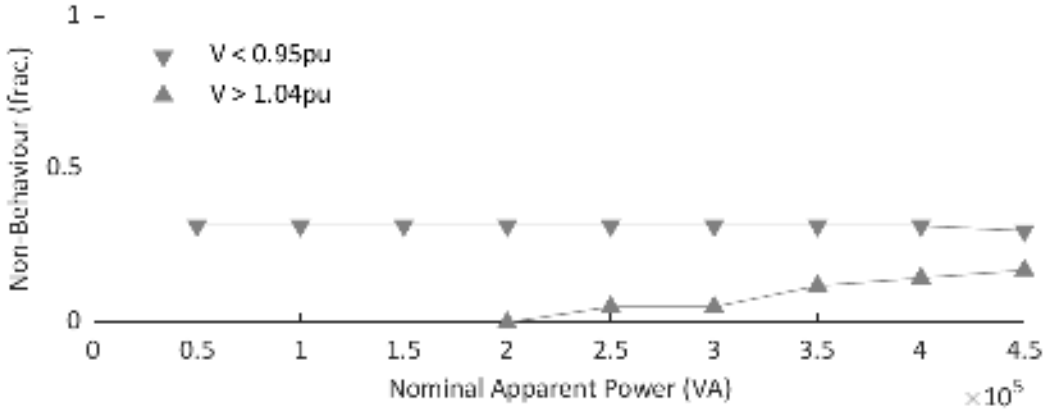

Figure 63: Fraction of Non-Behavioural Voltage Measurements for Line Switching Test Case 12

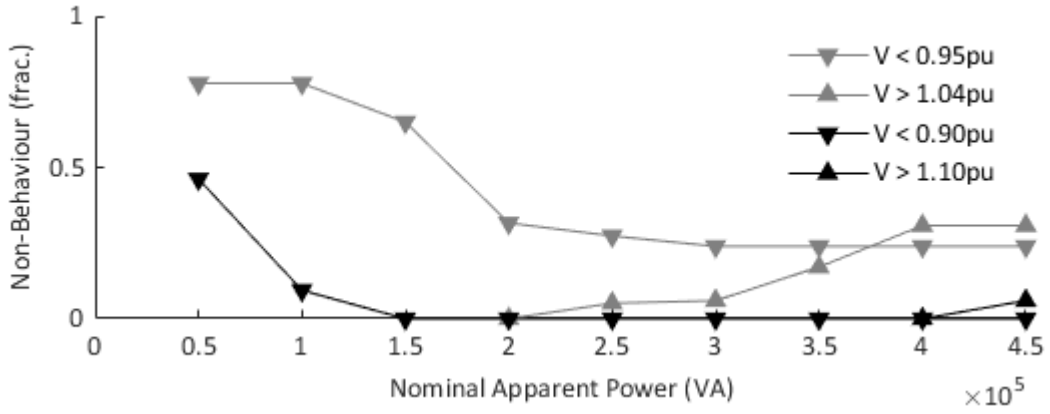

Figure 64: Fraction of Non-Behavioural Voltage Measurements for Line Switching Test Case 13

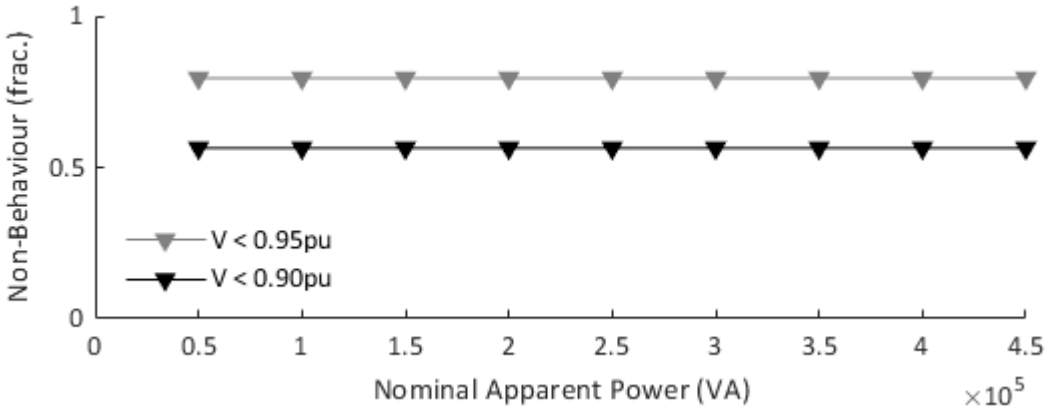

Figure 65: Fraction of Non-Behavioural Voltage Measurements for Line Switching Test Case 14

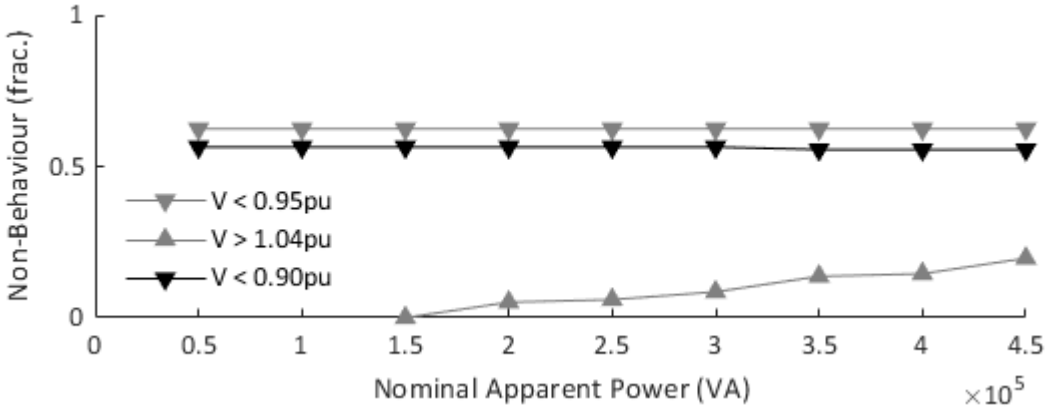

Figure 66: Fraction of Non-Behavioural Voltage Measurements for Line Switching Test Case 15

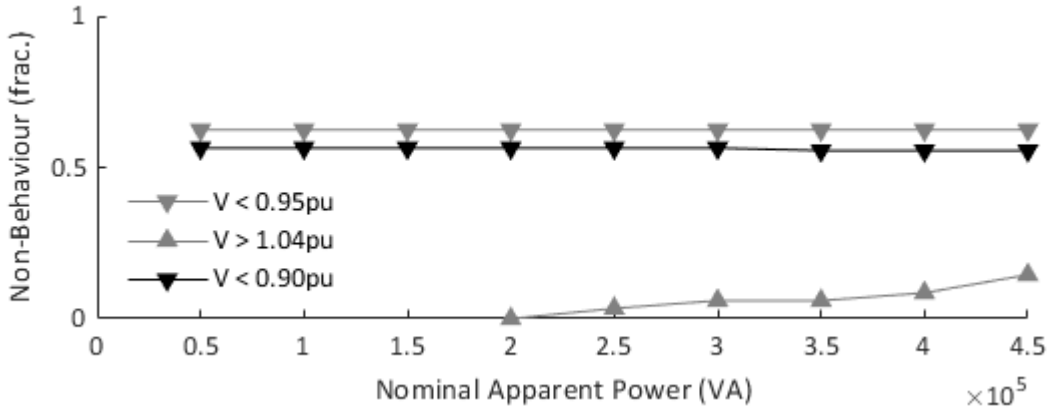

Figure 67: Fraction of Non-Behavioural Voltage Measurements for Line Switching Test Case 16

4.7.3 Generator G4

The results of the simulations performed for G4 are provided in Figure 68 to Figure 79. No voltage thresholds were exceeded for any scenarios for test cases 1, 2, 6, and 7. These test cases essentially define the proposed system configuration, with S6109 closed; S3788 open, opening, or closing; and S9609 open or closing. Furthermore, no frequency thresholds were exceeded for any of the scenarios.

Figure 68 to Figure 70 (test cases 3-5) show that the opening or closing of S6109 has a minimal impact on the system stability. The exceeded thresholds are largely due to the low voltage issue observed in the existing system, as discussed in more detail in the results of the energy balance simulations.

Figure 71 and Figure 72 (test cases 8 and 9) show that a significant number of under voltage thresholds are exceeded for 100% load on feeder 2 in the proposed system configuration. The fraction of non-behaviour decreases as the solar plant capacity increases, due to the location of the solar plant reducing the power flow through the feeder to the furthest end of the feeder.

Figure 73 and Figure 74 (test cases 10 and 11) show that, while still significant, a reduced number of under voltage thresholds are exceeded for 100% load on feeder 1 in the proposed system configuration as compared to 100% load on feeder 2. The fraction of non-behaviour was found to be minimally affected by the solar plant capacity.

Figure 75 (test case 12) shows that the closing of S9609, while in the existing system configuration, has a minimal impact on the system stability. The exceeded thresholds are largely due to the low voltage issue observed in the existing system, as discussed in more detail in the results of the energy balance simulations.

Figure 76 and Figure 77 (test cases 13 and 14) show that a significant number of voltage thresholds are exceeded for 100% load on feeder 2 in the existing system configuration. The fraction of non-behaviour for under voltage decreases with increasing solar plant capacity; however, the fraction of non-behaviour for over voltage increases with increasing solar plant capacity.

Figure 78 and Figure 79 (test cases 15 and 16) show that a significant number of under voltage thresholds are exceeded for 100% load on feeder 1 in the existing system configuration. The fraction of non-behaviour for under voltage was found to be minimally affected by the solar plant capacity; however, high solar plant capacities led to a small fraction of non-behaviour for over voltage.

In all cases, system instability was not observed to be caused by line switching, as evidence by comparison of the steady-state and switching test cases. System frequency was not observed to be impacted by line switching; however, due to the magnitude of non-behavioural voltage measurements, the simulation of the system loads with voltage dependence may cause changes in demand during switching events that could lead to larger frequency swings in the system.

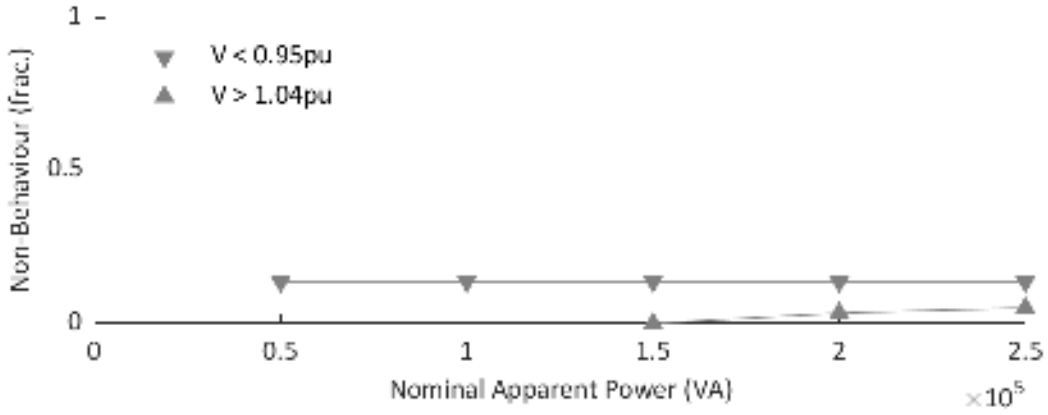

Figure 68: Fraction of Non-Behavioural Voltage Measurements for Line Switching Test Case 3

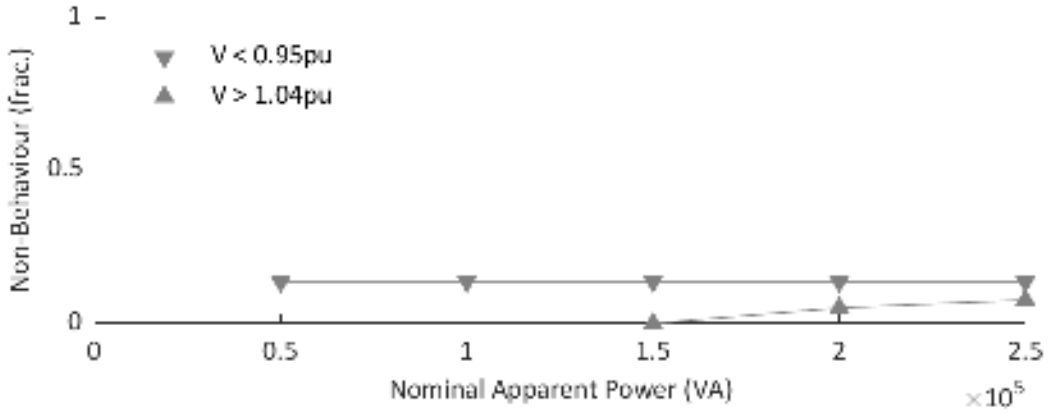

Figure 69: Fraction of Non-Behavioural Voltage Measurements for Line Switching Test Case 4

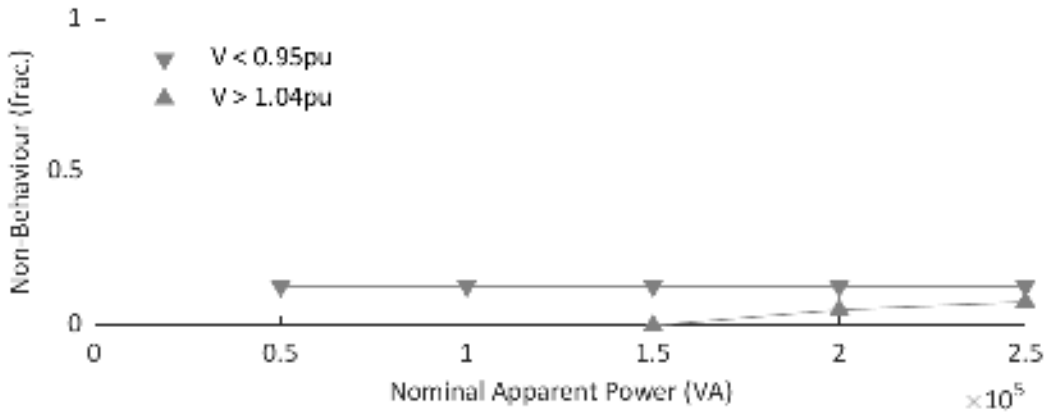

Figure 70: Fraction of Non-Behavioural Voltage Measurements for Line Switching Test Case 5

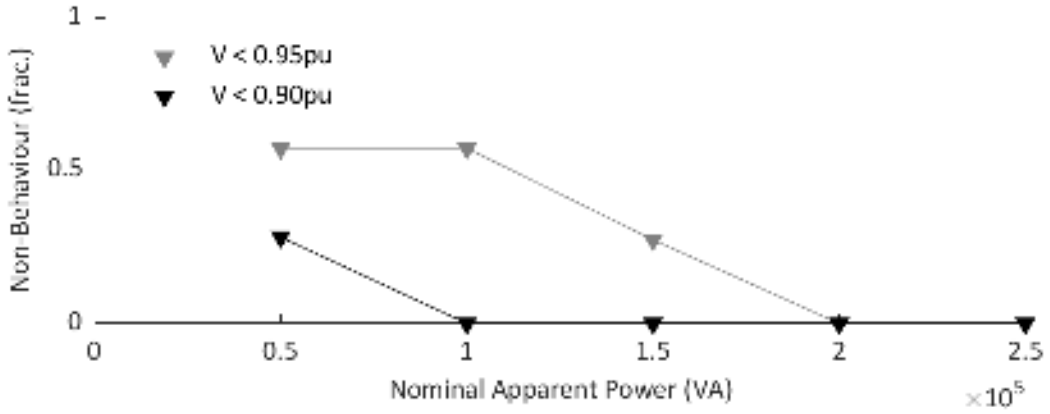

Figure 71: Fraction of Non-Behavioural Voltage Measurements for Line Switching Test Case 8

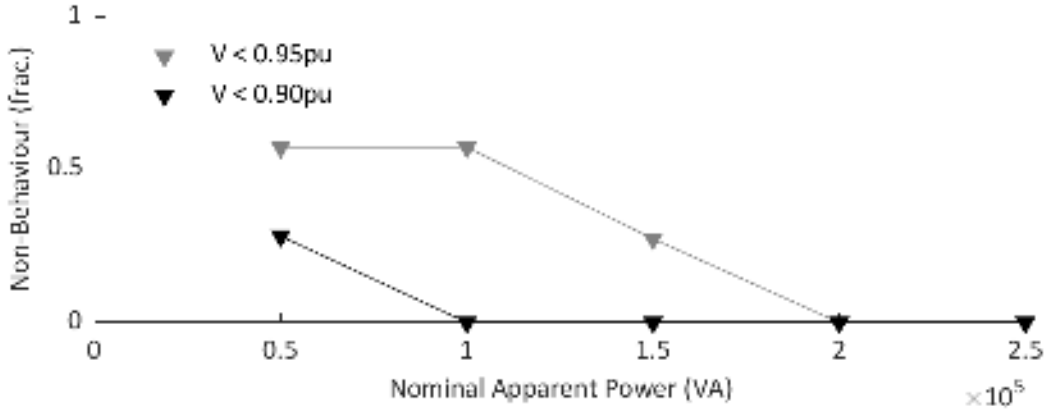

Figure 72: Fraction of Non-Behavioural Voltage Measurements for Line Switching Test Case 9

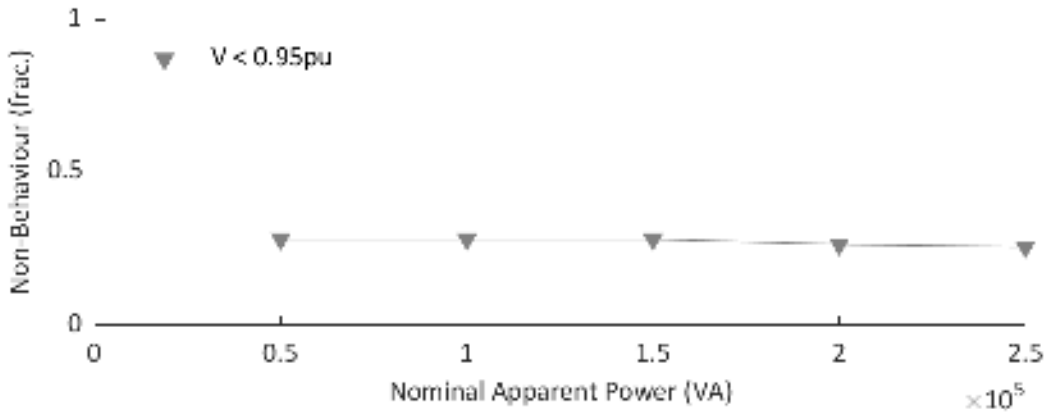

Figure 73: Fraction of Non-Behavioural Voltage Measurements for Line Switching Test Case 10

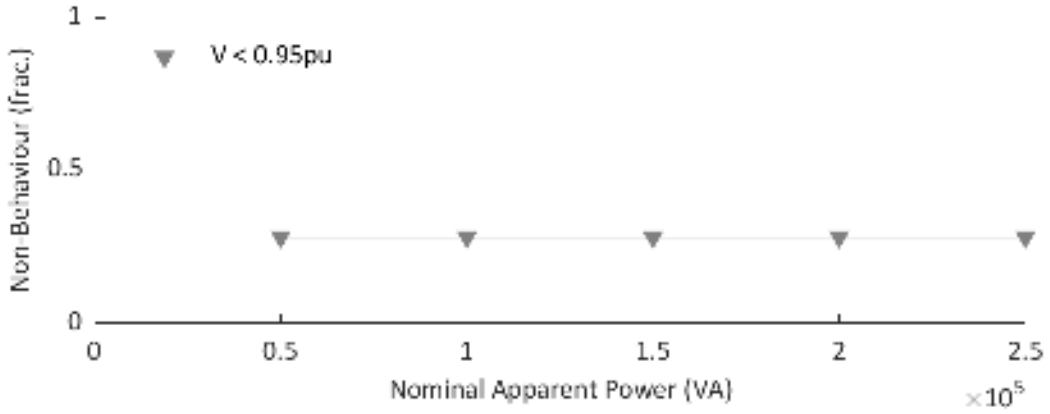

Figure 74: Fraction of Non-Behavioural Voltage Measurements for Line Switching Test Case 11

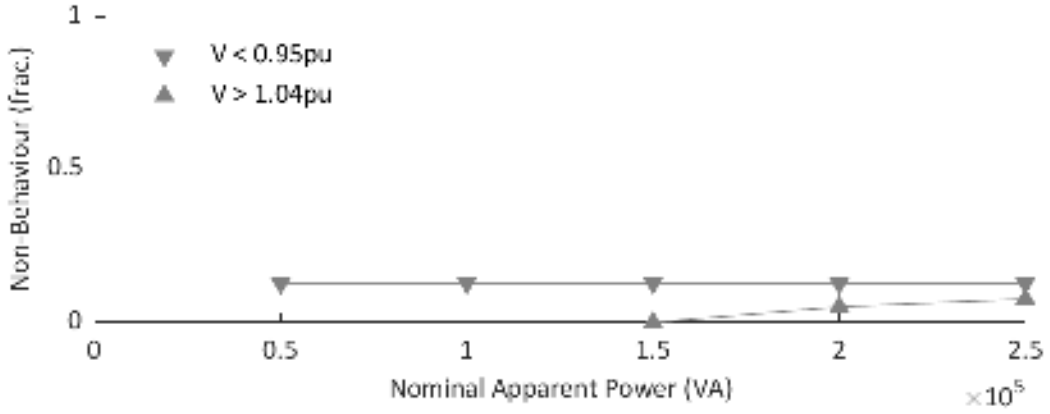

Figure 75: Fraction of Non-Behavioural Voltage Measurements for Line Switching Test Case 12

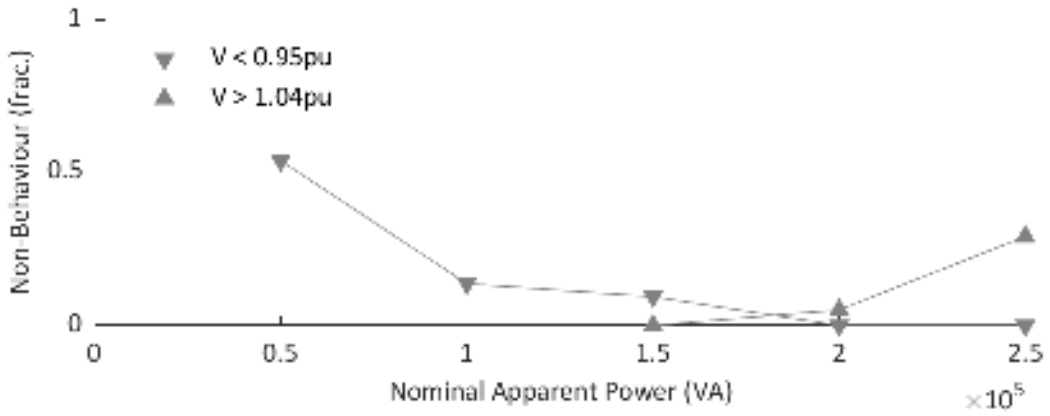

Figure 76: Fraction of Non-Behavioural Voltage Measurements for Line Switching Test Case 13

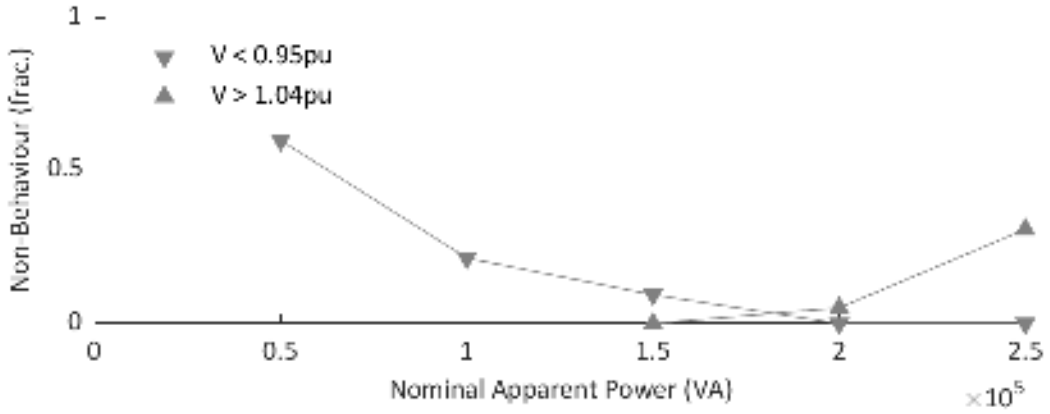

Figure 77: Fraction of Non-Behavioural Voltage Measurements for Line Switching Test Case 14

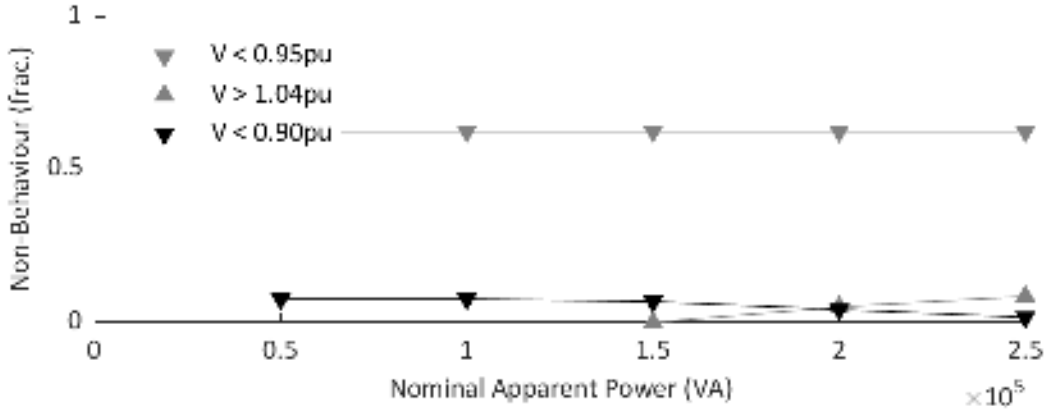

Figure 78: Fraction of Non-Behavioural Voltage Measurements for Line Switching Test Case 15

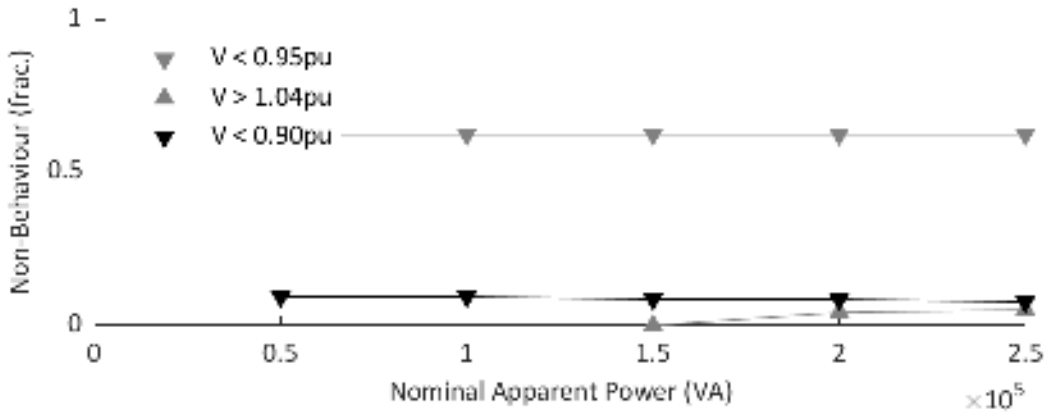

Figure 79: Fraction of Non-Behavioural Voltage Measurements for Line Switching Test Case 16

4.7.4 Summary

In all cases for each of the generators, system instability was not observed to be caused by line switching, as evidence by comparison of the steady-state and switching test cases. The proposed system configuration led to a reduction in exceeded under voltage thresholds over the existing system configuration; however, in either system configuration there was a significant fraction of non-behaviour for under voltage for 100% load on either feeder 1 or 2. System frequency was not observed to be impacted by line switching; however, due to the magnitude of non-behavioural voltage measurements, the simulation of the system loads with voltage dependence (as compared to constant impedance loads) may cause changes in demand during switching events that could lead to larger frequency swings in the system.

4.8 WIND SIMULATIONS

The feasibility of wind power within the Old Crow grid is evaluated through the energy balance studies. The wind generation profile provided by VGG is scaled to represent a wind farm of 0 to 10 turbines. The behaviour of the system is measured on multiple fronts: Total time diesel off, the number diesel off times through 1 to 24 hours, curtailment, ESS cycling, and renewable energy penetration. These parameters are examined for two ESS energy capacities of 616 kWh and 822 kWh as defined by VGG.

By examining the number of non-consecutive days of diesel off, it is found that the difference in energy capacity of the ESS has little change over the amount of time the diesel generators spend offline. Increasing the number of wind turbines in the system increases the amount of time the diesel

plant is inactive, increasing from 89 non-consecutive days for zero turbines to 249 non-consecutive days for ten turbines, as shown in Figure 80.

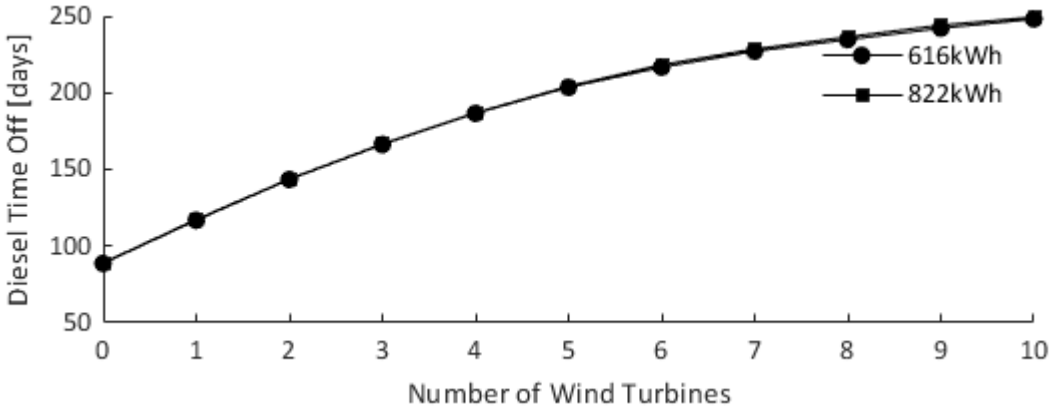

Figure 80: Diesel off times for examined ESS capacities of 616 and 822 kWh

The diesel off information can be broken down further, examining the number of times that the diesel plant is shut off for 1 to 2, 2 to 4, 4 to 6, 6 to 8, 8 to 12, 12 to 24 and greater than 24 hour timespans. Figure 81 shows the breakdown of the diesel time off timespans for a 616 kWh ESS. A high number of 1 to 2, 2 to 4 and 12 to 24 hour discharge times are observed proportionally to the other time bins. Despite the high number of 1 hour discharges, no discharges under 1 hour were observed within the simulations.

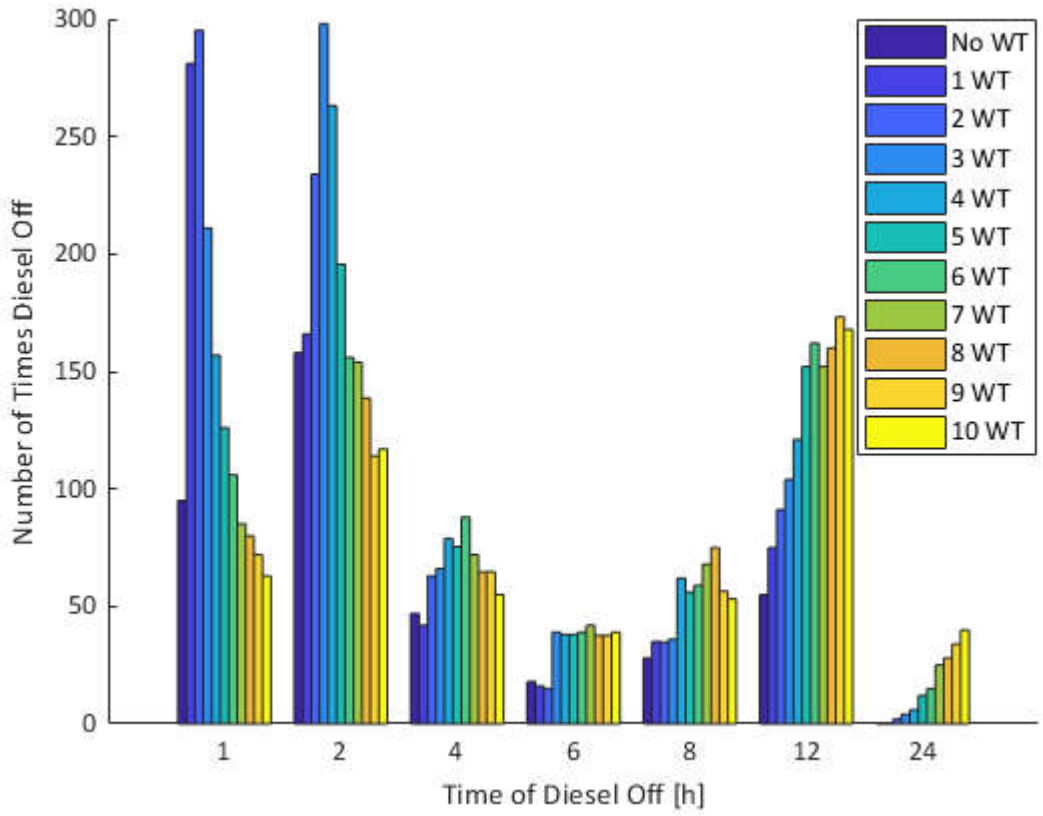

Figure 81: Histogram showing the number of diesel off times for specific timespans and wind plant size for a 616 kWh ESS.

Similarly, Figure 82 shows the histogram of diesel off timespans for the 822 kWh ESS. Similar to the smaller ESS a proportionally large number of discharges in the 2 to 4 hour timespan are observed. However, there were significantly fewer 1 to 2 hour discharges. Slight increases to the 4 hour and greater discharge time bins observed, however these are minimal. Furthermore, no discharges under 1 hour were observed for an ESS capacity of 822 kWh.

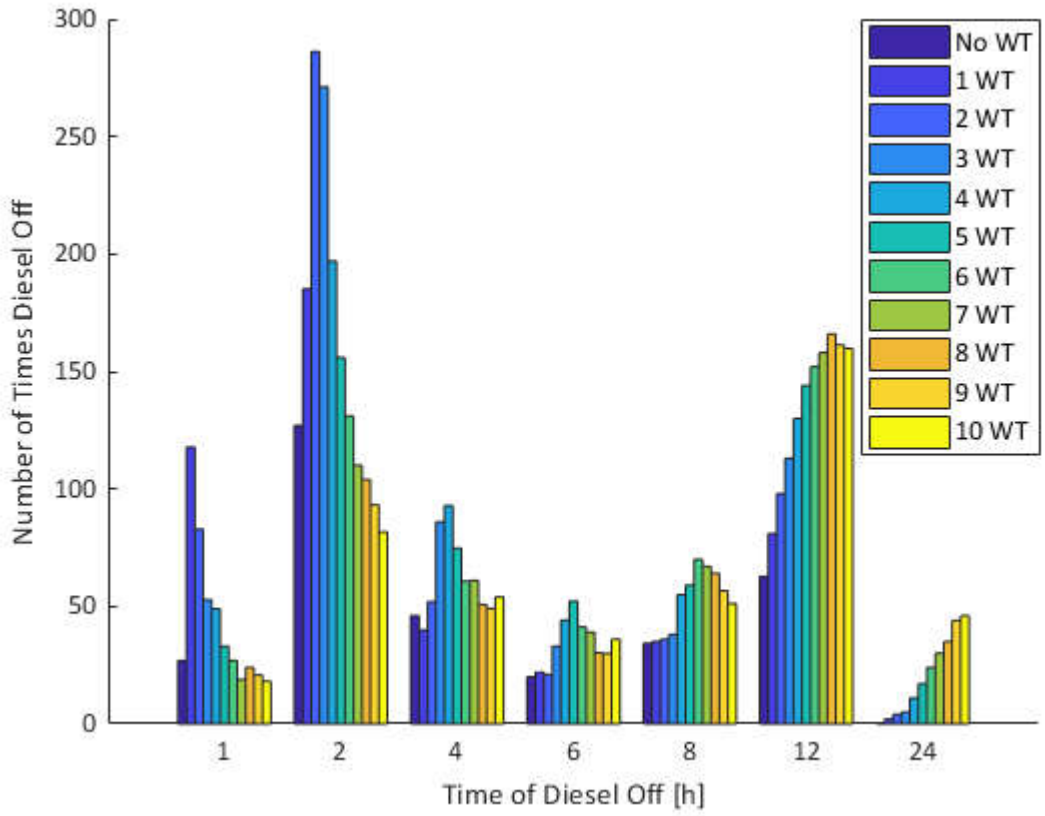

Figure 82: Histogram showing the number of diesel off times for specific timespans and wind plant size for an 822 kWh ESS.

Similar to the total diesel off time, the variation in ESS energy capacity has little influence over the amount of curtailed renewable resource. Figure 83 shows that increasing the number of wind turbines increases the amount of curtailed energy. With no curtailment each wind turbine could produce an estimated 2.62×10^5 kWh of energy to the grid. A wind plant of 7 wind turbines or greater curtails a greater amount of energy than any one wind turbine could be expected to produce.

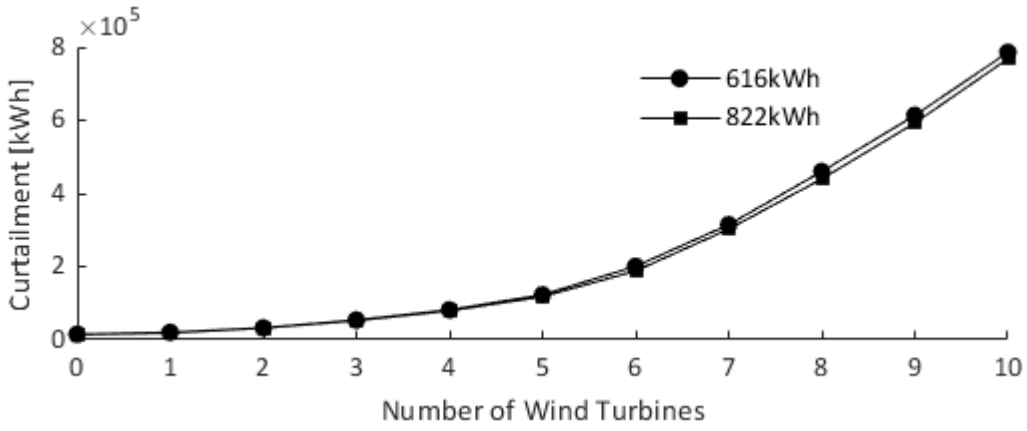

Figure 83: Total energy curtailed with respect to the number of wind turbines for 616 and 822 kWh energy capacities.

The introduction of wind turbines to the system increases the number of cycles undergone by the ESS. Unlike previous examined parameters the cycling of the ESS is highly dependent on the energy capacity, as shown in Figure 84. The decrease in the number of cycles of the battery with greater than 3 turbines is likely due to the wind plant's ability to provide the entire system demand for extended periods of time. This allows the battery to control voltage and frequency without charging or discharging.

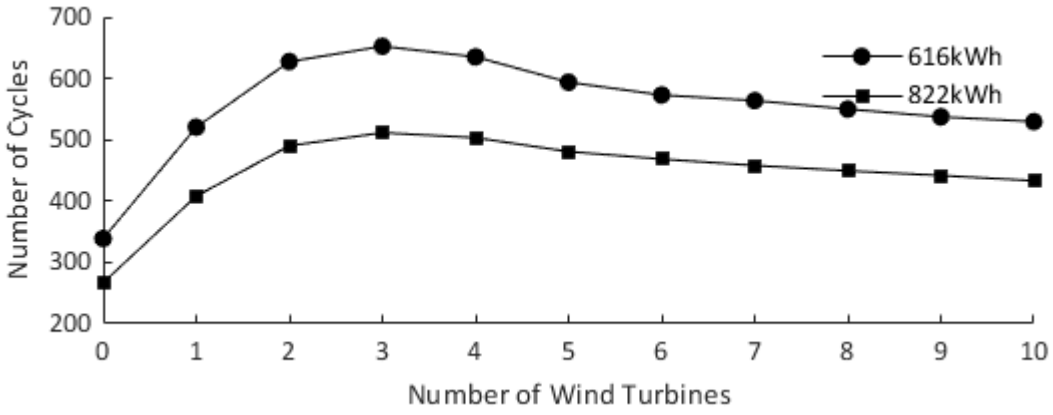

Figure 84: Number of total cycles of the ESS with respect to the number of wind turbines on the system.

It can be observed that the larger capacity of ESS experiences significantly less cycles than that of the smaller. This will dictate the lifespan of the ESS. Typically, a lithium battery is expected to provide 10,000 cycles before reaching 70 to 80% of its original capacity [7]. Ignoring the deterioration due to cycles it is observed that with 3 wind turbines connected, the peak number of cycles for both ESS are 511.5 and 652.4 for the 822 kWh and 616 kWh. With this amount of cycling observed, the expected life cycle of the ESS is expected to be 19.5 and 15.3 years respectively.

The penetration of these renewables is examined through both the average and maximum penetration. The average penetration of renewables on the system increases with diminishing returns as the number of wind turbines on the system increases, as seen in Figure 85. Slight deviations between the examined ESS energy capacities are observed, however minimal deviation is found.

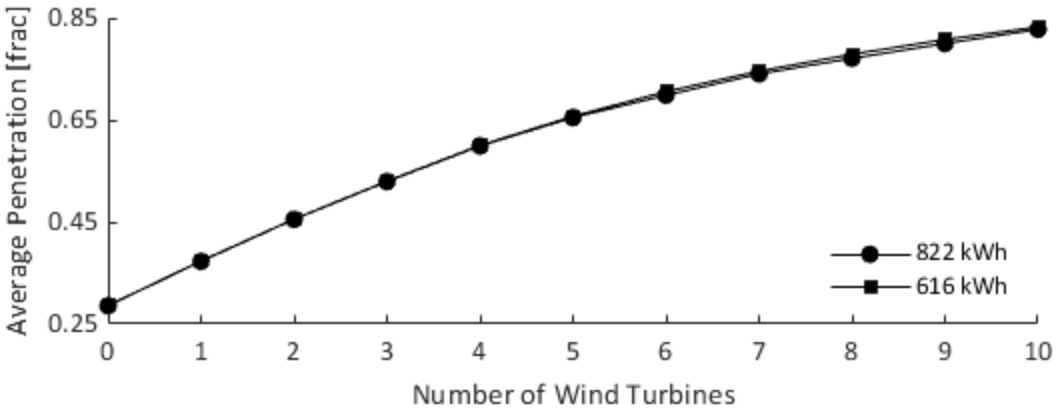

Figure 85: Average penetration of renewables with respect to the number of installed wind turbines.

The maximum penetration of renewables is observed to increase in a near linear fashion from 1.9 to 5.8, as shown in Figure 86. This expresses the difference between the average and instantaneous power penetration. Again, minimal deviation is observed between the energy storage capacities.

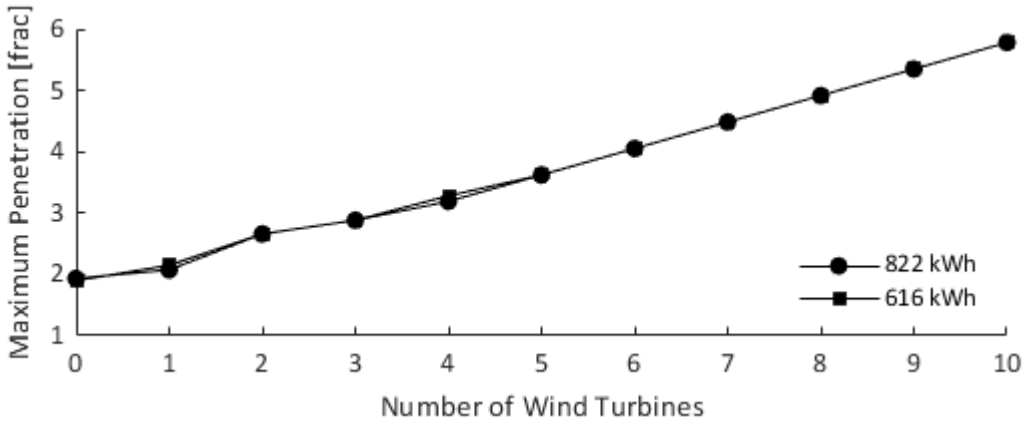

Figure 86: Maximum penetration of renewables with respect to the number of installed wind turbines.

Figure 87 shows the fuel consumed by the diesel generators with respect to the number of installed wind turbines, which is seen to decrease. The increase of wind turbines on the system is shown to decrease the amount of fuel consumed from 684,000 litres for no wind plant to 277,000 litres with ten wind turbines. The fuel consumption appears to follow a similar logarithmic trend to that of fuel consumption and curtailment. It can be concluded that there is a strong correlation these three

parameters. Furthermore, no discernable difference in fuel consumption is be observed between the examined energy capacities.

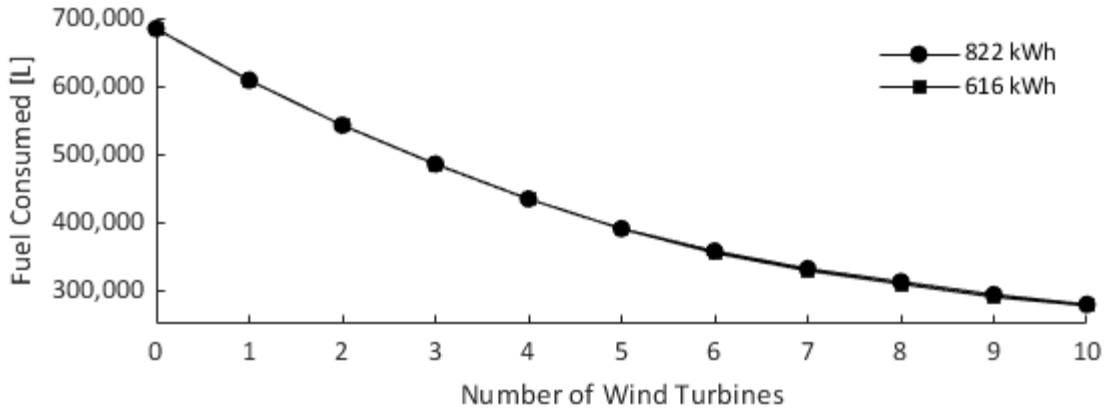

Figure 87: Fuel Consumption with respect to the number of installed wind turbines.

These results illustrate the behavior of the system with the introduction of multiple wind turbines and a varied energy capacity of the ESS through energy balance.

This study focuses exclusively on the energy balance of the system, and did not investigate the system voltages, line loading, protection, or stability. This study is intended as a preliminary investigation to provide insight on the impact of the proposed ESS capacities with consideration given to the potential of a wind farm. Given the potentially large power input of the wind farm at a remote location on the distribution system, it is expected that some means of voltage regulation will be required to address fluctuating voltages and voltage rise (similar to the voltage rise observed with the solar plant). Further investigation is required to conclude on the feasibility of the proposed wind farm; however, it is clear that the 822 kWh ESS capacity will reduce the battery cycling, thereby improving the life expectancy of the ESS by 4.2 years when compared to the 616 kWh ESS. Apart from the differences in cycling, little to no difference is observed between the examined ESS energy capacities.

5 CONCLUSION AND RECOMMENDATION

From the energy balance analysis, flags are identified regarding several factors. Over-production of solar (resulting in spilling) and over-loading of the battery in the simulations indicate an energy imbalance and are recorded. Flags are also identified when the energy storage system exits from the discharge state before 1 hour of being in voltage control mode, which indicates battery sizing (energy and/or power) limitations. Finally, line loading limits and voltage threshold violations indicate the potential for issues within the distribution system, and are recorded.

The voltage profile shows both under and over voltages on the system. The over-voltages particularly occur when the solar array is connected at bus 15691. The under-voltages occur on feeder 2; however,

this is in agreement with voltage profiles provided by ATCO from the CYME model, without the addition of PV and/or storage.

The current through the transmission lines never exceeds the set limits. This indicates that the thermal limits of the lines are never exceeded and line failures will not occur.

Modelling the size of the energy storage system over one year shows that every size is capable of discharging for up to 12 hours. However, only a few sizes are capable of discharging for up to 24 hours, and for only a few times each year. Sizing of the batteries show that for approximately 100 non-consecutive days every year, the diesel generator can be turned off. The flags of under one hour of discharge, and early exiting of the discharge state show that a capacity of 600 kWh and larger is required to avoid these errors. The dispatch logic used prevented the battery from experiencing demands that exceed the maximum power rating.

It was also found that larger battery sizes are not a solution for increasing diesel off hours. However, the lower the battery size, the more often the battery would complete a discharge cycle. Using a Saft estimate for battery life and the proposed battery logic, the 200 kWh battery may degrade before the anticipated lifespan of the project. Battery capacities of 600 kWh or larger experience less cycling and can be expected to have long life spans.

For the protection coordination study, it was found that R1N had relatively little impact on the protection coordination under the existing system. R1N contributed to a slight increase in the maximum observed current and a slight decrease in the clearing time of the fuses. Feeder relay operation was comparable both with and without R1N. The instantaneous time delay applied to the feeder 1B and feeder 2B over- and under-voltage relays prevented proper coordination with the fuses; however, this is an existing issue and is not caused by R1N. This study was not intended to select the protection settings of R1N; however, it will be important to select an appropriate anti-islanding protection scheme.

It was found that under normal operating conditions, generators G2 and G4 were capable of maintaining system frequency and voltage stability after the loss of a solar plant of 260kW and 270kW, respectively. The voltage was found to exceed the inner thresholds of 0.95pu and 1.04pu; however, this is likely due in part to the voltage rise on feeder 1 between the diesel generator and the point of interconnection of R1N, and voltage drop on feeder 2. A limitation on the maximum rate of change of active power of the solar PV plant is necessary to maintain system frequency and voltage during connection of the plant. Under abnormal operating conditions, generators G2 and G4 were found to have limitations on size of solar generation that could be lost instantaneously. A maximum solar plant size of 260kW is allowable under normal operating conditions without the implementation of an energy storage system and with 20.1kW of existing solar; however, this requires significant curtailment of the solar PV plant in order to maintain the minimum diesel generator loading at 30% of rated capacity.

The battery energy storage system was capable of maintaining system frequency and voltage under normal and abnormal operating conditions; however, a significant phase imbalance occurred which was likely due to the control system used in the model. It is apparent that the phase-locked loop used in the model did not have a sufficient response time to allow B1N to provide frequency support when operating in controlled-current mode.

Based on the methodology and results of the various studies, the following recommendations can be made:

1. Future system disturbances should be recorded for the purpose of generation model validation. System data should be recorded at a higher sampling rate than typically suggested in literature or other grid standards, due to the shorter timescale of system response relative to large interconnected grids. At minimum, voltage, frequency, active power, and reactive power at the point of interconnection should be recorded. Measurement resolution should be sufficient to ensure reasonable precision and accuracy. A 1/4-cycle sampling rate for 5s should provide sufficient data for validation; however, a 1/32-cycle sampling rate should provide sufficient resolution to observe the 2nd harmonics in an unbalanced system. Modern digital protective relays are typically capable of recording disturbances at a sufficient resolution.
2. The battery energy storage system should be specified:
    a. To maintain the phase imbalance at and acceptable level in an unbalanced system while in voltage and frequency control.
    b. To have a sufficient response time to maintain system frequency and voltage within the inner thresholds during a loss of 400kW of solar PV generation over 5 seconds.
    c. To have a phase-locked loop with sufficient response time to allow frequency support when the voltage-sourced converter is in controlled-current mode, if this type of control is required.
    d. To have sufficient fault current contribution to ensure proper protection coordination for the system when operated in diesel-off mode. Alternatively, a modification of the system protection should be implemented to allow the reduced fault current of the battery energy storage system.
3. The proposed PV array (R1N) should be specified:
    a. To include an anti-islanding protection scheme that is suitable for single-line open and double-line open series faults, in addition to islanding. Single-line and double-line open faults may be caused by blown fuses between the proposed PV array and the new plant.
4. The voltage rise between the new plant bus and bus 15691 should be addressed so as to prevent over-voltages. The over-voltage may cause tripping of protective devices at the proposed PV array, and may cause damage to both customer and/or utility equipment.

5. The feeder 1B and feeder 2B relays under- and over-voltage relays should be set appropriately so as to coordinate the relays with the fuses.

6 REFERENCES

[1] "Population Report – Second Quarter, 2017,," Yukon Bureau of Statistics, [Online]. Available: www.eco.gov.yk.ca/stats/pdf/populationJun_2017_R.pdf.

[2] "Canadian Climate Normals and Averags, Old Crow, YT 1981-2010," Government of Canada, [Online]. Available: www.climate.weather.gc.ca/climate_normals/results_1981_2010.

[3] University of Wisconsin-Madison, "Estimating Line-Flow Limits," Madison, 2013.

[4] C. S. Association, *Preferred voltage levels for AC systems, 0 to 50 000V,* Rexdale: Standards Council of Canada, 2015.

[5] X. Xu, B. Martin, O. G. Donna and C. Hao, "Application and Modeling of Battery Energy Storage in Power Systems," *CSEE Journal of Power and Energy Systems,* vol. 2, no. 3, pp. 82-90, September 2016.

[6] P. K. e. al., "Definition and Classification of Power System Stability," *IEEE Trans. Power Systems,* vol. 19, no. 2, May 2004.

[7] Saft, "Lithium-ion battery life," Saft, Bagnolet, France, 2014.

[8] J. Zrum, S. Sumanik and M. Ross, "An Automated Grid Impact Study Tool for Integrating a High Penetration of Intermittent Resources on Diesel-Based Isolated Systems," in *CIGRE Session 47*, Paris, 2018.

APPENDIX A - PROVIDED DATA

A.1 GENERAL INFORMATION

The following information has been provided through communication with ATCO [A1]-[A2].

Efficiency curves: Measured as a plant heat rate. 2015 average heat rate is 3.32kWh/L.

Diesel start times, shut down times and predicted minimum online running times: Start time is ~90s, and is defined as the time taken for a unit in auto to go online via a request from the dispatch PLC (crank, warmup, sync). Shutdown time is ~250s, and is defined as the time taken for a unit in auto to go offline and stop running (droop / load transfer, cool down, shut off).

Dispatch Strategy: assuming 30% to 80% of generator capacity.

Spinning reserve requirement: defined by the dispatch strategy.

Minimum diesel run time: Do not have

Minimum loading requirements: 30% of rated active power.

Maximum ramping (load) (duration, rate and kW): No defined rate. Dependent on response of each specific machine and system tolerances on voltage and frequency.

Maximum acceptable voltage variation: a) normal operation: 0.95-1.04 pu, b) large-disturbances: 0.90-1.10 pu at feeder relays.

Maximum acceptable frequency variation: a) normal operation: not provided, assuming 59.3Hz to 60.5Hz, b) large-disturbances: 58Hz to 66Hz.

Maximum acceptable phase imbalance variation: a) normal operation: i) voltage unbalance – less than 3% maximum (2% preferred), ii) current unbalance – less than 10% preferred, b) large-disturbances: not provided.

A.2 COST PER CAPACITY AND POWER

The cost of the battery electrical storage system is dependent on both the available output power of the battery, and the total energy capacity of the battery. These two types of costs can be normalized into a dollar per kW and dollar per kWh value to compare different technologies as well as different manufacturers. These types of data can be used in future examinations of parametric analyses of battery sizes or optimization examinations of the battery electrical storage system.

Several batteries are examined based on the dollar per kW and dollar per kWh basis provided within the information provided by CARMEN [A3] in 2015. Batteries that meet the standards set forward within the Table 15 below are placed within a chart depicting the dollar per kW with respect to dollar per kWh. The batteries examined within this section are either AC power capable (indicating that the

power electronic interface is AC compatible), or a battery module (indicating that the battery is independent or a replacement without a power electronic interface). These examples are used to best describe the normalized price of the battery storage systems. The AC power capable systems include the price of the necessary power electronic interfaces, as well as examples of the battery itself.

Table 15: Required parameters for analysis for charting power with respect to energy

AC power capable or Battery Module	Yes
Protection: Outage	Yes
Protection: Back up	Yes
Protection: Uninterruptable power supply	Yes
Price listed	Yes
DC power capable	No
Power listed	Yes
Capacity listed	Yes

With the information above provided for each of the battery models, Figure 80 was created comparing each model with respect to cost. Further information was collected from a Goldman Sachs report from 2015 [A4]. These values provided by each source vary considerably from the CARMEN supplied documentation, the exact reason for which is still unknown. This metric shows the data collected within the analysis. The data are time sensitive as the cost of batteries can vary. This figure is by no means conclusive for all battery types and all manufacturers.

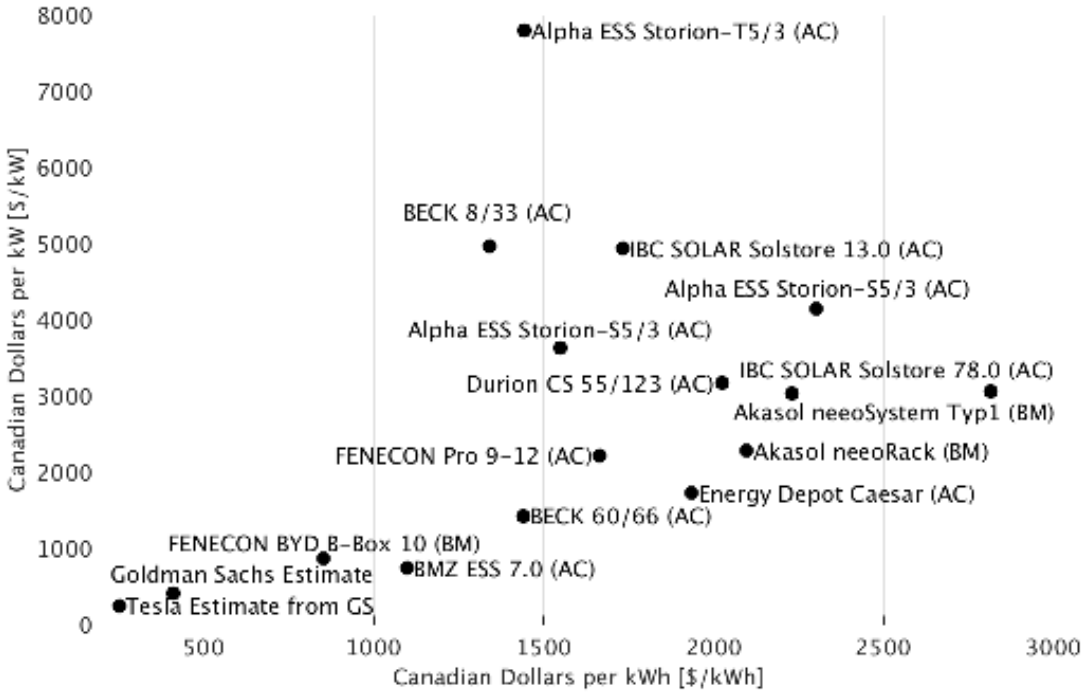

Figure 88: Normalized energy capacity and normalized power for a range of commercially available products

Figure 80 shows that the estimated values by Goldman Sachs are far lower than those provided by CARMEN. This may be due to the Goldman Sachs estimates neglecting the additional cost of a power electronic interface as well as perhaps being slightly optimistic, neither of which is made clear in the report. Furthermore, the differentiation could result due to the CARMEN report including taxes and representing smaller scale batteries. Regardless of the source of the differences in price it is clearly shown that the both the cost per kW and cost per kWh are dependent on the manufacturer.

A.3 RELAY SETTINGS

A.3.1 Generator Relay Settings (SEL700G and Crompton type relays):

A.3.1.1 OC1

Device No.	APL Ident. No.	Protected Device	Relay Type (Model, Rating, Range, etc.)	CT/ PT: Ratios	Setting and Comments
51		OC1 2.4kV MVA	Crompton 253k-PAPK Overcurrent Relay, 120V LL, 5A	200 /5	Phase O/C Not torque controlled; Reset 0.0167 seconds Pickup setting 90% (Minimum Operate = 180 A pri/4.5 A secd'y (748 KVA) Time Dial (51PTD) = 5 sec definite time Inst. =n/a Time Delay (67P1D) = n/a
32			Crompton 256-PATK Reverse Power 120V LL, 5A	200 /5	Pickup setting 9% (Minimum Operate = 25 KW Time Dial (51PTD) = 7 sec definite time

A.3.1.2 OC2

Device No.	APL Ident. No.	Protected Device	Relay Type (Model, Rating, Range, etc.)	CT/ PT: Ratios	Setting and Comments
51		OC2 2.4kV 412.5KVA	Crompton 253k-PAPK Overcurrent Relay, 120V LL, 5A	200 /5	Phase O/C Not torque controlled; Reset 0.0167 seconds Pickup setting 115% (Minimum Operate = 115 A pri/5.75 A secd'y (478 KVA) Time Dial (51PTD) = 6 sec definite time Inst. =n/a Time Delay (67P1D) = n/a
32			Crompton 256-PATK Reverse Power 120V LL, 5A	200 /5	Pickup setting 8% (Minimum Operate = 25 KW Time Dial (51PTD) = 7 sec definite time

A.3.1.3 OC3

Device No.	APL Ident. No.	Protected Device	Relay Type (Model, Rating, Range, etc.)	CT/ PT: Ratios	Setting and Comments
51		OC2 2.4kV MVA	Crompton 253k-PAPK Overcurrent Relay, 120V LL, 5A	75 /5	Phase O/C Not torque controlled; Reset 0.0167 seconds Pickup setting 100% (Minimum Operate = 75 A pri/3.75 A secd'y (312 KVA) Time Dial (51PTD) = 5 sec definite time Inst. =n/a Time Delay (67P1D) = n/a
32			Crompton 256-PATK Reverse Power 120V LL, 5A	75 /5	Pickup setting 7% (Minimum Operate = 25 KW Time Dial (51PTD) = 5 sec definite time

A.3.1.4 OCG3 (New)

Device No.	APL Ident. No.	Protected Device	Relay Type (Model, Rating, Range, etc.)	CT/ PT: Ratios	Setting and Comments
G3		Generator 680 KW 850 KVA 204.5 Amp Gen cable 2/0 AWG RW90 195 amp	SEL-700G Generator Protection Relay Part # 0700G02B1B1B0X850300 5A CT 120Vac PT	200:5 2400:120	32 Reverse Power: Minimum Operate = (5.55%) -34 kW pri/ -42.5W sec, Time Delay = 2.5s 50 Phase Overcurrent: Minimum Operate = 164.4 A pri/ 4.11A (680 KVA), Time Delay = 5s 59 Over Voltage: Minimum Operate = 2640 V pri/ 132 V sec, Time Delay = 2s 81 Over Frequency: Minimum Operate = 66 HZ = 0.5s 27 Under Voltage: Minimum Operate = 2160 V pri/ 108 V sec, Time Delay = 2.8s

A.3.1.5 OCG4

Device No.	APL Ident. No.	Protected Device	Relay Type (Model, Rating, Range, etc.)	CT/ PT: Ratios	Setting and Comments
G4		Generator 450 KW 563 KVA 135 Amp Gen cable #1 AWG RW90 145 amp	SEL-700G Generator Protection Relay Part # 0700G02B1B1B0X850300 5A CT 120Vac PT	150:5 2400:120	32 Reverse Power: Minimum Operate = (5.55%) -25 kW pri/ -41.66 W sec, Time Delay = 2.5s 50 Phase Overcurrent: Minimum Operate = 125A pri/ 4.17A (431 KVA), Time Delay = 5s 59 Over Voltage: Minimum Operate = 2640 V pri/ 132 V sec, Time Delay = 2s 81 Over Frequency: Minimum Operate = 66 HZ = 0.5s 27 Under Voltage: Minimum Operate = 2160 V pri/ 108 V sec, Time Delay = 2.8s Note: 27 Element torque controlled by breaker contact and only active when breaker is closed

A.3.2 Feeder Relay Settings

A.3.2.1 Bus Tie

Device No.	AE Ident. No.	Protected Device	Relay Type (Model, Rating, Range, etc.)	CT/ PT: Ratios	Setting and Comments
1		Bus Tie #1 Bus Tie Cable 4/0 AWG RW90 260 amp	SEL-751A Feeder Protection Relay Part# 751A02B1B1B71850300	300:5 2400:120	Settings for Group 1 51 Over Current: Minimum Operate = 396A pri/ 6.6A sec (1646kW), Time Delay = 3 sec

A.3.2.2 Feeder 1A

Device No.	AE Ident. No.	Protected Device	Relay Type (Model, Rating, Range, etc.)	CT/ PT: Ratios	Setting and Comments
1		Feeder 1A 3L405 Feeder Cable 1/0 AWG RW90 170 amp	SEL-751A Feeder Protection Relay Part# 751A02B1B1B71850300	300:5 2400:120	Settings for Group 1 27 Under Voltage: Minimum Operate = (90%) 2160V pri/ 108V sec, Time Delay = 2.0 sec, Torque Controlled by Loss of Potential, SV01 = 27P1T AND NOT LOP 51 Over Current: Minimum Operate = 160A pri/ 2.67A sec (440kW), Time Curve = U3, Time Dial = 0.8, Toque Control = Not SV08T 51 Over Current (Cold Load Pickup): Minimum Operate = 160A pri/ 2.67A sec (440kW), Time Curve = U3, Time Dial = 1.8, Toque Control = SV08T (Active 10s After Bkr Close) 59 Over Voltage: Minimum Operate = (110%) 2640V pri/ 132V sec, Time Delay = 1.5 sec 81 Under Frequency Stage 1: Minimum Operate = 58Hz, Time Delay = 3.0 sec

A.3.2.3 Feeder 1B

Device No.	APL Ident. No.	Protected Device	Relay Type (Model, Rating, Range, etc.)	CT/ PT: Ratios	Setting and Comments
51		Feeder 1 2.4kV MVA	Crompton 253k-PAPK Overcurrent Relay, 5A	150 /5	Phase O/C Not torque controlled; Reset 0.0167 seconds Pickup setting 60% (Minimum Operate = 90 A pri/3.0 A secd'y (374 KVA) Time Dial (51PTD) = 2.5 sec definite time Inst. =n/a Time Delay (67P1D) = n/a
27/59			Crompton 253-PVMK-PQBX Voltage relay 120V LL, 3phase	20 /1	U/V pickup setting 85% of 120 VAC DIFF 2% O/V pickup setting 110% of 120 VAC DIFF 2% Time Dial (51PTD) instantaneous definite time
81			Crompton	20 /1	Pickup setting 55Hz

A.3.2.4 Feeder 2A

Device No.	AE Ident. No.	Protected Device	Relay Type (Model, Rating, Range, etc.)	CT/ PT: Ratios	Setting and Comments
9		Feeder 2A 3L406 Feeder Cable 1/0 AWG RW90 170 amp	SEL-751A Feeder Protection Relay Part# 751A02B1B1B71850300	300:5 2400:120	Settings for Group 1 27 Under Voltage: Minimum Operate = (90%) 2160V pri/ 108V sec, Time Delay = 2.0 sec, Torque Controlled by Loss of Potential, SV01 = 27P1T AND NOT LOP 51 Over Current: Minimum Operate = 160A pri/ 2.67A sec (440kW), Time Curve = U3, Time Dial = 0.8, Toque Control = Not SV08T 51 Over Current (Cold Load Pickup): Minimum Operate = 160A pri/ 2.67A sec (440kW), Time Curve = U3, Time Dial = 1.8, Toque Control = SV08T (Active 10s After Bkr Close) 59 Over Voltage: Minimum Operate = (110%) 2640V pri/ 132V sec, Time Delay = 1.5 sec 81 Under Frequency Stage 1: Minimum Operate = 58Hz, Time Delay = 3.0 sec

A.3.2.5 Feeder 2B

Device No.	APL Ident. No.	Protected Device	Relay Type (Model, Rating, Range, etc.)	CT/ PT: Ratios	Setting and Comments
51		Feeder 1 2.4kV MVA	Crompton 253k-PAPK Overcurrent Relay, 5A	150 /5	Phase O/C Not torque controlled; Reset 0.0167 seconds Pickup setting 95% (Minimum Operate = 142.5 A pri/4.75 A secd'y (592 KVA) Time Dial (51PTD) = 3 sec definite time Inst. =n/a Time Delay (67P1D) = n/a
27/59			Crompton 253-PVMK-PQBX Voltage relay 120V LL, 3phase	20 /1	U/V pickup setting 85% of 120 VAC DIFF 2% O/V pickup setting 110% of 120 VAC DIFF 2% Time Dial (51PTD) instantaneous definite time
81			Crompton	20 /1	Pickup setting 55Hz

A.3.3 Existing PV Array Protection Settings

The existing PV array Protection settings are based off the IEEE Std. 1547-2003 and the Sunny Boy installation manual [A5].

10.4 Trip Limits / Trip Times

Nominal Freq. (Hz)	Trip Limit (Hz)	Trip Frequencies (Hz)	Trip Times (s)
60	> 60.5	60.45 - 60.55	max. 0.1602
	< 57.0 - 59.8 (default 59.3)	56.95 - 59.85 (default 59.25 - 59.35)	adjustable 0.16 - 300 (default max. 0.1602)
	< 57.0	56.95 - 57.05	max. 0.1602

Nominal Voltage (V)	Trip Limit	Trip Voltages Line-to-Neutral (V)*	Trip Voltages Line-to-Line (V)*	Trip Times (s)
208	50 %	57.6 - 62.4	99.8 - 108.2	max. 0.1602
	88 %	103.2 - 108.0	178.9 - 187.2	max. 2.002
	110 %	129.6 - 134.4	224.6 - 233.0	max. 1.001
	120 %	141.6 - 146.4	245.4 - 253.8	max. 0.1602
240	50 %	57.6 - 62.4	115.2 - 124.8	max. 0.1602
	88 %	103.2 - 108.0	206.4 - 216.0	max. 2.002
	110 %	129.6 - 134.4	259.2 - 268.8	max. 1.001
	120 %	141.6 - 146.4	283.2 - 292.8	max. 0.1602

*The intervals result from the measuring accuracies listed below.

Manufacturer's Accuracies:

Trip Limit Accuracy: ± 2 % of nominal grid voltage

Trip Time Accuracy: ± 0.1 % of nominal trip time

Trip Frequency Accuracy: ± 0.1 % of nominal frequency

Figure 89: Existing PV array protection settings

A.4 EQUIPMENT INFORMATION

Table 16: Line Information

Equipment ID	Nominal Rating [A]	Summer Rating [A]	Winter Rating [A]	Summer Emergency [A]	Winter Emergency [A]	Positive Sequence Resistance [mΩ/m]	Positive Sequence Reactance [mΩ/m]	Zero Sequence Resistance [mΩ/m]	Zero Sequence Reactance [mΩ/m]
ACSR 1/0 3PH	245	245	325	245	325	0.55178	0.462735	0.729616	1.927814
ACSR_1/0_2PH	245	245	325	245	325	0.55178	0.490116	0.729616	1.873052
ACSR_#4_3PH	140	140	185	140	185	1.3919	0.489454	1.569736	1.954533
DEFAULT	625	625	625	625	625	0.21748	0.398605	0.395316	1.863684
ACSR_#6_3PH	105	105	140	105	140	2.2121	0.500199	2.389936	1.992696
ACSR_#4_2PH	140	140	085	140	185	1.3913	0.516835	1.569736	1.899771
ACSR_266_3PH	485	485	640	485	640	0.21748	0.398605	0.395316	1.863684

Equipment ID	Positive Sequence Shunt Susceptance [mS/m]	Zero Sequence Shunt Susceptance [mS/m]	Positive Sequence Shunt Conductance [mS/m]	Zero Sequence Shunt Conductance [mS/m]	Lock Impedance	User Defined Impedances	Frequency [Hz]	Temperature [°C]
ACSR 1/0 3PH	3.769956	1.5624	0	0	1	1	60	25
ACSR_1/0_2PH	3.538644	1.659279	0	0	1	1	60	25
ACSR_#4_3PH	3.469493	1.508267	0	0	1	1	60	25
DEFAULT	4.124968	1.626662	0	0	0	1	60	25
ACSR_#6_3PH	3.406786	1.46488	0	0	1	1	60	25
ACSR_#4_2PH	3.27262	1.598356	0	0	1	1	60	25
ACSR_266_3PH	4.124968	1.620189	0	0	1	1	60	25

A.5 REFERENCES

[A1] Phil Borgel, ATCO Electric Yukon, *private communication*, 2017

[A2] Norm Curzon, ATCO Electric Yukon, *private communication*, 2017

[A3] Bayerisches Staatsministerium für Wirtschaft und Medien, Energie und Technologie, "Marktübersicht Batteriespeicher," Centrales Agrar-Rohstoff Marketing und Energie Netzwerk, Staubing, 2015.

[A4] B, Lee et al., "The Great Battery Race," Goldman Sachs, 2015.

[A5] “Solar Inverter – Sunny Boy (3000US, 4000US) – Installation Guide,” SMA, 2009, pp. 106.

APPENDIX B - MODELS AND PARAMETERS

Appendix B provides a description of models and parameters used to represent the Old Crow electric power system. The models are built in MATLAB 2017a and Simulink using the Simscape Power Systems and Stateflow toolboxes. Figure 82 shows a snapshot of the Old Crow model in Simulink. Figure 1 is a single-line diagram representation of Figure 82.

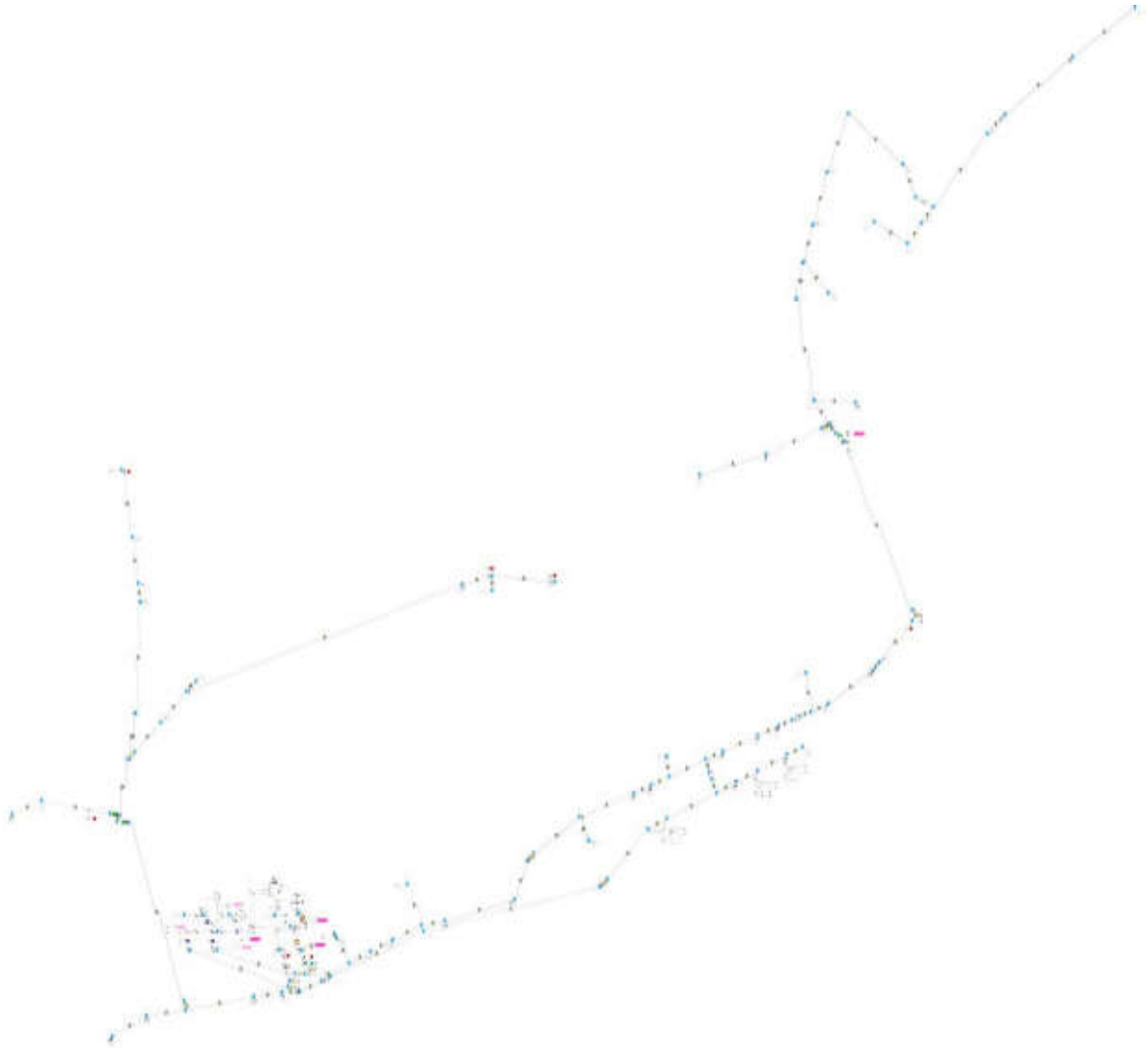

Figure 90: Snapshot of Old Crow System.

B.1 SYNCHRONOUS GENERATOR MODELS

The diesel generators are represented by the synchronous generator model, which is mainly comprised of a synchronous machine model, an excitation system model, a speed-governor model, and plant control model (i.e., automatic frequency control). The model structure is shown in Figure 83.

Each of the models in Figure 83 have several available variants, which are provided in Table 17. The model also includes a parasitic load to improve simulation stability, a breaker and controls to allow disconnection of the generator from the system model, a perturbation to the excitation system voltage reference for use with small-disturbance stability studies, and various measurements as needed for various studies. The model can be used in both discrete and phasor simulations.

Table 17 - Synchronous Generator Model Variants

Model Type	Model Variants
Synchronous Machine	IEEE Model 2.1, IEEE Model 2.2
Excitation System	AC1A, AC4A, AC5A, AC8B, DC1A, DC2A, ST1A, ST2A, BaslerAVC63-12[1]
Power System Stabilizer	None
Speed Governor	DEGOV1, Woodward2301A[2], GGOV1s[3]
Load Controller	None, LCFB1
Automatic Generation Control	None

Notes:

1. *Basler AVC63-12 model can be used to represent both the Basler AVC63-12 and AVC125-10 voltage regulators*
2. *Woodward2301A model exhibits instability at this point in time, but is not used in the studies*
3. *GGOV1s is a simplified version of GGOV1 for use with diesel generators only.*
4. *It is necessary to use a load controller and/or an automatic generation control model when using a speed governor model in droop control.*

It is important to understand that the models used to represent synchronous generators are typically valid for specific ranges of system variables. As an example, the excitation system models given in IEEE Std. 421.5-2005 are valid for frequencies within ±5% of 60Hz (57Hz to 63Hz) [B1]. The validity of each model may differ, and it is difficult to ascertain the range of validity without validating the models against real system data. For interpreting results, any simulations that exhibit frequencies beyond ±16.67% of 60Hz (50Hz to 70Hz) are assumed to be invalid and the results are rejected.

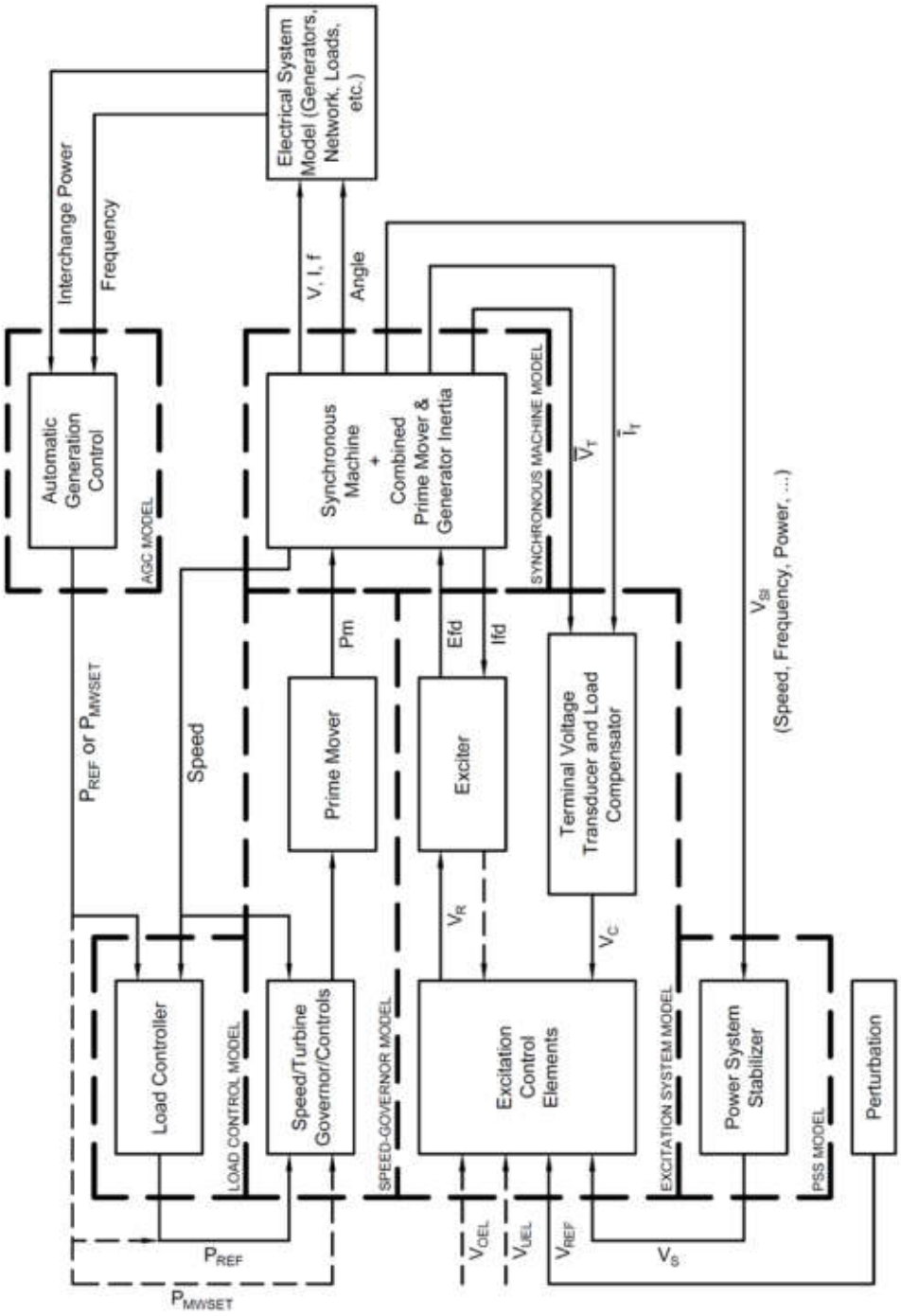

Figure 91: Synchronous Generator Model Structure

Note: figure adapted from [B1,B2,B3].

Synchronous Machines

A synchronous machine is a machine which has a rotor speed that is exactly proportional to the system frequency [B4]. The rotor windings, or field windings, are excited to create a magnetic field, which, when rotated at the synchronous speed, induces an alternating current and voltage in the stator windings at the system frequency. The field winding is excited by the excitation system. The rotor is driven at synchronous speed by the prime mover and regulated by the speed-governor. Both the excitation system and speed-governor are discussed later.

The synchronous machine model is an IEEE model 2.1 or 2.2 representation, and can be used for salient-pole or round-rotor machines, respectively. For further information on the synchronous machine models, the reader is directed to references [B5,B6,B7,B8,B9]. The IEEE model 2.1 representation of the synchronous machine for salient-pole machines is deprecated by NERC, where the GENTPJ model is recommended [B10]. The GENTPJ model provides improved performance in matching the response of synchronous generators; however, it has not been implemented in Simscape Power Systems at this time [B11,B12]. Due to the nature of the load flow tool within Simscape Power Systems, it is impractical/difficult to integrate new synchronous machine models such that they are initialized with the system model.

Excitation Systems

An excitation system provides direct current to the field winding of the synchronous machine, and controls the field voltage to regulate the field current, and consequently the terminal voltage, of the synchronous machine. It may provide protective functions, such as over and under-excitation limitation, to ensure damaging conditions do not occur. In addition, it can receive input from a power system stabilizer, which is discussed later. The excitation system model represents the synchronous machine exciter, the excitation control elements, and the terminal voltage transducer and load compensator. The excitation control elements are sometimes referred to as an automatic voltage regulator. For further information on excitation system models, the reader is directed to references [B1,B7,B9,B13,B14,B15,B16].

The available excitation system models are based on IEEE Std 421.5-2005, as recommended by NERC, and can be used to represent a wide range of excitation systems [B1,B10]. It is important to note that the IEEE models are valid for frequency deviations of ±5% from nominal frequency and oscillation frequencies up to approximately 3Hz [B1]. This may cause inaccuracies in an unbalanced system model, wherein a 2^{nd} harmonic (120Hz) oscillation occurs.

In addition, an excitation system model for the Basler AVC63-12 and AVC125-10 voltage regulators has been implemented, based on the mathematical model provided by Basler and the exciter model from the AC5A model [B1,B17,B18]. The model is functionally identical for both the AVC63-12 and AVC125-10 voltage regulators.

Power System Stabilizers (PSS)

A power system stabilizer acts to increase the damping of power system oscillations through control of the excitation system [B1]. They can accept a variety of inputs such as speed, frequency, and power, and produce a biasing signal for the excitation control elements. Power system stabilizers can be used to address issues with resonance phenomena, such as subsynchronous resonance.

At this time, no power system stabilizer models have been implemented. In remote power systems, there is typically a lack of long transmission lines (with lengths on the order of hundreds of kilometers), and multiple synchronous generation plants. These conditions are generally requisite for resonance phenomena to occur, and so the use of power system stabilizers is not expected.

Turbine-/Speed-Governors

Turbine-/speed-governor models represent the prime mover and control system that acts to regulate, or govern, the power output from the prime mover. The resulting power balance in the electro-mechanical system causes changes in the rotor speed, and thus frequency. The typical control schemes include isochronous and speed-droop.

The available turbine-/speed-governor models are based on the models recommended by NERC that are suitable for use with diesel generator speed-governors. For further information on speed-governor or turbine-governor models, the reader is directed to references [B7,B9,B19,B20].

The DEGOV and DEGOV1 models, which are recommended by NERC, were created exclusively for modeling diesel generator speed-governors are the DEGOV and DEGOV1 models [B10,B21,B22]. The DEGOV1 model has been modified to incorporate the DEGOV model, allowing the model to use both isochronous and speed-droop control methods. Previously, the DEGOV model was used for isochronous control, whereas the DEGOV1 model was used for speed-droop control. When using the DEGOV1 model, care must be taken in the selection of the governor gain; a large governor gain when coupled with a small inertia constant (which is a combined value for the synchronous machine and prime mover) will result in instability in the mechanical system.

The GGOV1 model is a generic thermal turbine-governor model, which is intended to represent steam (conventional or nuclear) plants, simple cycle gas turbines, and combined cycle gas turbines that are controlled by a PID governor [B10,B20,B23]. The model can also be used to represent diesel generators [B20]. The model allows both isochronous and speed-droop control methods, and includes a supervisory load controller. The supervisory load controller serves to represent the outer layer of control used to regulate the prime mover power to a desired value. The GGOV1 model was simplified by removing the turbine acceleration limiter, the turbine load limiter, and the low value select logic. With these pieces removed, the logic within the GGOV1 model becomes very similar to that of the DEGOV1 model.

The Woodward2301A model is based on the mathematical model provided by Woodward [B24,B25]. The model was modified to remove the torque balance and engine acceleration from the model. This

matches the convention used by other governor models used in power system models, wherein the inertia of the prime mover is combined with the synchronous machine and input into the mechanical system of the synchronous machine model.

Load Controller

A load controller acts to regulate the prime mover power to the power set point. Under normal operation in speed-droop control, deviations in speed (i.e., frequency) will cause an increase or decrease in power output, which must be counteracted by the load controller to maintain the power set point. Load controllers are an outer loop of control, and act much slower than speed-droop control.

A load controller control can be represented by the LCFB1 model, as recommended by NERC [B10,B20,B23]. The LCFB1 model provides supervisory load control, and has an identical structure to the supervisory load controller in the GGOV1 model. LCFB1 can be used in conjunction with any other governor model that accepts a load reference.

Automatic Generation Control

Automatic Generation Control acts to regulate the power set point of one or more generators. It can act on a single control area or a multi-area interconnection, and can focus on a number of factors, such as system frequency, economic dispatch, or tie-line power flow. AGC is essentially an outer layer of control for the generator load controllers, and acts to replace manual control of generators.

At this point in time, no AGC models have been implemented. The response time of AGC is typically well beyond the timespan of interest for large-disturbance simulations for remote systems.

B.1.1 Generator G1

No data available from manufacturer for synchronous machine; the generator was not modeled due to lack of information.

B.1.2 Generator G2

Models and model parameters are provided in excel spreadsheet ‘g2_model_data.xlsm’.

Information obtained from:

1. Synchronous Machine – datasheets from Caterpillar and Kato Engineering
2. Excitation System – assuming the AC5A model can be used i) per standardized models recommended by NERC, ii) Per similarity to AVC63-12, which replaces the SR4
    a. Exciter – datasheet from Kato Engineering
    b. Voltage Regulator – no datasheet available (does not exist) from Basler Electric for voltage regulator (model SR4)
3. Speed-Governor – datasheet from Woodward (model 2301A), assumed DEGOV1 model (per standardized models recommended by NERC).

B.1.3 Generator G3O

Models and model parameters are provided in excel spreadsheet ‘g3o_model_data.xlsm’.

Information obtained from:

1. Synchronous Machine – datasheets from Caterpillar and Kato Engineering

2. Excitation System – assuming the AC5A model can be used (i. per standardized models recommended by NERC, ii. Per similarity to AVC63-12, which replaces the SR4)
    a. Exciter – datasheet from Kato Engineering
    b. Voltage Regulator – no datasheet is available (does not exist) from Basler Electric for voltage regulator (model SR4).
3. Speed-Governor – datasheet from Woodward (model 2301A)

B.1.4 Generator G3N

Models and model parameters are provided in excel spreadsheet 'g3n_model_data.xlsm'.

Information obtained from:

1. Synchronous Machine – datasheets from Caterpillar
2. Excitation System
    a. Exciter – datasheet from Caterpillar
    b. Voltage Regulator – datasheet from Basler Electric (model AVC63-12)
3. Speed-Governor – datasheet not available (proprietary) from Caterpillar, assuming the DEGOV1 model can be used (per standardized models recommended by NERC).

B.1.5 Generator G4

Models and model parameters are provided in excel spreadsheet 'g4_mode_data.xlsm'.

Information obtained from:

1. Synchronous Machine – datasheets from Caterpillar and Marathon Electric
2. Excitation System
    a. Exciter – datasheet from Marathon Electric
    b. Voltage Regulator – datasheet from Basler Electric (model AVC63-12)
3. Speed-Governor – datasheet not available (proprietary) from Caterpillar, assuming the DEGOV1 model can be used (per standardized models recommended by NERC).

B.2 RENEWABLE ENERGY AND BATTERY ENERGY STORAGE SYSTEM MODELS

Renewable energy system models can be described as either generic model or detailed models.

Generic Models

Generic models are used for a variety of reasons, such as model transparency and documentation; model availability in various software platforms; and for studies where a detailed model is not available or actual equipment has yet to be chosen [B26]. The generic models are positive sequence models, and can be used to represent a wide range of systems from a wide range of manufacturers with reasonable accuracy. At present, the WECC models necessary to represent solar PV arrays, solar PV plants, distributed solar PV arrays, and battery plants (the REPC_A, REEC_B, REEC_C, REGC_A, and PVD1 models) have been implemented [B10]. These models can be used to represent solar PV arrays, solar PV plants, battery plants, and distributed solar PV arrays [B27,B28]. Further models can be implemented which can be used to represent generic wind turbines or plants [B29]. A separate set of models were developed by the IEC, and have many similarities to the models developed by WECC [B26,B30,B31].

The generic models are positive sequence and output an active and reactive current (i.e., the currents are in the dq-frame). Simscape Power Systems simulates time domain voltages and currents in multi-phase networks, which requires the dq-frame currents to be converted into a single-phase or three-phase frame.

Conversion between the abc-frame (three-phase) and dq-frame uses the Park transformation synchronized to the abc-frame with a phase-locked loop. The current commands are then fed into controlled current sources that inject real time currents into the three-phase network.

To convert a single phase frame, a second (imaginary) signal that is orthogonal to the real signal is created (a 90° phase shift from the real signal). The imaginary signal can be created by differentiating the real signal, applying an all-pass filter, or applying a time delay [B32,B33,B34]. At this point in time, differentiation is used. Conversion between the RI-frame uses the dq transformation synched to the real frame with a phase-locked loop. The current command is then fed into a controlled current source that injects real time currents into the single-phase network.

Detailed Models

Detailed models are specific to the actual power electronic converters (i.e., voltage-sourced converter and/or switch-mode dc-dc converters), power/energy source (e.g., solar photovoltaics, wind turbines, batteries, fuel cells, etc.), and controls. A detailed or averaged model of the power electronic converters can be used within these models. Detailed models of the power electronic converters are necessary if the effects of switching transients must be observed (i.e., for studies looking at harmonics or resonance). Averaged models of the power electronic converters neglect transients; however, they allow substantially larger simulation time steps (i.e., faster simulations).

B.2.1 Battery B1N

Battery B1N is the proposed energy storage system. B1N is assumed to have a base voltage of 600V line-to-line (rms), and is connected to the new plant bus through a grounded wye-delta transformer.

Detailed Model

A detailed model of B1N was built to allow both controlled-current and controlled-frequency. The structure of the model is shown in Figure 84.

The model assumes an averaged 3-arm voltage-sourced converter, and a controller based on the phase-locked loop and dq-frame controls presented in [B35]. Values for the control parameters in the voltage-sourced converter controller are assumed from the examples in [B35].

The voltage on the dc-link of the voltage-sourced converter is controlled according to the mode of operation of the battery. When charging, the dc-link voltage is controlled by the voltage-sourced converter, and bucked to the battery voltage with the buck converter. When discharging, the dc-link voltage is controlled by the boost converter, and is boosted from the battery voltage with the boost converter. Controlling the voltage at the battery terminals from the dc-link allows the magnitude of

power flow into the battery to be controlled. Controlling the voltage at the dc-link from the battery terminals allows the magnitude of power flow out of the battery to be controlled. The duty cycle for both the buck converter (charge) and the boost converter (discharge) is set using the averaged converter equations according to the real power command [B36]. The direction of power flow indicated by the real power command is used to determine which converter should be acting and which should be blocked.

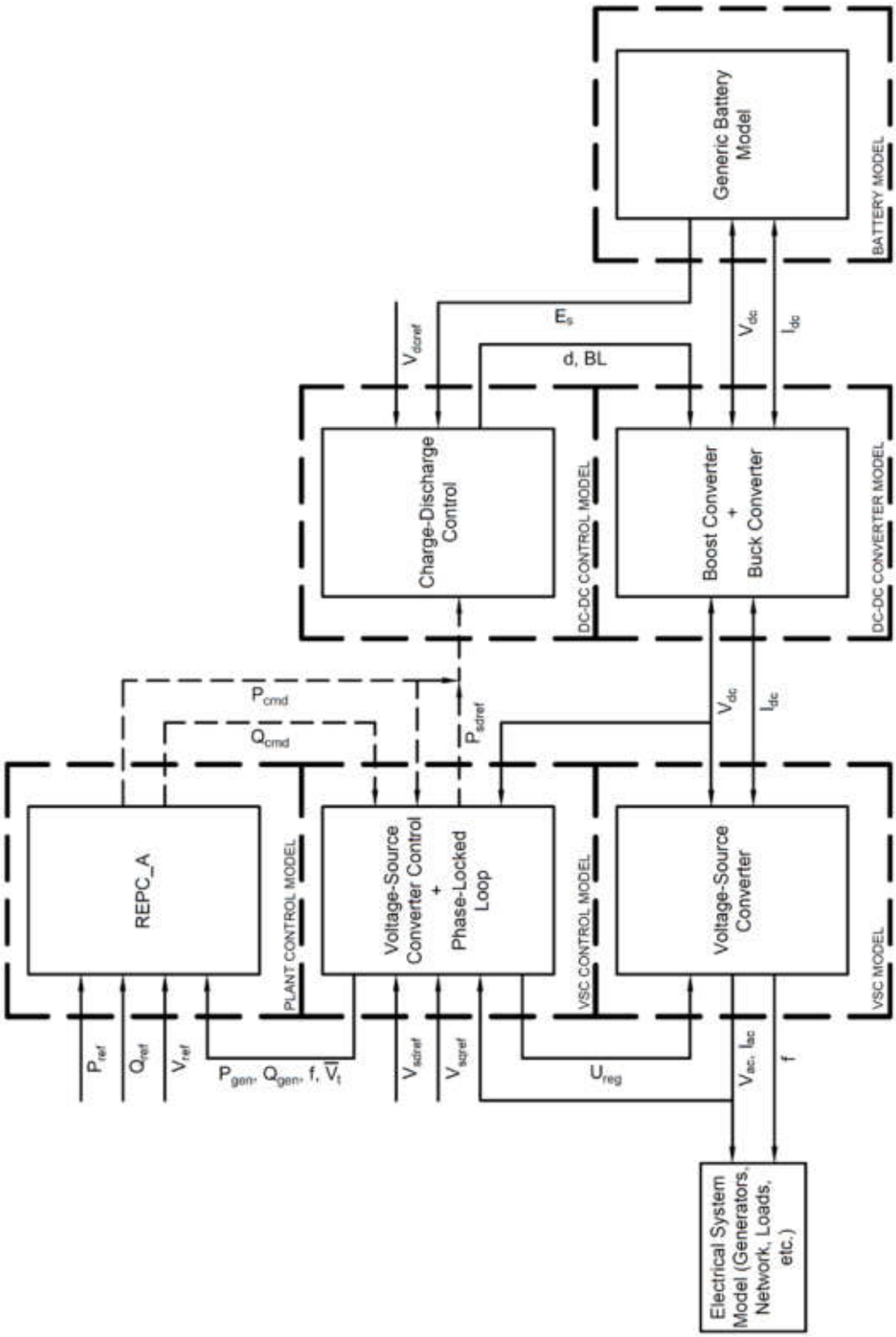

Figure 92: Battery Energy Storage System B1N Model Structure

The source of the power commands depends on the control mode (i.e., controlled-current or controlled-frequency). In controlled-current, the REPC_A model (one of the generic models) is used to generate active and reactive power commands that are used in both the charge-discharge controller and the voltage-sourced converter controller. In controlled-frequency, the voltage-sourced converter controller acts to regulate the magnitude and frequency of the ac-side voltage, and so the real power command is generated by the voltage-sourced converter controller to ensure power flow on the ac-side and dc-side of the converter are balanced.

The battery model is a simplified, generic model, which can be used to represent many types of batteries [B37]. The effects of temperature and aging are assumed to not be required due to i) the time span of the dynamic simulations, and ii) the focus of the studies using dynamic simulations is not concerned with the effects on the battery. The battery model approximates the discharge curve, and controls the battery voltage according to the state-of-charge. The charge characteristics are assumed to be the same as the discharge characteristics [B37].

B.2.2 PV Array R1N

PV Array R1N is the proposed PV array. R1N is presently modeled with the REPC_A, REEC_B, REGC_A, and network interface models. When the PV array design has been finalized, the present model may be replaced with a detailed plant model to improve the accuracy of simulation results. The assumed model parameters are based on typical values provided by WECC [B27].

B.2.3 PV Array R1E

PV Array R1E is the existing 11.8kW PV array at the Arctic Research Facility. R1E is connected on the secondary side terminals of the load transformer at bus 1587. R1E is modeled with the PVD1 model due to a lack of information on the power electronic inverter that is necessary for an array specific model. The assumed model parameters are based on the test system for the PVD1 model given by WECC [B27].

B.2.4 PV Array R2E

PV Array R2E is the existing 3.3kW PV array at the VIOC is connected on the secondary side terminals of the load transformer at bus 1586. R2E is modeled with the PVD1 model due to a lack of information on the power electronic inverter that is necessary for an array specific model. The assumed model parameters are based on the test system for the PVD1 model given by WECC [B27].

B.2.5 PV Array R3E

PV Array R3E is the existing 5.0kW PV array at the bus 1583. R3E is connected on the secondary side terminals of the load transformer at bus 1583. R3E is modeled with the PVD1 model at present. The assumed model parameters are based on the test system for the PVD1 model given by WECC [B27].

B.3 PROTECTION MODELS

Protection devices are represented by a number of device models, which are mainly comprised of one or more measurements, one or more device or function models, and a circuit breaker (1ph or 3ph). The model settings are as specified in the relay settings provided by ATCO.

Fuses

Fuses are modeled as a time-current characteristic curve. The rms current is used to determine the total clearing time from an interpolation between points on the time-current characteristic curve. At each simulation time step, the inverse of the total clearing time is fed into an integrator. By taking the inverse, the saturation limit of the integrator is held constant at 1; however, the rate at which the saturation limit is approached is set by the total clearing time (i.e., it takes the same amount of time as the total clearing time to reach the saturation limit). By this method, if the current increases or decreases from its present value, the fuse model will 'remember' how much longer it will take to clear. On clearing, the circuit breaker that represents the fuse is opened.

At this point in time, fuses do not have a 'reset' function modeled; however, due to the short timeframe of the simulations performed, it is assumed to not be necessary (i.e., only a single event is simulated).

Protective Relays

Protective relays are modeled as a compilation of protective functions. Each function is defined according to the device numbers provided in IEEE Std. C37.2-2008 [B38]. The method of implementation for each function, where available, is defined according to the logic provided by the manufacturers [B39,B40]. Multiple device functions can be used to represent one complete protective relay such as the SEL-700G and SEL-751 relays. At this point in time, only the relay functions specified for the system have been modeled. Relays such as the SEL-700G and SEL-751 relays have a vast number of functions available, many of which are not in use in Old Crow.

The measurement model determines rms values of voltages and currents. Frequency is measured using a zero-crossing method. The effects of potential transformers and current transformers, which are used to transform system voltages and currents to the levels required by the relays, are neglected. This removes the necessity of also including the possible PT/CT configurations as variants in the protection device model. Device settings used in the protection model assume values on the primary side of the PT/CT.

Inverter Protection (Response to Abnormal Conditions)

The protection of the existing PV arrays (R1E, R2E, and R3E) is based on the response to abnormal conditions given by IEEE Std. 1547-2003 [B41,B42,B43,B44]. The response is defined as a clearing time (i.e., the maximum time allowed for the resource to clear from the system) for a given range of voltages or frequencies. The measurement accuracies indicated in the manufacturer's installation

manuals are neglected, as it is not practical to determine the measurement error of the existing devices. Frequency and voltage are assumed to be the measured values provided by the PV array models.

B.3.1 SEL-700G and SEL-751A Relays

The SEL-700G relays provide protection to G3N (PCG3N) and G4 (PCG4). The SEL-751A relays provide protection to Feeder 1A (PCF1A), Feeder 2A (PCF2A), and the bus tie (PCBT1) between the new plant and old plant.

R1N was also assumed to be protected by a SEL-700G relay with functions 27 (under-voltage), 59 (over-voltage), and 81 (frequency) enabled. It was necessary to assume a base level of protection for R1N to prevent islanding; however, no specific anti-islanding protection logic was used at this time. Function 27 was set to trip at voltages below 0.9pu with a definite time delay of 0.5s. Function 59 was set to trip at voltages above 1.1pu with a definite time delay of 0.5s. Function 81 was set to trip at frequencies below 58Hz with a definite time delay of 0.5s. Specific relay settings should be as determined by ATCO. Future studies should incorporate actual relay settings.

Information obtained from:

1. Instruction Manuals from Schweitzer Engineering Laboratories, Inc. [B39,B40]
2. Relay Setting Orders from ATCO Electric Yukon

B.3.2 Crompton 250 Series Relays

The Crompton 250 series relays (Crompton 253-PAPK, 253-PVMK-PQBX, 256-PATK, etc.) provide protection to Feeder 1B (PCF1B), Feeder 2B (PCF2B), G1 (PCG1), G2 (PCG2), and G3O (PCG3O). At this point in time, the device functions are assumed to be identical to those used to model the SEL-700G and SEL-751 relays. The following assumptions were made in simulating the Crompton 250 Series Relays

1. The inverse-time overcurrent relay (device no. 51) is specified with a definite time delay and no inverse-time curve. For this reason, the device is modeled as a definite time overcurrent relay (device no. 50TD).
2. A definite time delay of 1ms (i.e., one simulation time step) is used to represent any devices with no time delay (i.e., an instantaneous definite time). Where a device is not specified with a definite time delay (excluding device no. 51), a 1ms time delay is used.

Information obtained from:

1. Relay Setting Orders from ATCO Electric Yukon

B.3.3 Kearney 30K and 50K Fuses

The Kearney 30K and 50K Fuses are modeled as a melting time-current characteristic curve in the fuse model. The time-current characteristic curves were obtained from the fuses in the CYME model provided by ATCO.

Information obtained from:

1. Melting Time-Current Characteristic Curves from Cooper Power Systems [B45,B46]
2. CYME model from ATCO Electric Yukon

B.4 LOAD MODELS

The load models used are dependent on the type of simulation / study being conducted. Static load models are assumed for the dynamic simulations (i.e., the protection coordination and large-disturbance stability studies). Dynamic load models are assumed for the energy simulations (i.e., the energy balance studies).

Static Load Models

Single-phase loads are assumed to have a 120/240V distribution transformer with a solidly grounded centre-tap. The primary side of the transformer model can be connected in either line-to-line or line-neutral configuration. The load is assumed as a series impedance applied across the x1 and x3 terminals (i.e., 240V) so as to balance the load across the secondary side windings of the transformer. The model also allows the connection of single-phase renewable energy system models to the secondary side terminals.

Three-phase loads are assumed to have three single-phase transformers configured into a three-phase to three-phase transformer. The transformer model can be connected delta-delta, delta-wye, and wye-wye. Wye connections can be floating, to neutral, or to ground. The load is assumed as a balanced three-phase impedance, and is constant at the nominal system frequency [B47]. The load can be configured in a floating wye, a neutral wye, a grounded wye, or a delta configuration [B47]. The model also allows the connection of three-phase renewable energy system models to the secondary side terminals.

In the Old Crow system model, the following specific configurations are used:

1. Single-phase loads are connected in line-line on the primary side of the distribution transformer.
2. Three-phase loads are connected with a delta-wye (grounded) transformer, and assume a grounded wye load configuration.

Dynamic Load Models

The single-phase and three-phase dynamic load blocks shown in Figure 85 (single phase depiction) and Table 18 model the power consumption of a dynamic load using the exponential model retrieved from Power System Stability and Control [B7, pp. 272-273].

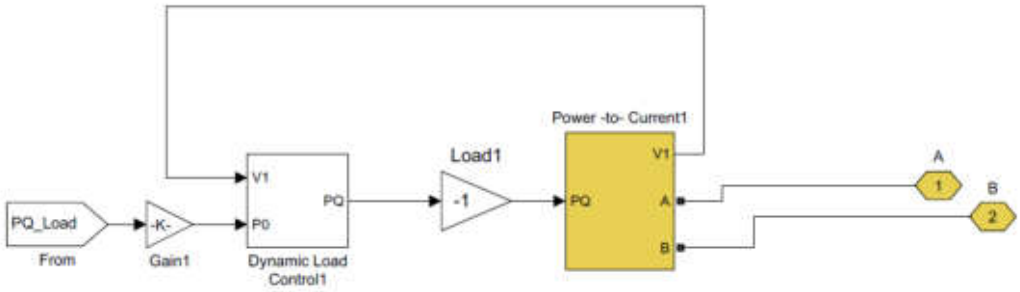

Figure 93: Dynamic Load Block.

Table 18 – Parameters used in dynamic load block

Block Parameter	Units	Description	Variable Name
Nominal L-L voltage	V	Nominal rated voltage of the system. For Old Crow the nominal voltage is 2400V.	Vnom
Power Factor	No units	The power factor is the ratio of the real power to the apparent power of the circuit. For this block, the power factor is used to calculate the apparent power of the system since the total power is given.	PF
Parameters	No units	Parameter a and b represent the type of power injected to the system. These values typically range from 0 to 2 for composite loads. See detailed information on the subject [B7, pp. 272-273].	np_nq
Seasonal Load Data	W	This data is read in automatically from the total load data supplied by the utility.	a2j_load

The equations below are implemented in the Dynamic Load Control block that outputs real and reactive power to the Power to Current Block. This equation uses the initial power (real and reactive) of the current time step (P_o and Q_o) to determine P and Q using the equations stated below, where the bus voltage is V.

$$P = P_o(\overline{V})^a$$

$$Q = Q_o(\overline{V})^b$$

The variables a and b represent the type of power injected to the system. These exponents will be equal to 0, 1 or 2 representing constant power, constant current and constant impedance characteristics respectively. Since this system is built to represent constant power the constants are set to a = 0 and b = 0.4 [B7].

The per unit voltage ($\overline{V}$) is also calculated at each time step using the equation,

$$\overline{V} = \frac{V}{V_0}$$

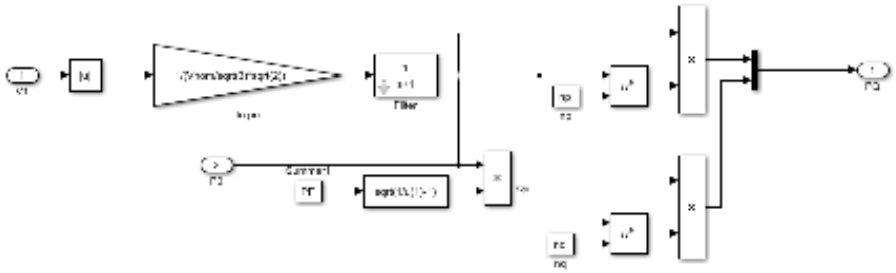

Figure 94: Dynamic Load Control.

The Power to Current block in three phase, Figure 87 and in a single phase Figure 88, convert the input power to a current with the equations,

$$V_1 = \frac{1}{3}(V_{ab} - a^2 V_{bc})$$

$$S = \frac{3}{2} V I^*$$

The first equation is used to determine the total voltage from a balanced three-phase circuit [B48, Sec. 1.8, eq. 1.29].

The second equation is the power equation where the complex power (S) is equal to the product of Voltage (V) by the complex conjugate of current (I^*). The 3/2 is derived from the conversion from peak voltage and current to RMS and converting to phase to ground. The two blocks differentiate with a single phase and three-phase by the amount of power going through each line and the resulting current.

The single-phase power to current block can represent a load that is only connected across two lines of the power system. This allows for the grid impact study to perform experiments on an imbalanced system. This type of power to current block requires a different logic scheme than the three-phase block. The single-phase system uses the same process without the addition of the final phase, Figure 88.

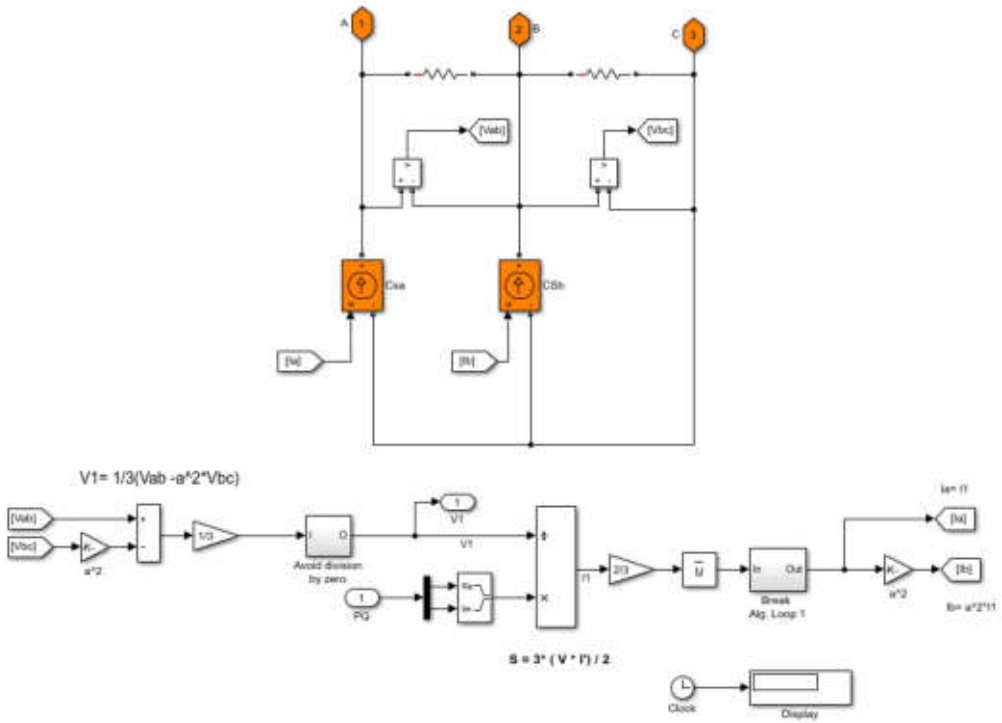

Figure 95: Three-Phase Power to Current block.

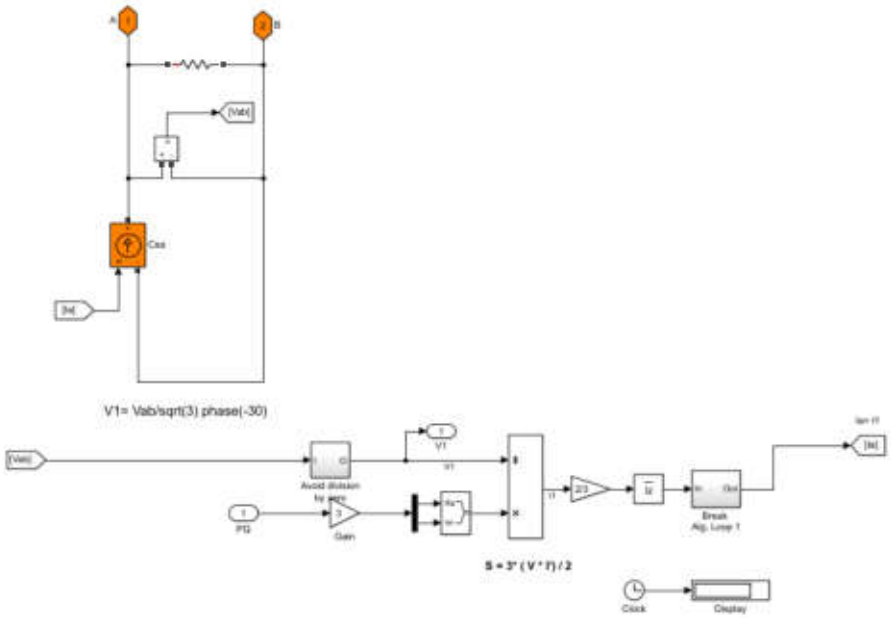

Figure 96: Single phase dynamic load block

B.5 LINE MODELS

Line models are classified according to the type and line length. Several assumptions were made from the data contained in the CYME model:

1. Transmission lines in CYME with zero length were assumed to have a length of 1×10^{-5}m in the model. This is necessary to ensure non-zero resistances/inductances associated with a zero length transmission line. This is necessary in Matlab since parameters are implemented in matrices, which will result in either errors when inverting the matrix.
2. Unbalanced lines (i.e., #4 outside #6 center) were assumed to be balanced lines. For the case of the #4 outside #6 center line type in the CYME model, an ACSR_#4_3PH line type was used.

Distribution Line Models

Distribution lines are modeled as a series impedance (resistance and inductance), and are accurate for distances less than 50km [B7] The impedance is calculated from the line length and the impedance per unit length. The impedance per unit length is unique for each line type/configuration.

Transmission Line Models

Short transmission lines are modeled as a series impedance (resistance and inductance), and are accurate for distances less than 50km [B7]. The impedance is calculated from the line length and the impedance per unit length. The impedance per unit length is unique for each line type/configuration.

B.6 REFERENCES

[B1] *IEEE Recommended Practice for Excitation System Models for Power System Stability Studies*, IEEE Std. 421.5-2005

[B2] "Dynamic Models for Steam and Hydro Turbines in Power System Studies," IEEE Trans. Power Apparatus and Systems, Vol. 92, No. 6, pp. 1904-1915, 1973

[B3] "Dynamic Models for Fossil Fueled Steam Units in Power System Studies," IEEE Trans. Power Systems, Vol. 6, No. 2, pp. 753-761, 1991

[B4] *Authoritative Dictionary of IEEE Standard Terms – Seventh Edition*, IEEE Std. 100-2000

[B5] https://www.mathworks.com/help/physmod/sps/powersys/ref/synchronousmachine.html

[B6] *IEEE Guide for Synchronous Generator Modeling Practices and Applications in Power System Stability Analyses*, IEEE Std. 1110-2002(R2007)

[B7] P. Kundur, *Power System Stability and Control*, McGraw-Hill, 1994

[B8] P. Krause et al., *Analysis of Electric Machinery and Drive Systems*, 3ed, Wiley, 2013

[B9] M.J. Gibbard, P. Pourbeik, and D.J. Vowles, *Small-Signal Stability, Control and Dynamic Performance of Power Systems*, University of Adelaide Press, 2015

[B10] "NERC Library of Standardized Powerflow Parameters and Standardized Dynamics Models – Version 1," NERC, 2015

[B11] J. Undrill, "The Gentpj Model", 2012

[B12] P. Pourbeik et al., "Modeling of synchronous generators in power system studies," CIGRE Science & Engineering, vol. 6, pp. 21-31, 2016

[B13] "Computer Representation of Excitation Systems," IEEE Trans. Power Apparatus and Systems, Vol. 87, No. 6, pp. 1460-1464, June 1968

[B14] "Excitation System Models For Power System Stability Studies," IEEE Trans. Power Apparatus and Systems, Vol. 100, No. 2, pp. 494-509, February 1981

[B15] *IEEE Recommended Practice for Excitation System Models for Power System Stability Studies,* IEEE Std. 421.5-1992

[B16] *IEEE Recommended Practice for Excitation System Models for Power System Stability Studies*, IEEE Std. 421.5-2016

[B17] T. Gaines, Basler Electric Company, *private communication*, September 2017

[B18] "Mathematical Per-Unit Model of the AVC63-12 and AVC125-10 Regulator," Basler Electric, June 2002

[B19] L.L.J. Mahon, *Diesel Generator Handbook*, Elsevier, 1992

[B20] P. Pourbeik et al., "Dynamic Models for Turbine-Governors in Power System Studies," IEEE Power & Energy Society, Technical Report PES-TR1, January 2013

[B21] K.E.Yeager and J.R.Willis, "Modeling of Emergency Diesel Generators in an 800 Megawatt Nuclear Power Plant," IEEE Trans. Energy Conversion, Vol. 8, No. 3, September 1993

[B22] L. Hannett et al., "Validation of Nuclear Plant Auxiliary Power Supply Test," IEEE Trans. Power Apparatus and Systems, Vol. 101, No. 9, September 1982

[B23] L. Pereira et al., "New Thermal Turbine Governor Modeling for the WECC," WECC MVWG, October 2002

[B24] T. Hinde, Woodward, private communication, June 2017

[B25] "Woodward 2301A Governor and EGB-13 P Actuator Mathematical Model," Woodward, April 2009

[B26] P. Pourbeik et al., "Value and Limitations of the Positive Sequence Generic Models of Renewable Energy Systems," WECC, December 2015

[B27] WECC REMTF, "WECC PV Power Plant Dynamic Modeling Guide," WECC MVWG, April 2014

[B28] WECC REMTF, "WECC Battery Storage Dynamic Modeling Guideline," WECC MVWG, 2016

[B29] WECC REMTF, "WECC Wind Power Plant Dynamic Modeling Guide," WECC MVWG, 2014

[B30] *Wind Turbines – Part 21-1: Electrical simulation models – Wind turbines*, IEC 61400-27-1:2015

[B31] A. Honrubia-Escribano et al., "Generic dynamic wind turbine models for power system stability analysis: A comprehensive review," Elsevier Renewable and Sustainable Energy Reviews, 2017

[B32] M. T. Haque and T. Ise, "Implementation of Single-Phase pq Theory," IEEE Power Conversion Conference, Osaka, pp. 761-765, 2002

[B33] B. Crowhurst et al., "Single-Phase Grid-Tie Inverter Control Using DQ Transform for Active and Reactive Load Power Compensation," IEEE Power and Energy Conference, Kuala Lumpur, pp. 489-494, 2010

[B34] A. Roshan et al., "A D-Q Frame Controller for a Full-Bridge Single Phase Inverter Used in Small Distributed Power Generation Systems," IEEE Applied Power Electronics Conference and Exposition, 2007, pp. 641-647

[B35] A. Yazdani and R. Iravani, *Voltage-Sourced Converters in Power Systems: Modeling, Control, and Applications*, Wiley, 2010

[B36] N. Mohan, T. Undeland, and W. Robbins, "dc-dc Switch-Mode Converters" in *Power Electronics: Converters, Applications, and Design*, 3rd ed., Wiley, 2003, ch. 7, pp. 161-199

[B37] O. Tremblay, L. Dessaint, A. Dekkiche, "A Generic Battery Model for the Dynamic Simulation of Hybrid Electric Vehicles," IEEE Vehicle Power and Propulsion Conference, 2007, pp. 284-289

[B38] *IEEE Standard for Electrical Power System Device Function Numbers, Acronyms, and Contact Designations*, IEEE Std. C37.2-2008

[B39] "SEL-700G Generator and Intertie Protection Relays – Instruction Manual," SEL, 20160831

[B40] "SEL-751 Relay Feeder Protection Relay – Instruction Manual," SEL, 20160930

[B41] *IEEE Standard for Interconnecting Distributed Resources with Electric Power Systems*, IEEE Std 1547-2003

[B42] "Solar Inverter – Sunny Boy (3000US, 4000US) – Installation Guide," SMA, 2009

[B43] "Solar Inverter – Sunny Boy (5000US / 6000US / 7000US) – Installation Guide," SMA, 2009

[B44] "SolarEdge Installation Guide – For North America, Version 4.1," SolarEdge, 2017

[B45] "Melting Time-Current Characteristic Curves for Kearney Type K Fuse Links," Cooper Power Systems, No. K-31000A, 1981

[B46] "Total Clearing Time-Current Characteristic Curves for Kearney Type K Fuse Links," Cooper Power Systems, No. K-31000B, 1981

[B47] https://www.mathworks.com/help/physmod/sps/powersys/ref/threephaseseriesrlcload.html

[B48] J. J. Grainger, *Power System Analysis*, McGraw-Hill, 1994